

Study of the Impact of Power Converters Equipped with LC-
LCL Filters Interfacing Renewable Energy Sources to the
Grid

by

Naima ARAB

MANUSCRIPT-BASED THESIS PRESENTED TO ÉCOLE DE
TECHNOLOGIE SUPÉRIEURE IN PARTIAL FULFILLMENT
FOR THE DEGREE OF DOCTOR OF PHILOSOPHY
Ph.D.

MONTREAL, 12 JUNE, 2021

ÉCOLE DE TECHNOLOGIE SUPÉRIEURE
UNIVERSITÉ DU QUÉBEC



Naima Arab, 2021



This Creative Commons license means that it is permitted to distribute, print or save on another medium part or all of this work provided the author is acknowledged, that these uses are made for non-commercial purposes and that the content of the work has not been modified

BOARD OF EXAMINERS

THIS THESIS HAS BEEN EVALUATED
BY THE FOLLOWING BOARD OF EXAMINERS

Mr. Kamal Al-Haddad, Thesis Supervisor
Department of Electrical Engineering, École de Technologie Supérieure

Mr. Gabriel J. Assaf, Chair, Board of Examiners
Department of Electrical Engineering, École de Technologie Supérieure

Mr. Handy Fortin Blanchette, Examiner
Department of Electrical Engineering, École de Technologie Supérieure

Dr. Arezki Merkhouf, Examiner
Hydro Quebec Research Institute

Mr. Sheldon S. Williamson, Independent External Examiner
Department of Electrical, Computer and Software Engineering, University of Oshawa, Ontario

THIS THESIS WAS PRESENTED AND DEFENDED IN THE PRESENCE

OF A BOARD OF EXAMINERS AND THE PUBLIC

ON JUNE 29TH, 2021

AT ÉCOLE DE TECHNOLOGIE SUPÉRIEURE

ACKNOWLEDGMENTS

I would like to express my deep gratitude to my thesis director, Mr. Kamal Al-Haddad, who gave me the benefit of his expertise, his appreciable advice, his availability, and his financial support.

I would also like to thank the examiners, who accepted to review my thesis, I am deeply grateful to you.

I would like to thank the staff of the electrical engineering department at ÉTS and, in particular, all the members of the GREPCI laboratory.

I would like to express my utmost respect to Mr. Abdelhamid Hamadi and thank him for his unreserved assistance and for answering all my questions during the process of reviewing my papers. I would also like to thank him and Mr Auguste for attending my pre-defense.

I would like to thank Mr Bachir Kedjar who participated in the research project proposal and in the choice of the control, and for his help in the redaction of my first paper.

I would also like to thank Alireza Javadi who helped me in real-time implementation using dSPACE.

My sincere thanks to Hani Vahedi whose I had a good experience during this work.

I want to express my greatest gratitude to my dearest family. I will not be there, and this thesis would never have seen the light of day without your unfailing support, without your advice throughout this work and without your unconditional love.

Thanks to my little angel who gives me the will and power to complete this work. I dedicate this thesis to my dear Rayana Meriem and to my husband.

Study of the impact of power converters equipped with LC-LCL filters interfacing renewable energy sources to the grid

Naima ARAB

ABSTRACT

The demand and variety of power converters interfacing with renewable energy sources have been increasing steadily in recent years, presenting new challenges for the current centralized power grid. The microgrid is a new alternative that increases the penetration rate of the renewable energies (wind and photovoltaic energy, etc.) while the electrical power quality is improved. However, the increased penetration rate of the distributed generators DGs systems can pose problems with reverse power flow, voltage fluctuations and other issues to distribution networks. Beside this, the loads variations, the power generated by the renewable energy sources, and also the transition between grid-connected and the islanded modes impact the microgrid stability. The instabilities are linked to the fact that the power flow in this type of network is bidirectional. In addition, the power fluctuations generated by the renewable energy sources in MGs require the coordinated control of DGs, which allows further stable MG operation. Therefore, the reliability and stability are the major concerns in a microgrid system. On the other hand, distributed generators are equipped with an LC-LCL filter to produce higher power quality while relieving it for reactive power compensation and harmonic elimination.

As part of this doctoral thesis, the local control of a distributed generator which is connected to the loads and to the grid via an LCL filter has been optimally designed as to have the active damping based on LQR control. In addition, this proposed control takes into consideration the perturbation and the tracking of a desired reference model in order to guarantee the stability and robustness of the distributed generator. The controllers have been experimentally implemented using real time with dSPACE. Two applications have been successfully completed; first application is a distributed generator connected to the grid via an LCL filter (PUC5-LCL) and the second one is a single stage multifunctional SPV-APF-LCL which was designed to achieve optimal multifunctional operation for residential power supply.

In order to improve the power sharing between the distributed generators in a microgrid, a new droop control in the primary control has been proposed to keep the voltage and frequency of the microgrid constant. This droop control is based on supplementary control loop (stabilizer) added in the conventional droop control and is applied to several converters interfacing with renewable energy sources connected in parallel on the AC bus. The microgrid application with the proposed droop control has been verified in the real time environment using dSPACE and RT-LAB.

The application of its commands involves the modeling of these complete systems as well as the design of the appropriate regulators to deal with the resonances problems, instabilities and the high quality of energy transfer as well as the suitable power sharing performance.

VIII

All the theoretical studies are completely validated by simulation and experimentation analyses and discussions.

Keywords: Active damping, LCL filter, Microgrid, optimal control, Power sharing, PUC5 multilevel converters, stability, stabilizer.

Étude de l'impact des convertisseurs de puissance munis de filtres LC-LCL interfaces des sources d'énergies renouvelables au réseau

Naima ARAB

RESUMÉ

La demande et la variété de convertisseurs de puissance d'interface avec des sources d'énergie renouvelables n'ont cessé d'augmenter ces dernières années, présentant de nouveaux défis pour le réseau électrique centralisé actuel. Le micro-réseau est une nouvelle alternative qui permet d'augmenter le taux de pénétration de ces énergies renouvelables (éolien et photovoltaïque, etc.) et qui permet d'améliorer la qualité de l'énergie électrique. Cependant, la pénétration croissante des systèmes de générateurs distribués DGs peut poser des problèmes de flux d'énergie inversé, de fluctuations de tension et d'autres problèmes aux réseaux de distribution. La stabilité du micro-réseau est influencée par les variations de charges, la puissance produite par les sources d'énergie renouvelables et aussi la transition entre le mode connecté au réseau et en mode îlot, les instabilités sont liées au fait que la puissance d'écoulement dans ce type de réseau est bidirectionnelle. De plus, les fluctuations de puissance générées par les sources d'énergie renouvelables dans les MGs nécessitent un contrôle coordonné des DGs, ce qui permet un fonctionnement plus stable des MGs. Ainsi, la fiabilité et la stabilité deviennent des préoccupations majeures dans un micro-réseau. Les générateurs distribués sont équipés d'un filtre LC-LCL pour produire une meilleure qualité de puissance tout en le soulageant pour la compensation de la puissance réactive et l'élimination des harmoniques.

Dans le cadre de cette thèse de doctorat, un contrôle local d'un générateur distribué connecté aux charges et au réseau via un filtre LCL au moyen d'un contrôle optimal doté d'un amortissement actif basé sur le contrôle LQR a été proposé. De plus, cette commande proposée prend en compte la perturbation et le suivi d'un modèle de référence souhaité afin de garantir la stabilité et la robustesse du générateur distribué. Les contrôleurs ont été implémentés en temps réel avec dsPACE. Deux applications ont été faites, la première est un générateur distribué connecté au réseau via un filtre LCL (PUC5-LCL). La deuxième application est un SPV-APF-LCL multifonctionnel a un seul étage conçu pour obtenir un fonctionnement optimal multifonctionnel pour une alimentation électrique résidentielle.

Afin d'améliorer le partage de puissance entre les générateurs distribués dans un micro-réseau, une nouvelle commande de statisme dans le contrôle primaire a été proposée pour maintenir la tension et la fréquence du micro-réseau constantes. Ce contrôle de statisme est basé sur une boucle de contrôle supplémentaire (stabilisateur) ajoutée dans le contrôle de statisme conventionnel et qui est appliqué à plusieurs convertisseurs en interface avec des sources d'énergie renouvelables, connectés en parallèle sur le bus AC. L'application de micro-réseau avec le contrôle de statisme proposé a été implémentée en temps réel à l'aide de dsPACE et RT-LAB.

L'application de ses commandes implique la modélisation de ces systèmes complets ainsi que la conception des régulateurs appropriés pour faire face aux problèmes de résonances et

X

d'instabilités ainsi que la bonne qualité de transfert d'énergie et de bonnes performances de partage de puissance.

Toutes les études théoriques sont entièrement validées par simulation et expérimentation.

Mots-clés : Amortissement actif, convertisseurs multiniveaux PUC5, contrôle optimal, filtre LCL, Micro-réseau, partage de puissance, stabilité, stabiliser.

TABLE OF CONTENTS

	Page
INTRODUCTION	1
CHAPTER 1 LITERATURE REVIEW AND STATE OF THE ART OF DISTRIBUTED ELECTRICITY GENERATION SYSTEMS.....	11
1.1 Introduction.....	11
1.2 Control Strategies of Power Converter for Distributed Generation.....	11
1.2.1 Passive and Active Damping	12
1.2.1.1 Passive damping.....	12
1.2.1.2 Active damping.....	12
1.3 Control methods of primary loop.....	21
1.3.1 Conventional droop controller	22
1.3.2 Droop controller with virtual impedance and other variants	22
1.3.3 Improved droop controller	23
1.3.4 Hierarchical control strategies	24
1.4 Microgrid power quality	25
1.5 State of the art on microgrids.....	26
1.5.1 Concept, definition and challenges of microgrid.....	26
1.5.2 Control Structures	27
1.5.2.1 Centralized control structure.....	27
1.5.2.2 Decentralized control structure.....	27
1.5.3 Classification of microgrid	27
1.5.4 Microgrid Architecture	29
1.5.5 Power converters used in microgrids.....	29
1.5.6 Methods of controlling an AC microgrids.....	30
1.5.6.1 Control strategies in grid-connected mode.....	30
1.5.6.2 Control of power converters for grid forming	31
1.5.6.3 Control of power converters supplying a network.....	32
1.5.6.4 Control of grid supporting power converter	33
1.5.7 Control technique in islanded mode	33
1.5.7.1 Master-slave control	33
1.5.7.2 Peer-to-peer control	34
1.5.7.4 Control of the multi-agent system	35
1.5.8 Microgrid control strategy, power management and optimization.....	35
1.5.8.1 Primary control	36
1.5.8.2 Secondary control	37
1.5.8.3 Tertiary control	37
1.5.9 Control strategy of autonomous microgrids	37
1.6 Conclusion	38

CHAPTER 2	LQR CONTROL OF SINGLE-PHASE GRID-TIED PUC5 INVERTER WITH LCL FILTER	41
2.1	Introduction.....	41
2.2	Gid-Tied PUC5-LCL Inverter.....	45
2.2.1	Configuration	45
2.2.2	LCL Filter Design.....	47
2.3	Single-Phase d-q Model.....	50
2.4	Design and implementation of optimal control for grid-tied PUC5-LCL	52
2.4.1	Comparison between LQR and PI controller.....	57
2.5	Experimental validation.....	60
2.5.1	Performance under grid current variations	64
2.5.2	Performance under system parameter changes	65
2.5.3	Performance under grid voltage sag and swell	67
2.5.4	Performance under DC voltage variation	69
2.6	Conclusion	70
CHAPTER 3	A MULTIFUNCTIONAL SINGLE-PHASE GRID-INTEGRATED RESIDENTIAL SOLAR PV SYSTEMS BASED ON LQR CONTROL	73
3.1	Introduction.....	73
3.2	Modeling OF SPV-APF-LCL	78
3.2.1	3.2.1. LCL Filter Design	78
3.3	Controller Design and Implementation.....	81
3.4	Simulation and experimental results.....	89
3.4.1	Simulation results.....	89
3.4.1.1	Controller performance under load power changes.....	93
3.4.1.2	Controller Performance under change in insolation	93
3.4.2	Comparison between proposed control and conventional p-q /d-q control.....	94
3.5	Experimental results.....	96
3.5.1	Comparison between proposed control scheme and with others existing in the literature	101
3.6	Conclusion	102
CHAPTER 4	A ROBUST STABILIZER FOR POWER SHARING BASED ISLANDED AC MICROGRID	105
4.1	Introduction.....	106
4.2	Microgrid model	109
4.3	New droop control	110
4.3.1	Stabilizer design.....	112
4.4	Voltage and current control loop design.....	115
4.5	Stability analysis with dynamic phasor model (DPM)	115
4.6	Simulation and experimental results.....	117
4.6.1	Simulation results.....	118
4.6.2	Experimental results.....	122

4.7	Conclusion	129
	CONCLUSION AND FUTURE WORK	131
	LIST OF REFERENCE	135

LIST OF TABLES

	Page
Table 1.1	Converters used in microgrids29
Table 2.1	All states of PUC5 Inverter.....46
Table 2.2	A comparison between PUC5-L with PI controller and PUC5-LCL with LQR controller.....60
Table 2.3	Experimental tests parameters61
Table 3.1	System parameters89
Table 3.2	Pv array parameters.....89
Table 3.3	Comparative study of the proposed control with d-q/p-q control.....95
Table 3.4	Comparison of the proposed system with the existing work in the literature102
Table 4.1	System parameters118

LIST OF FIGURES

	Page
Figure 1.1	A block diagram of virtual resistance13
Figure 1.2	Lead-leg compensator control structure.....14
Figure 1.3	Notch filter control structure.....15
Figure 1.4	Capacitor current feedback control structure16
Figure 1.5	Block diagram of the GCC damping method19
Figure 1.6	Conventional droop control curves21
Figure 1.7	Microgrid architecture26
Figure 1.8	AC microgrid architecture28
Figure 1.9	DC microgrid architecture28
Figure 2.1	Single-Phase PUC5 inverter connected to the grid via LCL filter.....45
Figure 2.2	Five-level pulse-width modulation (PWM) scheme47
Figure 2.3	Bode plots of the designed LCL filter.....49
Figure 2.4	Designed controller for single-phase grid-tied PUC5-LCL inverter56
Figure 2.5	Block diagram of the design of the PI controller58
Figure 2.6	Conventional vector control.....58
Figure 2.7	Grid current components in D-Q reference frame, (a) with conventional59
Figure 2.8	Experimental setup. (1) PUC5 inverter, (2) LCL filter, (3) dSPACE 110361
Figure 2.9	Steady state voltage, grid current and DC source voltage waveforms63
Figure 2.10	Grid current, voltage waveforms, and their Harmonic analysis (THD)63
Figure 2.11	Power analyzer results64
Figure 2.12	Snapshot of grid current in α - β coordinates measured by64

Figure 2.13 Experimental results of the grid current reference variations in d-q65

Figure 2.14 Grid voltage, grid current and DC source voltage waveforms for a grid current variations from 4A to 8A and back to 4A66

Figure 2.15 Grid voltage and current, inverter output voltage, dc bus voltage for a decrease in grid inductance value66

Figure 2.16 Harmonic analysis (THD) of the grid current and voltage for.....67

Figure 2.17 Power analysis results when grid inductance is reduced67

Figure 2.18 Grid voltage and current, DC voltage under grid voltage sag68

Figure 2.19 Grid voltage and current, DC voltage under grid voltage swell69

Figure 2.20 Performance under DC voltage variation from 200V to 220.....70

Figure 3.1 Residential solar photovoltaic systems76

Figure 3.2 Electrical scheme of the system under study79

Figure 3.3 Implemented controller in Matlab80

Figure 3.4 Design of LQR control with fixed R and iterating Q.....85

Figure 3.5 Design of LQR control for fixed Q (large value) and iterating R.....85

Figure 3.6 Placement of the closed-loop eigenvalues86

Figure 3.7 The phase-locked loop (PLL)88

Figure 3.8 System response under load power variations90

Figure 3.9 System response when load is switched on/off and off/on91

Figure 3.10 System response under insolation variations92

Figure 3.11 System response when insolation is switched on/off.....92

Figure 3.12 Dynamic response under insolation variations95

Figure 3.13 Laboratory setup96

Figure 3.14 Steady state waveforms in presence of load97

Figure 3.15 System response in the presence of load when insolation is switched on98

Figure 3.16	System response under insolation variations in presence of load.....	99
Figure 3.17	Waveforms during load variations (a) increase and (b) decrease	99
Figure 4.1	Stabilizer under nonlinear load variations, (a) the active power of converter 1 and converter 2, (b) frequency of converter 1 and converter 2, (c) current of converter 1, (d) load current, (e) PCC voltage	121
Figure 4.2	Stabilizer under unbalanced load variations, (a) the active power of converter 1 and converter 2, (b) frequency of converter 1 and converter 2, (c) current of converter 1, (d) load current, (e) PCC voltage	122
Figure 4.3	Stabilizer when the unbalanced load is switched on/off and then off/on, (a) the active power of converter 1 and converter 2, (b) frequency of converter 1 and converter 2, (c) current of converter 1, (d) load current , (e) PCC voltage.....	122
Figure 4.4	Experimental setup used for HIL implementation.....	123
Figure 4.5	Experimental results of AC microgrid with the proposed droop control under balanced equal power sharing	125
Figure 4.6	Experimental results of AC microgrid with the proposed droop control under unbalanced equal power sharing	126
Figure 4.7	Waveforms of the proposed droop control during balanced load variations,	127
Figure 4.8	Waveforms with the proposed droop control during unbalanced load variations, (a, b) increased and (c, d) decreased	127
Figure 4.9	Waveforms with the proposed droop control during balanced unequal power sharing.....	128
Figure 4.10	Waveforms with the proposed droop control during unbalanced unequal power sharing	128

INTRODUCTION

The increased of the energy consumption has growingly reduced the fossil fuel reserves. Over 85% of the generated energy is obtained from fossil materials such as natural gas, oil, or nuclear energy ... etc. Figure 0.1 shows the growth in annual global fuel demand for all current sources (BP, 2016).

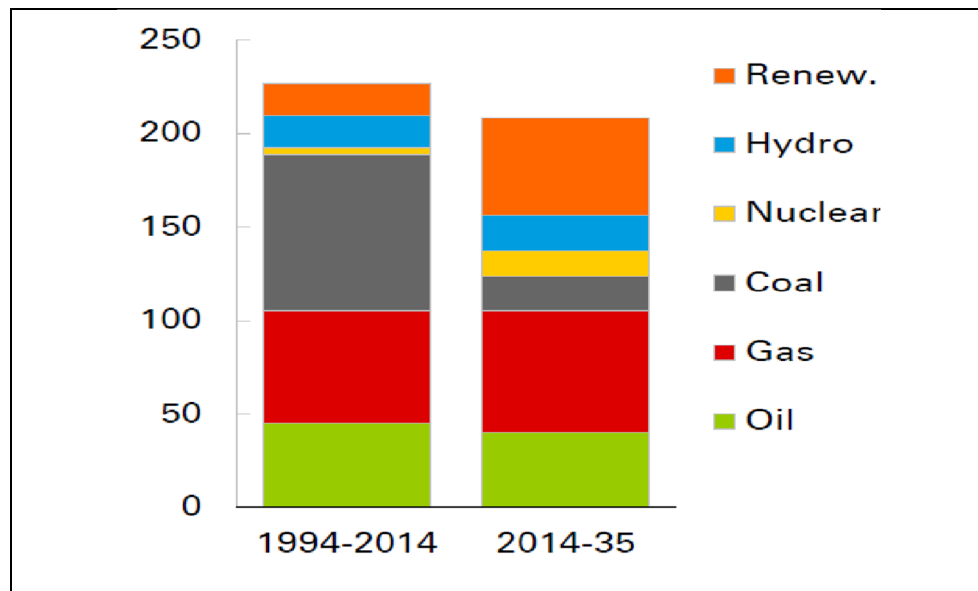


Figure 0.1 Growth in annual fuel demand

Non-renewable energy sources cause high environmental pollution by emitting greenhouse gases that have a negative impact on the environment. Renewable energies, which are alternative solutions, are therefore paths towards which we must embark. These sources offer great security of supply to consumers while respecting the environment (J. Chen & Song, 2016). Another advantage of using of renewable energies is the switch from the centralized model to the decentralized model as presented in Figure 0.2 (Farrell, 2011). The centralized model has always been based on fossil fuels (coal, oil and gas) or nuclear.

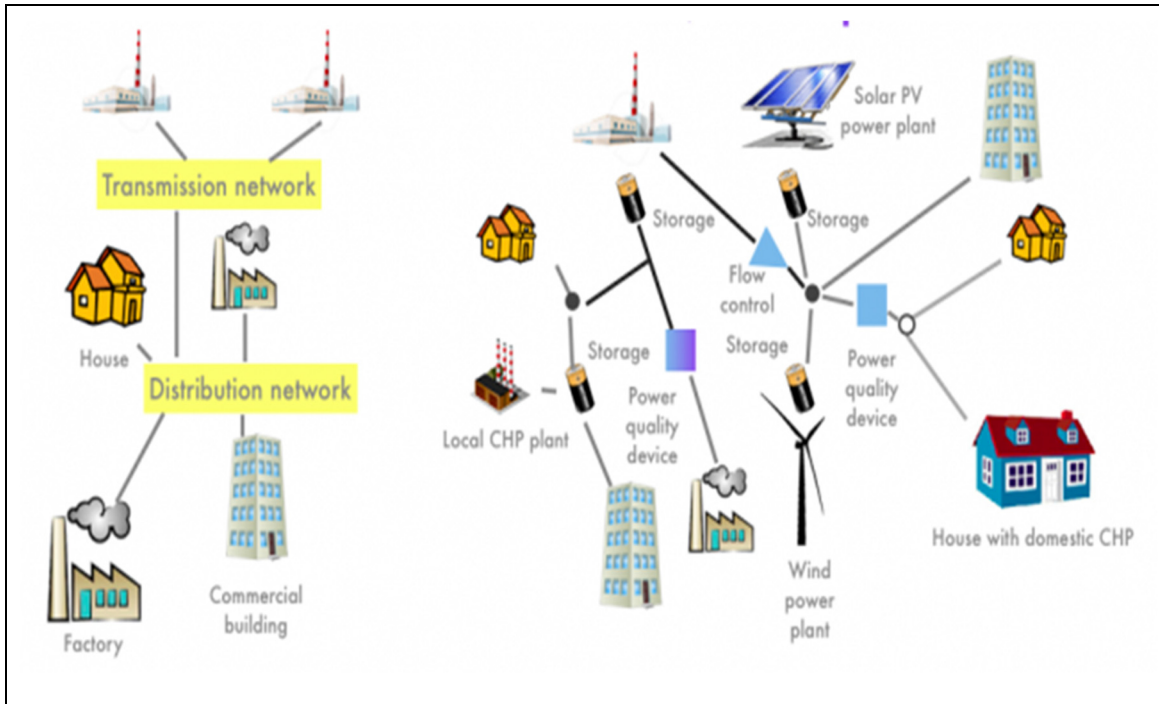


Figure 0.2 Centralized V. Decentralized electricity system

This explains the growing and exponential use of wind and photovoltaic energy in recent years as shown in Figure 0.3 (BP, 2015).

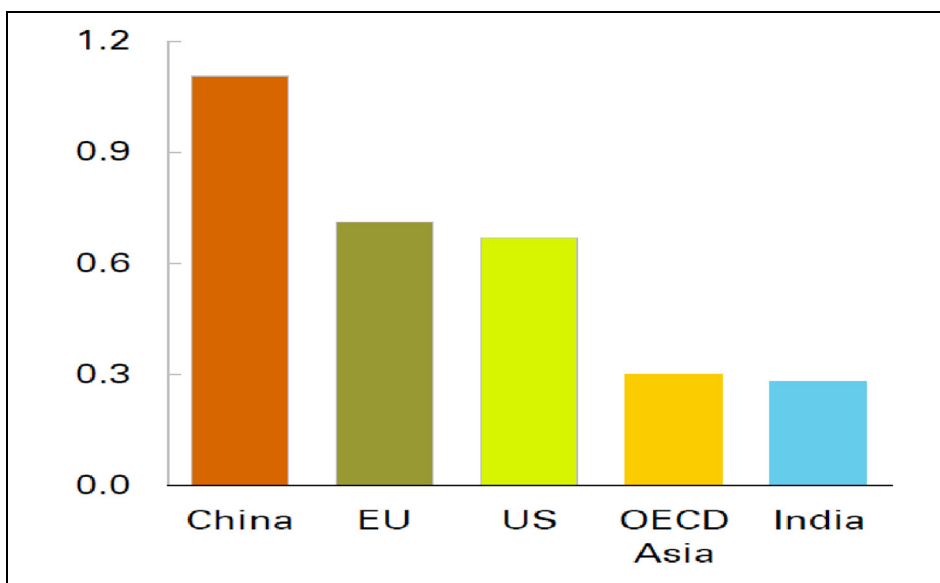


Figure 0.3 The growth of renewable energy 2013-2035

Power converters can find very wide and important applications in modern electrical systems as a result of the development of power semiconductors and power electronics technologies.

Converters interfacing with renewable energy sources have received considerable attention in latest years due to their increasing interest on the environmental issues and electricity demand. The aim of these systems is to supply energy (solar and wind) to the grids through a filter (Komurcugil, Ozdemir, Sefa, Altin, & Kukrer, 2016c).

However, the increased penetration of the distributed power generation systems DGs can pose problems with reverse power flow, voltage fluctuations and other issues for distribution networks (Y. Han, Shen, Zhao, & Guerrero, 2016). In order to solve this issue and overcome these challenges, a microgrid was proposed several years ago (Y. Han et al., 2016).

These DGs units are connected to the AC bus via an LCL filter to reduce switching harmonics. The microgrid stability is greatly sensitive to the power variations from renewable energy sources or loads sides. In order to dampen the LCL filter resonance, a robust control algorithm is provided to solve the resonance and stability problem of parallel converters equipped with an LCL filter which forms an AC microgrid.

A new droop control based on stabilizer for robust power sharing which is integrated in the conventional droop control has been proposed to improve the power sharing between the distributed generators in MG.

Therefore, the main contribution of this thesis is to apply controls to one or several DGs forming a microgrid with several parallel converters interface with renewable energy sources to dampen the resonance of the LCL filter, and to guarantee the stability. In addition, a compensator that allows regulating the voltage and frequency of the microgrid has been proposed.

Research Issue

The main problem of this research work is to apply robust controls to a microgrid which has n units (DG) connected in parallel on an AC bus each unit is composed of a renewable energy source with its interface converter which is fitted by an LCL filter as to provide the high quality sinusoidal current (IEEE519 standard). The microgrid is connected to the main grid or is operated in the islanded mode. However, the interaction between the LCL filters and the power converters generates instabilities on the AC bus. This issue is largely responsible for the instability of the system and the degradation of the electrical energy quality, which demands a compensation system to ensure the stability of the AC microgrid. This latter keeps the microgrid voltage and frequency constant. The application of stabilizer which is equipped by compensators allows to produce better quality of energy and to stabilize the AC microgrid while an excellent electrical energy transfer is ensured. A complex control strategy must be designed to keep the AC bus voltage and frequency constant where the dynamic performance remains acceptable in autonomous operation mode and in grid-connected mode under normal and faulty conditions. The control application involves these complete systems modeling as well as the appropriate regulators design to handle the microgrid critical problems and the high energy transfer quality.

Objectives of This Thesis

As the integration of renewable energy sources has been grown, the new challenges have been emerged for the electrical grid. In order to increase the integration ratio of the renewable energies and improve the quality of electrical energy, the microgrid is an appropriate alternative for the current electrical grid. Distributed generators (DGs) interfacing with voltage source inverters (VSIs) establishes a microgrid system. The VSIs which are operating in parallel are responsible for the frequency and voltage controls where the system stability is influenced by the generated power and the connected loads.

The main objective of this research work is to develop a control technique which solves the robustness and stability problems of a single-stage voltage source inverter. Another objective is to provide solutions for improving the microgrid performance including one or more distributed generation units (DGs) with voltage and a fixed frequency to ensure optimal power sharing among the inverters. To do this, the improved controls which have the stabilization techniques are developed. The goal is to enhance the electrical power quality, minimize the resonance impact, maintain an optimal power sharing and insure the system stability.

The overall objective which was already mentioned will be achieved by studying an AC microgrid. The AC microgrid system is established based on converters which are connected in parallel and accordingly their effects in terms of power sharing and stability need to be studied.

The purposes of the research can be summarized as follows:

1. Minimizing the impact of LCL filter resonance problems by a local control using robust control algorithms;
2. The solution for the certain problems of the distributed generators interfaced by a voltage source inverter to improve stability, robustness and performances;
3. Improvement and development of DG and MG controllers;
4. Improving the transient performance and stability of conventional droop control;
5. Experimental implementation of a DG and MG using dsPACE and OPAL-RT control card.

Methodology

This research work was carried out in three stages: theoretical model realization, simulation validation and experimental implementation.

As the first step, a literature review has been done for better understanding of latest development of the microgrid systems as to choose an appropriate interface converters topology in terms of performance and the adopted control methodologies. This part also helps to choose the right type of control technique as well as damping algorithm which would be suitable for solving the resonances problems of the LCL filter. The existing models and controllers of the distributed generations have been simulated in Matlab/Simulink SimPowerSystems to deeply analyze the advantages and drawbacks of those reported techniques.

Accordingly, the theoretical model of the existing and the proposed DGs which is fitted with the local stabilizer solution has been comprehensively performed. The proposed systems have been simulated in Matlab/Simulink SPS with the proposed controls scheme to verify the theoretical analyses as to attenuate disturbances because of LCL filter resonances and to prove the excellent dynamic performance in grid-connected and autonomous modes of operations. Many tests have been carried out which have been examined first by simulation to avoid any failure in hardware implementation. Moreover, the controllers have been practically implemented using dSPACE ds 1103 and tested under different operational conditions including the load changes, parameters variations, and AC or DC voltage variations.

Finally, the entire AC microgrid system based on the distributed generators which are connected in parallel and equipped by LCL filters with the stabilizing solutions has been simulated in Matlab/Simulink/SimPowerSystems environment. The robustness of the proposed compensator has been evaluated by simulation using two single-stage three-phase converters which are parallel connected and are switched by six PWM signals.

The proposed system has been also implemented in real time in the laboratory using a hardware-in-the-loop (HIL) of the OPAL-RT technologies using dSPACE control platform.

Originalities of the Proposed Works

The main contributions of this thesis are as follows:

The proposed stabilizer control has the advantage of controlling microgrid voltage and frequency, where it is in charge of ensuring microgrid stability, the power sharing, and reliability. This work will concentrate on the study, modeling, simulation and experimental validation of AC microgrid systems in islanded mode. The distributed generators are also connected to the linear and non-linear loads through the AC bus. Therefore, the contribution of this thesis can be listed as below:

1. Robust Control

A robust control strategy based on LQR controller with the integration of active damping in the control of the single-stage single phase PUC5 inverter which is equipped by the LCL output filter and connected to the grid has been proposed. The proposed control method is designed using the d-q reference frame. The proposed local control provides better control on the uncertainties and the resonance of the LCL filter. It also obtains the suitable monitoring reference of the current and voltage, a low Total Harmonic Distortion (THD), robustness under system disturbances and a rapid response to the current reference variations. The objective is to ensure the connectivity and efficiency of the grid-connected single-phase PUC5-LCL inverter in terms of the energy transfer, adaptability, and power quality. The optimal control which is designed by the active damping integration exhibits better dynamic performance with fast-tracking feature in comparison to a PI controller.

A robust control scheme based on LQRI control of a single-stage multifunctional SPV-APF-LCL is designed to achieve optimal multifunctional operation for a residential power supply.

Additional functions such as an active power regulator and voltage stabilizer have been incorporated into the control. In addition, the method of the maximum power tracking (P&O) was used to generate the reference of the DC voltage. The multifunctional grid-connected SPV system operates as an APF when the insolation is unavailable. The proposed control scheme makes it possible to obtain an excellent dynamic performance, low grid current THD, and small settling time and overshoot. As part of the Smart Grid initiative, it is shown that effective management of the active power on the solar panels, the single-stage configuration can compensate the harmonic current generated by distorted supply voltage or by nonlinear loads.

2. Power Sharing Control

The stabilization signals are added to the classical droop control for robust power sharing in AC microgrid system. The microgrid contains several parallel connected inverters with LCL filters where they are controlled by the proposed droop control to guarantee an overall stability of MG. The stabilizer will continue the operation even during transients.

Connecting converters in parallel requires a precise power sharing mechanism to ensure proper operation. To this end, a droop controller based on the stabilizer is proposed in this work. The performed analysis illustrates that the proposed method obtains a better power sharing in the presence of balanced and unbalanced loads.

Organization of the Thesis

This thesis includes five chapters starting with a general introduction and a literature review about distributed generators control and microgrid. Chapters 2, 3 and 4 will present the work results in form of articles; either published (chapters 2 and 3) or submitted for publication (chapter 4).

CHAPTER 1 presents a complete literature review on the distributed generators controls as well as microgrid control techniques which are previously reported.

CHAPTER 2 discusses the detailed modeling in d-q reference frame and the optimal control design of the grid-connected single-phase PUC5 inverter which is equipped by the LCL filter. In this chapter, the PUC5 inverter topology with sensorless voltage control is introduced. The experimental results are presented to confirm the excellent dynamic performance of the proposed controller. A comparison analysis with the classical controller is also presented.

CHAPTER 3 introduces a multifunctional single-stage residential photovoltaic power supply based on Linear Quadratic Regulator (LQR). The system uses a single-phase power converter, linear and non-linear loads and it is connected to the grid via LCL filter. The proposed controller insures the robustness and stability of the system with a desired reference tracking.

CHAPTER 4 Describes some droop control techniques which are used for controlling of the parallel connected distributed generators of a microgrid system. This chapter also offers a new method of the droop control to address the weaknesses of conventional one. The new controller based on compensators was designed and it is evaluated by simulation and experimentation under various operational conditions to improve the power sharing performance among the parallel DGs.

CHAPTER 5 Discusses the conclusions and prospects of this thesis.

CHAPTER 1

LITERATURE REVIEW AND STATE OF THE ART ON THE DISTRIBUTED ELECTRICITY GENERATION SYSTEMS

1.1 Introduction

Distributed generation plays a vital role in modern electricity systems. The microgrid is an innovative technique that includes a series of distributed generators, energy storage systems, loads and power electronics interfaces. Most DGs do not produce a constant power; therefore, it is necessary to use an appropriate control techniques to maintain the stability and reliability of microgrid system (Z. Yang & Ho, 2016).

This chapter presents the literature review on the microgrids based on the distributed generators (DGs) with LCL filters which are operating in grid-connected mode or in islanded mode. Besides the definitions and development of MG has been also examined considering the distributed generators controls, power management and droop control in microgrids, and hierarchical control of MG.

1.2 Control Strategies of Power Converter for Distributed Generation

Power converters interfacing with renewable energy sources are fitted with an LCL filter to produce higher power quality and also suitable for reactive power compensation and harmonic elimination. The LCL filter is more attractive in many industrial applications because of their small size and low cost. However, LCL filter also leads to the resonance problem where many methods including the active and passive damping have been proposed to overcome this imposing challenge (Chi, Dragicevic, Vasquez, & Guerrero, 2014a).

1.2.1 Passive and Active Damping

Several solutions for attenuating the LCL filter resonances are proposed in the literatures which are mainly based on two methods, passive damping and active damping.

1.2.1.1 Passive Damping

Passive damping consists of adding a resistance in series (R. N. Beres, Wang, Blaabjerg, Liserre, & Bak, 2016; R. N. Beres, Wang, Liserre, Blaabjerg, & Bak, 2016; Peña-Alzola et al., 2013; Zhao & Chen, 2009) or in parallel with the inductance or filter capacitance. These methods are simple and reliable, but the increased resistance increases the dissipated losses by the Joule effect (Houari et al., 2015). The damping purpose is to insert an impedance at the resonant frequency so as to avoid oscillations by means of the switching (R. Beres, Wang, Blaabjerg, Bak, & Liserre, 2014).

1.2.1.2 Active Damping

The active damping technique is integrated into the control scheme to stabilize the system without additional losses. Their principle is based on the injection of the compensation signals into the internal control loop (Houari et al., 2015). Various researches on the active damping methods have been done which could be considered as an alternative to dampen the resonance problems of the LCL filter. Many active damping methods have been also proposed to remedy this problem (Juntunen et al., 2015; Lazzarin, Bauer, & Barbi, 2013; Lu, Wang, Loh, & Blaabjerg, 2015; X. Wang et al., 2014). Some active damping methods can be mentioned as below:

Virtual Resistance Method

Virtual resistance is proposed as an active damping solution to damp the resonance at the resonant frequency (J. He & Li, 2012). This latter can be damped without losses in system efficiency using control loops, instead of the real resistance which greatly reduces system

efficiency due to the losses. A robust strategy for regulating the current injected into the network has been proposed by (Twining & Holmes, 2002). An active damping method based on the virtual resistance is designed by (Jinwei, Yun Wei, Bosnjak, & Harris, 2013) to be used for a parallel inverter in a microgrid. The strategy includes two regulation loops; an external regulation loop to regulate the grid current using a PI regulator, and an internal loop regulation to regulate the capacitor current for stabilizing the system. The virtual resistance is realized by controlling the capacitor current, which is added to the converter control loop. Therefore, the resonance peaks and harmonics at the high frequency can be reduced without reducing the system efficiency. A block diagram of the virtual resistance is shown in Figure 1.1 (Chi, Dragicevic, Vasquez, & Guerrero, 2014b):

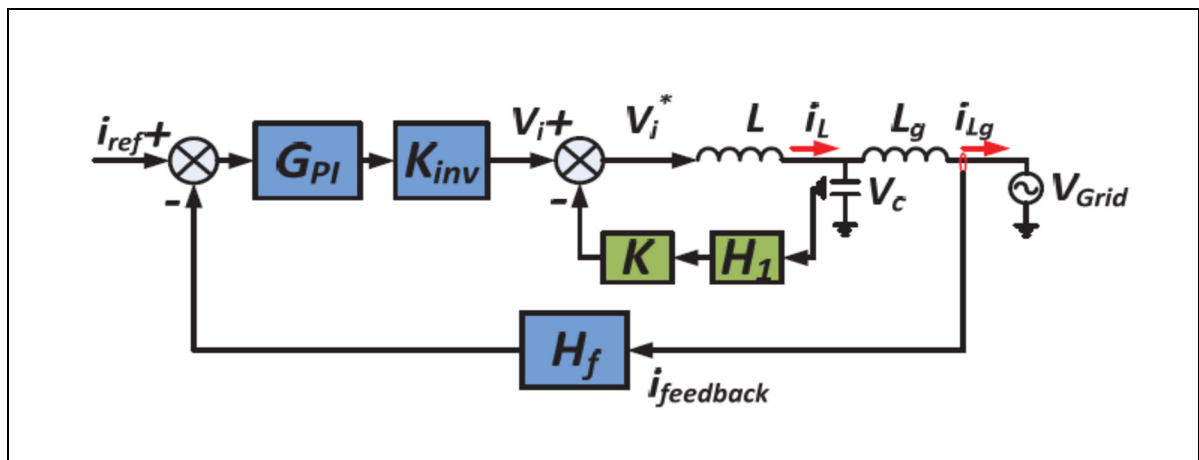


Figure 1.1 A block diagram of virtual resistance

Lead-Lag Compensator

The active damping method with lead-lag compensator was originally proposed in (Blasko & Kaura, 1997) to compensate the phase changes which are caused by the filter. An example of a lead-lag compensator control structure is shown in Figure 1.2 (Chi et al., 2014b):

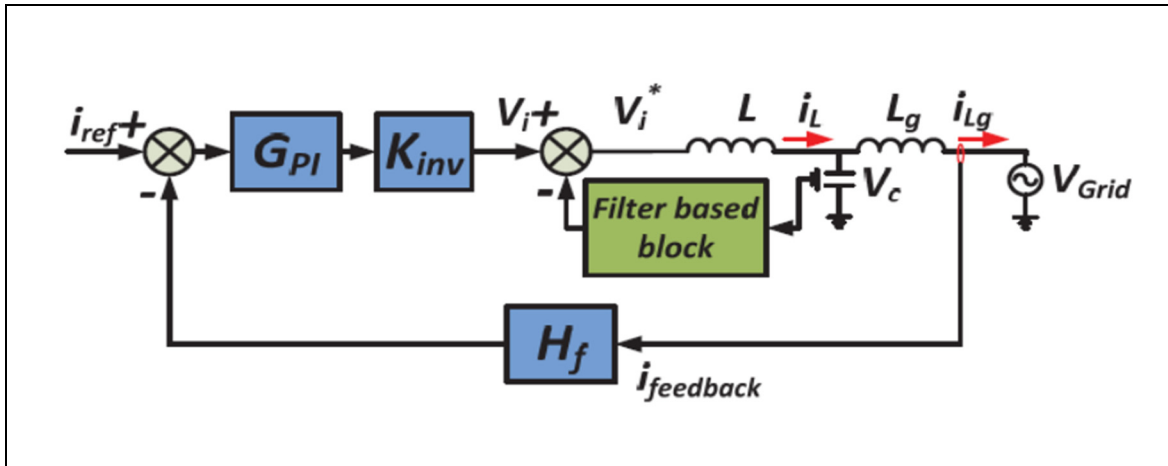


Figure 1.2 Lead-leg compensator control structure

In (Liserre, Dell'Aquila, & Blaabjerg, 2002) a guide for choosing the damping resistance value and the three parameters of the grid advance phase at resonant frequencies is proposed to achieve the active damping. However, the maximum advance phase selection does not take into account computer tools and the PWM delay. A lead-lag compensator is added into the current loop by (Ricchiuto, Liserre, Kerekes, Teodorescu, & Blaabjerg, 2011) to operate for a small interval around the resonant frequency, but no loop is considered for low frequency and switching frequency. In (S. Y. Yang, Zhang, Zhang, & Xie, 2009) the lead-lag active damping method is improved through the inclusion of a capacitor voltage observer. A procedure for adjusting network phase lead-lag is also developed using a software tools which is presented in (Peña-Alzola, Liserre, Blaabjerg, Ordonez, & Yang, 2014b).

Notch Filter

Another type of active damping method is the notch filter (Liserre, Dell'Aquila, & Blaabjerg, 2003b; Peña-Alzola, Liserre, Blaabjerg, Sebastián, et al., 2014; Yao, Yang, Zhang, & Blaabjerg, 2015) which is inserted into the control path to allow the resonance peak cancellation. The idea is to compensate the resonance peak by an anti-peak of the notch filter (Dannehl, Liserre, & Fuchs, 2011a).

An example of a notch filter control structure is presented in Figure 1.3 (Stewart G. Parker, July 2014).

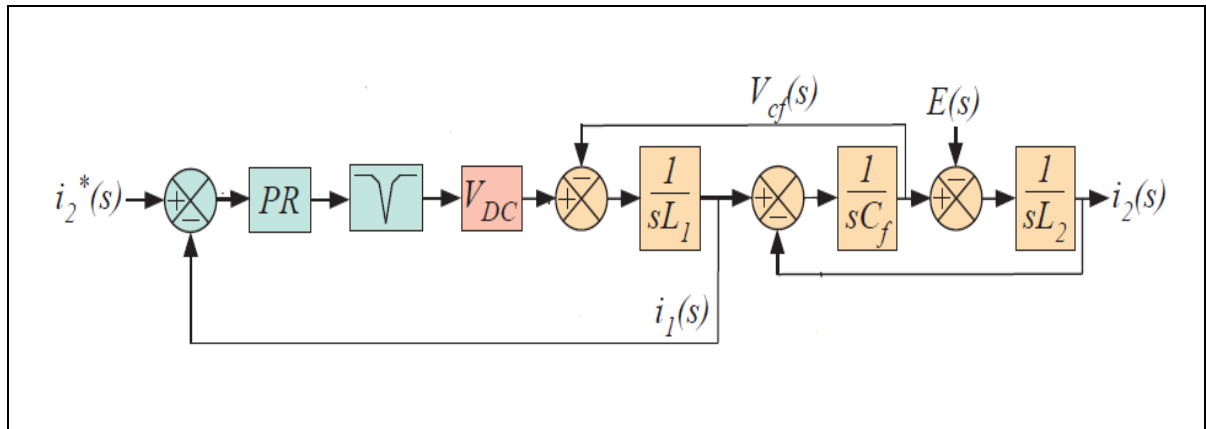


Figure 1.3 Notch filter control structure

An active damping is introduced in (Liserre, Dell'Aquila, & Blaabjerg, 2003a) where a notch filter is considered into the modulator reference voltage to produce an optimum voltage reference for the converter. The filter and the control parameters are optimized using genetic algorithms (GA). A simple, straightforward tuning procedure for a self-commissioning notch filter has been proposed by (Pen et al., 2014). In order to take into consideration the grid inductance changes, the resonant frequency is estimated using the Goertzel algorithm to adjust the notch filter. The proportional gain is estimated to dampen the resonance. In (Wenli, Yongheng, Xiaobin, & Blaabjerg, 2015) an active damping method based on a notch filter and no need of additional sensors is proposed where the inverter output current is used as a feedback variable. Therefore, the notch filter frequency is designed smaller than the resonant frequency to make the controller robust under impedance changes.

Capacitor Current and Converter Current Feedback

Another damping solution for the LCL filter resonance is to add an additional current loop or capacitor current or voltage feedback (Dannehl, Fuchs, Hansen, & Thogersen, 2010; Pan, Ruan, Bao, Li, & Wang, 2014; S. G. Parker, McGrath, & Holmes, 2014b; J. Wang, Yan, &

Jiang, 2016; X. Wang, Ruan, Liu, & Tse, 2010) as shown in Figure 1.4 (Stewart G. Parker, July 2014).

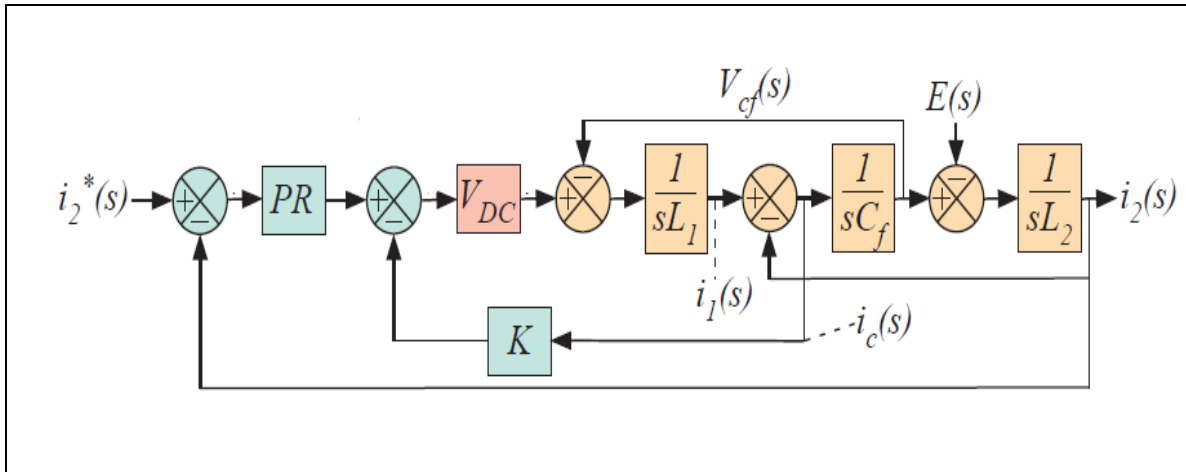


Figure 1.4 Capacitor current feedback control structure

A robust tool to compensate instability problems in a grid-connected converter via an LCL filter has been developed by (Houari et al., 2015). A large signal stabilizer based on Lyapunov's direct theorem has been proposed to eliminate uncertainties because of the LCL filter resonance. Lyapunov's theory allows the construction of stabilizing feedback signals that maintain both active damping performance and robustness against the parameter uncertainty or load variation. Full feedback of capacitor current and the injected current to the grid has been proposed by (Xuehua, Xinbo, Shangwei, & Tse, 2010), this proposed control strategy can effectively remove the current distortion caused by voltage harmonics of the network, and the static error at steady state of the injected current is ensured by a PI regulator. (Dannehl, Fuchs, Hansen, Th, et al., 2010), studied different feedback loops to evaluate their performance. The current of the C capacitor analysis and comparison, as well as voltage feedback was done to damp the resonance. The active damping method with additional feedback provides high resonance rejection. However, the overall cost of the system will increase and the system implementation will be further complex. On the other hand (S. G. Parker, McGrath, & Holmes, 2014a) discusses the theoretical identification of three distinct regions for the LCL filter when the grid current is the feedback variable. It shows that active damping is important for the

control stability in the region of the low frequency. The grid current feedback is the only condition which needs to be satisfied so as to design a stable system. The critical resonant frequency where the system is unstable will be independent of the used controller. The design of the maximum gains for each controller that matches the identified regions is then presented. (Donghua, Xinbo, Chenlei, Weiwei, & Xuehua, 2014), proposes an active damping model based on the capacitor current feedback. This latter is like a virtual impedance parallel to the C capacitor as a result of the computation and the PWM delay. The reduction in the calculation time is obtained by shifting the single time of the capacitor current to the sampling time of the PWM reference. Thanks to this method, unstable poles are eliminated; thus, one obtains a great robustness to the variations of the network impedance. However, the system becomes unstable due to the resonant frequency shifting. In order to improve the capacitor current feedback of the grid-connected converter via the LCL filter, a stability analysis in the discrete domain was presented by (Xiaoqiang et al., 2015). The active damping zone is extended to $f_s/4$, which can encompass all possible resonant frequencies. An optimal damping is obtained at a resonance frequency equal to $(f_r + f_s/4)/2$. A pseudo-derivative feedback (PDF) method has been applied by (Jianguo, Jiu Dun, & Lin, 2016) as a control method, to control the current of the three-phase inverter which is connected to the grid via an LCL filter to improve the transient response. In addition, an active damping method which uses the inductance current feedback instead of the capacitor current feedback has been presented by (Lazzarin et al., 2013), whose control strategy is realized for the parallel operation of a single-phase inverter (VSI). The principle of this control strategy is to use the feedback of the inductance current of the output filter to change the input voltage of the same filter. This control method has been validated by the experimental tests of the three single-phase inverters which are connected in parallel and supply a 10 kVA output load. The authors analyze the modeling and control of the parallel inverters which are connected to the grid through the LCL filters in photovoltaic system. Another active damping method which has been applied to the several parallel converters is carried out by (Agorreta et al., 2011). The performed analyses could obtain an inverter equivalent to N inverters of a photovoltaic installation. The capacitor current feedback is used as an active damping. However, internal information on the stability poles is lost which is requiring the use of stability criteria to ensure overall system stability.

Other Controls and Methods of Active Damping

Control with Sliding Mode

The sliding mode control (Komurcugil, Ozdemir, et al., 2016c; Vieira, Stefanello, Tambara, & Gründling, 2014) consists of a moving trajectory of the system state to a predetermined surface which is called the sliding surface where it is controlled to maintained around the latter with an appropriate logic (Boulâam & Boukhelifa, 2014). In (Komurcugil, Ozdemir, Sefa, Altin, & Kukrer, 2016b), sliding mode control with double-band hysteresis is proposed. The function of the sliding surface is formed using the grid current error, and the capacitor voltage error, and its derivative, which requires only three sensors. A dual band hysteresis system has been used to attenuate the switching frequency; so, the VSI semiconductors switches will be modulated only for one half cycle while it stays ON or OFF the other half cycle of the fundamental period. A multi-loop controller with sliding mode has been proposed by (Padilha Vieira, Stefanello, Varella Tambara, & Grundling, 2014) to control the inverter current which is connected to the grid with an LCL filter. The inner loop uses the converter current error as the sliding surface. The model allows the application of an external reference model with adaptive control (MRAC) for monitoring grid voltage in a robust way with disturbance rejection.

Control with H^∞ Method

H^∞ is an optimization method that is used to design optimal controls. (Cobreces, Bueno, Rodriguez, Pizarro, & Huerta, 2010), propose a control procedure with H^∞ method to control the current loop of power converter (VSC) which is connected to the grid through LCL filter. In addition, (S. Yang, Lei, Peng, & Qian, 2011) proposes a H^∞ controller with low steady state error to guarantee the system stability even with variations in grid impedance, and also to ensures low THD of mains current.

Model GCC (Generalized Closed-Loop Control)

The GCC model is introduced based on two virtual impedances loops in the control technique. The virtual impedances are divided as the internal and external loops where an internal virtual impedance is to dampen the LCL filter resonance and an external virtual impedance is to control the instability due to grid impedance variations. This process is considered for the microgrid applications (Chi et al., 2014a; J. He & Li, 2012). An example of the GCC damping control is presented in Figure 1.5 (Chi et al., 2014b).

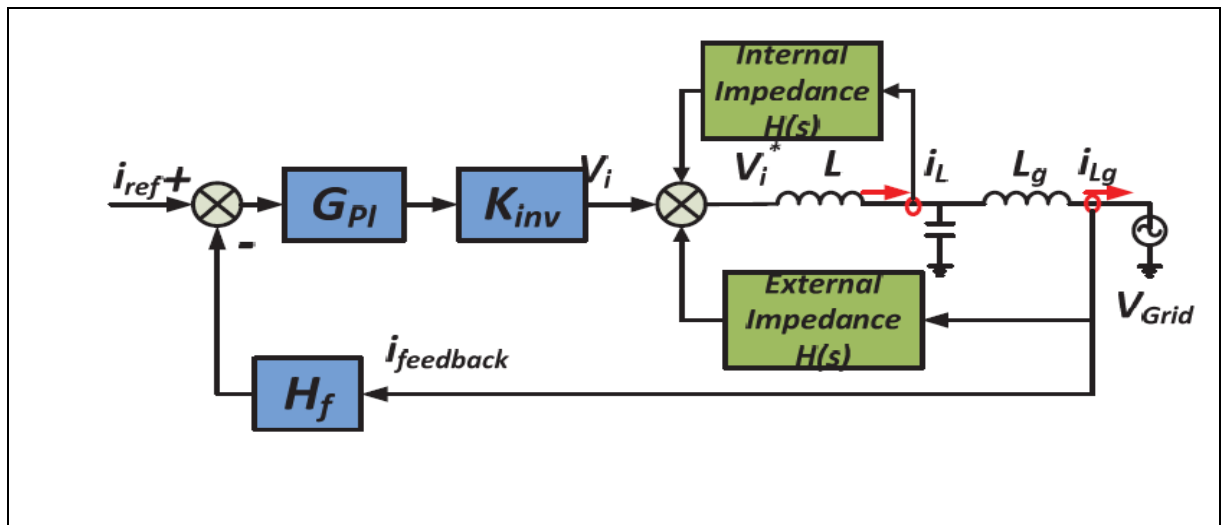


Figure 1.5 Block diagram of the GCC damping method

Predictive Control and Deadbeat

The deadbeat control principle is to force the inverter output current to reach the reference current at the end of each switching period (Y. Han et al., 2011; J. He, Li, Bosnjak, & Harris, 2013; Y. He, Chung, Ho, & Wu, 2016; Nishida, Ahmed, & Nakaoka, 2014). Predictive controllers use an internal system model to determine voltage output. Active damping is generally used to treat LCL filter resonance (Y. Han et al., 2011; J. He et al., 2013; Y. He et al., 2016; Nishida et al., 2014).

Optimal Control (LQR)

Various researches have been done on the optimal control of different types of converters (shunt active filter, the vienna rectifier, etc.) and electrical machines (Kedjar & Al-Haddad, 2009a; Kedjar, Kanaan, & Al-Haddad, 2014a). The performed review focus on the applications of this robust control for the parallel converters interfacing with renewable energy sources in stand-alone mode or grid-connected through an LCL filter (Dirscherl, Fessler, Hackl, & Ipach, 2015; Huerta, Bueno, Cobreces, Rodriguez, & Giron, 2008; Huerta, Pizarro, Cobreces, Rodriguez, Giron, et al., 2012; Kaszewski, Grzesiak, & Ufnalski, 2012; Maccari, Santini, Oliveira, & Montagner, 2013; Maccari, Santini, Oliveira, & Montagner, 2014; Maccari, Santini, Pinheiro, Oliveira, & Montagner, 2015; Santini, Maccari, & Montagner, 2014; Ufnalski, Kaszewski, & Grzesiak, 2015). In (Dirscherl et al., 2015), an observer and a control by LQR states feedback is proposed to control a converter which is connected to the grid through the LCL filter. (Kaszewski et al., 2012) presents the synthesis of control system with the LQR for the three-phase three-levels inverter with an output LC filter to ensure a high quality voltage waveform for the unbalanced and non-linear loads. An optimization of the cost function weighting factors in the LQR control technique is presented by (Ruiz, Muñoz, & Cano, 2015). The proposed optimization approach is based on the particle swarm method. On the other hand, the LQR control has been used in discrete domain (DLQR) in (Maccari, Santini, et al., 2013; Maccari et al., 2014; Maccari et al., 2015; Santini et al., 2014) in order to control the three-phase grid-connected inverter with variable inductance. (Maccari, Santini, et al., 2013; Maccari et al., 2014; Maccari et al., 2015; Santini et al., 2014), shows its applicability also for the time varying situation. In (Huerta et al., 2008), a multi-variable LQ servo controller as the current regulator of the inverter which is connected to the grid via LCL filter has been proposed; however, this method presents an error at steady state due to the absence of integral action. Another method has been proposed in (Huerta, Pizarro, Cobreces, Rodriguez, Giron, et al., 2012) based on linear quadratic (LQ) and Gaussian (LQG) technique which associates the LQ regulator and the Kalman filter (KF). LQG servo controller cooperates with THD=4.4%, while LQ servo controller and Luenberger estimator works with THD=4.7%. (Brabandere et

al., 2007) present a Gaussian Linear Quadratic (LQG) decentralized control method for inverters in parallel operation in a stand-alone or connected to an infinite bus.

1.3 Control Methods of Primary Loop

Much work has been done to study the stability, reliability, and protection issues of microgrids. The development of the applied control strategies has received great interest in recent years. The main objective is to control the power converters switching, the voltage and frequency-level control, the power control, and the power sharing at the point of interconnection to guarantee a correct and continuous supply of the load. These strategies use a mathematical approach and each of these strategies is based on one or more combinations of: active power (P)/reactive power (Q), voltage (V), frequency (f), phase angle (δ), and state of charge. Hence, the use of droop control to ensure a good power sharing between several DGs connected in parallel in a MG. However, the conventional droop control presents some weaknesses like poor power sharing accuracy, slow dynamic performance, and voltage and frequency deviations (Abdikarimuly, Familant, Ruderman, & Reznikov, 2016a). Figure 1.6 illustrates the conventional droop technique P - F / Q - E curves.

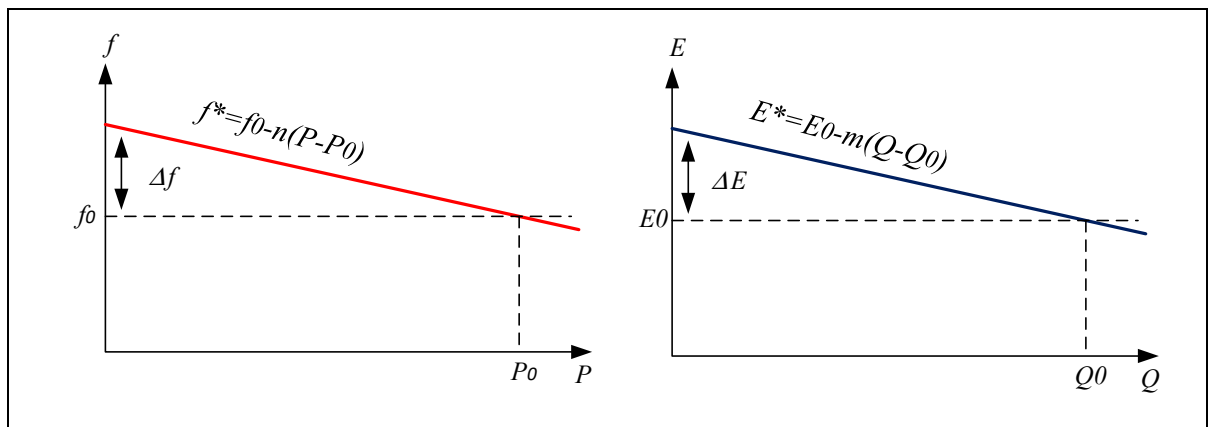


Figure 1.6 Conventional droop control curves

1.3.1 Conventional Droop Controller

This technique is the most used for local power sharing. It is capable of power sharing without communication links among different control points. Accordingly, several researches were performed on power sharing to ensure optimal MG conditions.

In (Borup, Blaabjerg, & Enjeti, 2001) present a power-sharing method that is equipped by an active compensation. However, the dynamic performance are not improved. A control structure for the microgrid converters has been presented by (Mohamed, Zeineldin, Salama, & Seethapathy, 2012) to have seamless transition and to improve the dynamic stability of the MG in grid-connected and islanded modes of operations. Furthermore, in (Vandoorn, Kooning, Meersman, Guerrero, & Vandeveld, 2012) the P/V and P/f droop control strategies are compared with the consideration of the power sharing modification and the line losses.

1.3.2 Droop Controller with Virtual Impedance and other Variants

When the concept of virtual inductance is used, the DG output impedance becomes more inductive while it improves the system stability and reduces the power oscillations and circulating currents (Y. Han, Shen, Zhao, & Guerrero, 2017). In (Y. Han, Shen, et al., 2017), a virtual impedance loop is proposed that contains a positive and negative virtual impedance sequence. In (Yao, Chen, Matas, Guerrero, & Qian, 2011), a complex virtual impedance loop to minimize the fundamental and harmonic current is also presented. Another adaptive virtual impedance concept is proposed by (Mahmood, Michaelson, & Jiang, 2015a) to improve the power sharing precision in an isolated microgrid and to compensate the voltage and frequency offset. On the other hand, a P/V droop control method has been proposed in (J. Chen et al., 2020) to decouple the powers and improve the precision of power sharing among DGs where a positive and negative virtual impedance strategy has been adopted for this purpose. In (Zhu et al., 2016) a wireless control strategy is presented where an optimized virtual impedance controller is used and a local load measurement for reactive power sharing is also realized. A Virtual Impedance Controller (VIC) is presented in (Hoang & Lee, 2020) to have precise power sharing and voltage harmonic compensation in island microgrids. An adaptive virtual impedance control method is proposed by (B. Liu et al., 2019) for power sharing in island

microgrids. This method is based on the injection of an extra small ac signal into the output voltage of each inverter. In (Y. Han, Shen, et al., 2017), a virtual impedance loop is proposed that contains a positive and negative virtual impedance sequence to ensure the system stability and to reduce power oscillations and circulating currents. (Sreekumar & Khadkikar, 2016) a control strategy for harmonic power sharing in an island microgrid is proposed where the virtual impedance is applied only at harmonic frequencies and it does not affect the power sharing. This strategy uses negative virtual harmonic impedance to compensate the line impedance effect. A complex virtual impedance loop to reduce the circulating current is presented in (Yao et al., 2011). (Zhang, Kim, Sun, & Zhou, 2017), introduces an adaptive virtual impedance control of MG's for precise reactive power sharing under the effects of the unsuitable line impedance. On the other hand, a virtual capacitor technique based on the conventional droop control is presented in (Yao et al., 2011) to reduce the steady state reactive power sharing error in multi-paralleled distributed generator.

1.3.3 Improved Droop Controller

A modified droop control has been developed in literature to enhance the power-sharing performance. In (Golsorkhi & Lu, 2015), a control strategy is proposed based on V-I characteristic which is introduced to exploit the flexibility and rapid dynamics of the converters which is interfacing the distributed energy sources. A piecewise linear droop characteristic is adopted to improve the power sharing accuracy under high load conditions when DERs are vulnerable to overload. As in (Joung, Kim, & Park, 2019), a modified decoupled voltage and frequency controller for DGs is presented to maintain the frequency and voltage amplitude of MG constant. According to the proposed technique, a frequency recovery loop is added to the classical droop control for efficient power sharing and the frequency response stabilization. (Imran, Wang, & Flaih, 2019) also proposes a modified d-q voltage droop control for power-sharing among DGs. A voltage-current (V-I) droop control has been proposed in (Y. Li & Fan, 2017) for an accurate power sharing among converters. In (Das, Chattopadhyay, & Palmal, 2017), a d-q voltage droop control for equal power sharing is presented where the performance does not depends of the line parameters nature. A washout filter based power sharing is added

in the classical droop control to restore the voltage and frequency without any communication links and without any additional control loops; but, the washout filter design is not presented (Y. Han, Li, Xu, Zhao, & Guerrero, 2018; Yazdani & Mehrizi-Sani, 2016). A control scheme based on V-I characteristics is presented to have fast dynamics and flexibility of the distributed generator (Golsorkhi & Lu, 2015). In (Mohamed & El-Saadany, 2008), an adaptive droop controller for converters connected in parallel is presented to ensure power sharing stability. (Savaghebi, Jalilian, Vasquez, & Guerrero, 2013), introduces a stationary-frame control method to compensate for the voltage unbalance in autonomous microgrid. In order to calculate the active and reactive powers of the positive sequence, the positive and negative sequence components of the voltage and current are applied. Furthermore, an adaptive voltage droop control is presented in (Mahmood, Michaelson, & Jiang, 2015b) to share an accurate reactive power. The effect of the supply impedances incompatible is compensated by the adaptive droop coefficients; but, only linear load results are shown. In (H. Han, Liu, Sun, Su, & Guerrero, 2015), a modified droop control method is proposed. The method essentially includes two parts; the first one shows the error reduction operation and the second one displays the voltage recovery operation.

1.3.4 Hierarchical Control Strategies

In order to solve the problems of unequal power sharing, an improved hierarchical control structure with several damping current loop schemes has been proposed by (Y. Han et al., 2016), to compensate harmonics and unbalanced voltage in a stand-alone AC microgrid. A hierarchical control with three levels of the control has been proposed in (Guerrero, Vasquez, Matas, Vicuna, & Castilla, 2011). Similarly, the concept of hierarchical control is also presented by (Savaghebi, Jalilian, Vasquez, & Guerrero, 2012) which includes primary and secondary control. The primary control consists of local distributed generators controls, which contain a current and voltage control loop as well as the virtual impedance loop. The secondary controller is designed to compensate the voltage imbalance at the point of common coupling (PCC) in autonomous MG. The compensation is performed by the control signals which are sent to the local control of the DGs. In (Mahmood et al., 2015a), a control strategy has been

proposed to improve power sharing in an isolated MG. Hierarchical control strategy has been introduced by (Z. Li, Zang, Zeng, Yu, & Li, 2018) for an autonomous AC microgrid where the frequency and voltage control is achieved through a cascade structure which includes a droop control loop, a virtual impedance control loop, a mixed H^2/H^∞ based on sliding mode control for voltage and current control loop.

1.4 Microgrid Power Quality

The proposed methods for improving the microgrid power quality can be generalized in three ways: energy storage, filtering, and appropriate control systems (such as PI, PR, and nonlinear). In (Balanuta, Vechiu, & Gurguiatu, 2012), a three-phase three-level NPC converter was used to improve the microgrid power quality . In (Rafiei, Moallem, Bakhshai, & Yazdani, 2014) a decentralized approach is proposed to improve the energy quality in smart microgrids. An adaptive digital notch filter is introduced to extract the harmonic content of the power system variables, such as current or voltage. In (Trivedi & Singh, 2017), a repetitive controller (RC) is proposed to mitigate the negative impact of the disturbances on the output voltage. Furthermore, a grid-connected multifunctional inverters (MFGTI) are presented in (Zeng, Zhao, & Yang, 2014) to be used as interface with renewable energy resources so as to improve the microgrid power quality. (Al-Saedi, Lachowicz, Habibi, & Bass, 2011) presents an optimal power control strategy for autonomous microgrid based on the real-time method (PSO) "Particle Swarm Optimization" with the aim of improving the power supply quality where the units (DGs) are connected to the network.

As a conclusion, although there is a large body of research, existing droop control methods do not generally guarantee the desired power sharing. Another important challenge which has not been fully investigated yet in the literature it is to deal with the MGs stability under non-linear loads, faults and switching from grid-connected mode to island mode.

1.5 State of the Art on Microgrids

1.5.1 Concept, Definition and Challenges of Microgrid

Modern electrical systems confront great challenges such as social demands, ensuring electrical reliability and maximizing environmental benefits. Figure 1.7 (Kim, Jeon et al. 2010) demonstrates a new type of power grid so-called as microgrid which has emerged as a promising alternative to address these challenges.

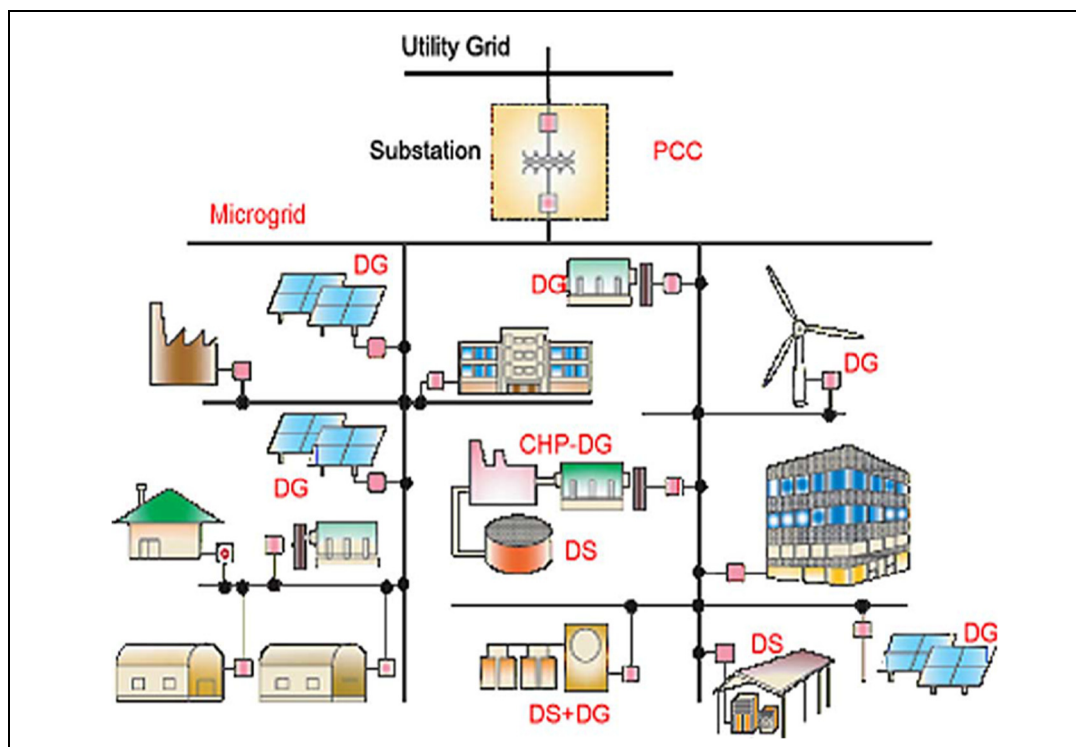


Figure 1.7 Microgrid architecture

The microgrid is usually established by various distributed generators (DGs), storage devices and loads, and can operate in grid-connected mode or in islanded mode (Dou, Li, Yue, & Liu, 2016; Marnay et al., 2015), where the MG can separate from the main network each time a disturbance of power quality occurs on the main grid (Banerji et al., 2013). It should be noticed that grid-connected operation is the normal operating mode of a MG without the current quality disturbance on the main connected network.

1.5.2 Control Structures

The microgrid control system role is to ensure equal and precise power sharing among the MG and to ensure voltage and frequency adjustment; two distinct approaches can be identified.

1.5.2.1 Centralized Control Structure

These structures require a central controller for all data and measurements to determine the control actions for all systems to keep the power sharing balancing among the distributed generators. However, this structure requires the presence of a wide bandwidth communication system for a rapid information sharing. This communication system has weaknesses when the microgrid is distributed in a long-distance zone as this system can fail the control guarantee, so the whole system may stop operation.

1.5.2.2 Decentralized Control Structure

This structure does not require the presence of a communication system. Indeed, each unit can be managed independently by a local controller which allows regulating the voltage and the frequency; so, each unit can share the requested power.

1.5.3 Classification of Microgrid

There are two main categories of MGs (AC and DC microgrid) depending on the nature of the output voltage that supplies the sensitive load, the two categories are illustrated in Figure 1.8 and Figure 1.9 (Z. Yang & Ho, 2016).

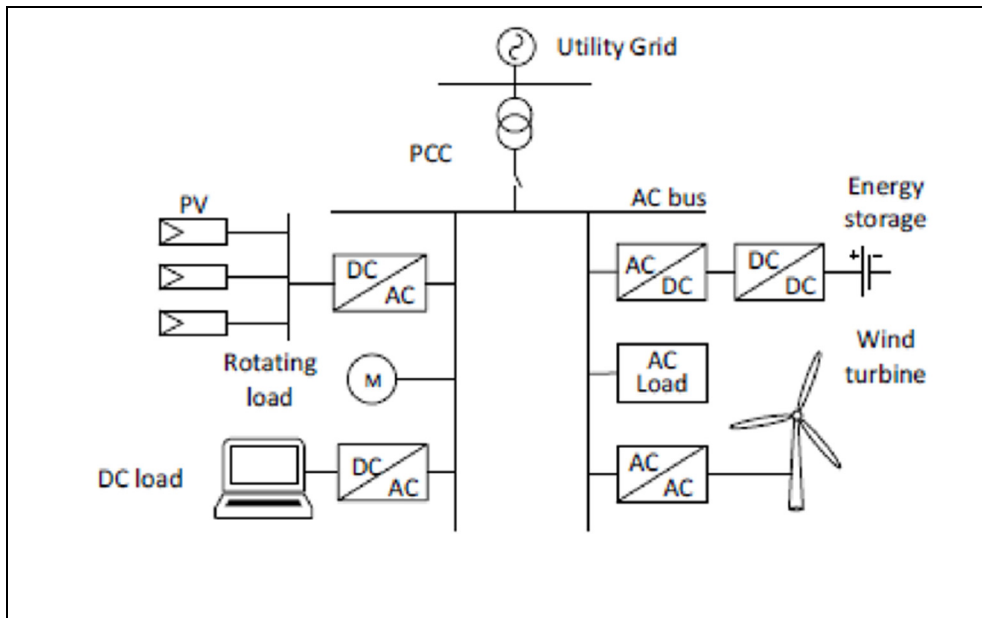


Figure 1.8 AC microgrid architecture

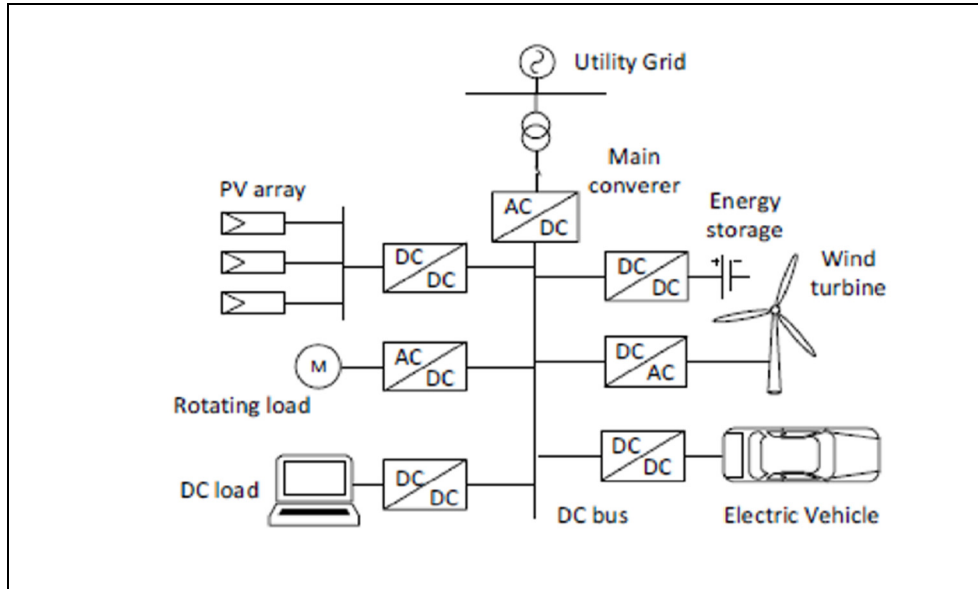


Figure 1.9 DC microgrid architecture

1.5.4 Microgrid Architecture

The microgrid structure contains numerous varieties of the distributed energy sources (DER), such as solar panels, wind turbines, micro turbine, etc. Each in the form of the distributed generator (DG), including energy storage systems (Dou et al., 2016). The electrical connection points of microgrid are connected to the PCC (common coupling point). The loads connected to the AC or DC bus are residential types, commercial buildings, campuses and industrial complexes (Hartono, Budiyanto et al. 2013, Z. Yang & Ho, 2016).

1.5.5 Microgrids Power Converters

Power converters play an important role in the microgrid system, as they are a gateway among energy resources and the transfer of the energy among different microgrid components. Table 1.1 summarizes the converters most used in microgrids (Z. Yang & Ho, 2016).

Table 1.1 Converters used in microgrids

Interface	Applications in microgrid
DC-DC	Energy storage systems (battery), DC loads (EV chargers), DC generators (PV), etc.
AC-DC	Main converter to DC microgrid, AC microgrid power supply for DC loads, DC motor control, PFC, active PFC.
DC-AC	Drive motor, uninterruptible power supplies, active power filter, PV panel interfaces.
AC-AC	Air conditioning compressor.
AC-DC-AC	Wind turbine, micro-turbine.

1.5.6 Methods of Controlling an AC Microgrids

1.5.6.1 Control Strategies in Grid-Connected Mode

Power converters are classified into three categories according to their operation in an AC microgrid which are grid-feeding, grid-supporting, and grid-forming power converter (Rocabert, Luna, Blaabjerg, & Rodríguez, 2012). The figure below shows the different types of power converter (Rocabert, Luna, Blaabjerg, & Rodríguez, 2012).

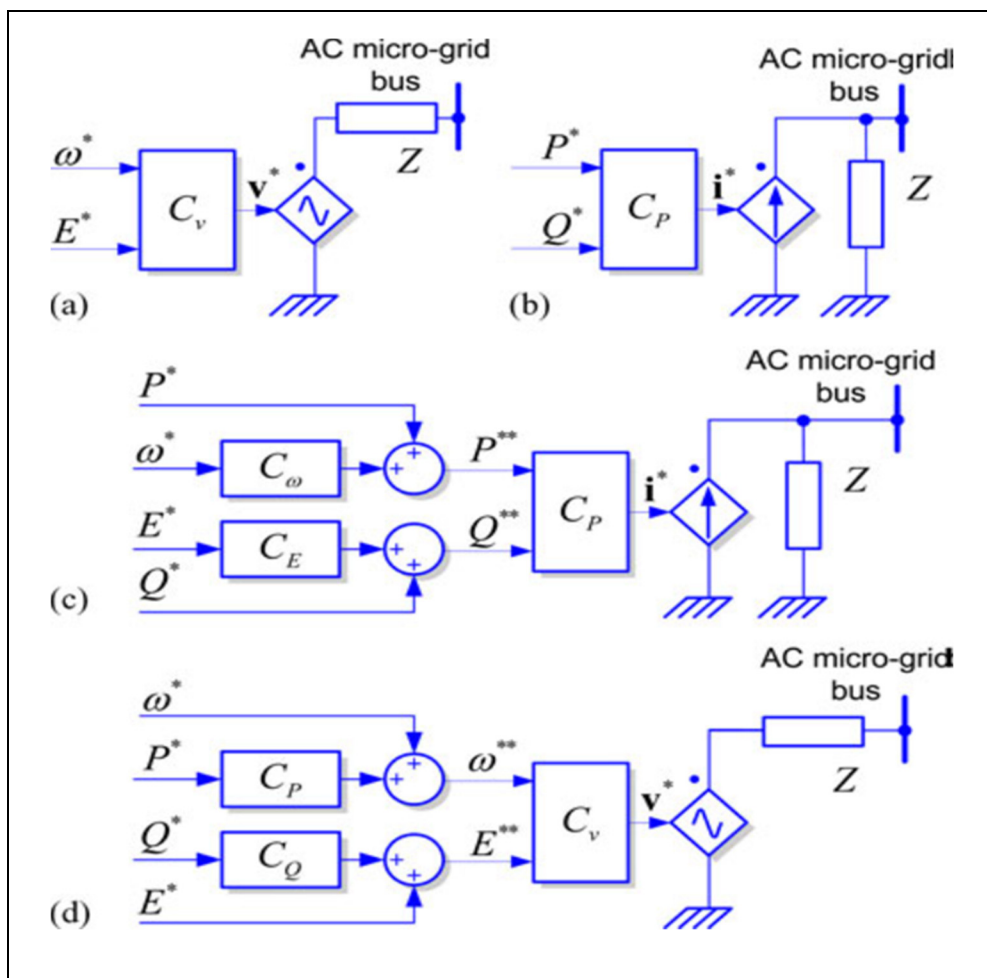


Figure 1.10 Basic representation of power converters connected to the grid
 (a) grid-forming, (b) grid-feeding, (c) current-source-based grid-supporting,
 (b) and (d) voltage-source-based grid-supporting

1.5.6.2 Control of Power Converters for Grid Forming

Grid-forming power converters are controlled to function as an ideal AC voltage source with an amplitude (E^*) and a frequency (ω^*). As voltage sources, they have small output impedance; so they require extreme precision of a synchronization system to work in parallel with other converters forming a network. The power sharing between converters forming a network connected in parallel is a function of the value of their output impedance (Rocabert et al., 2012). Figure 1.11 shows the block diagram of the grid forming power converter (Rocabert et al., 2012).

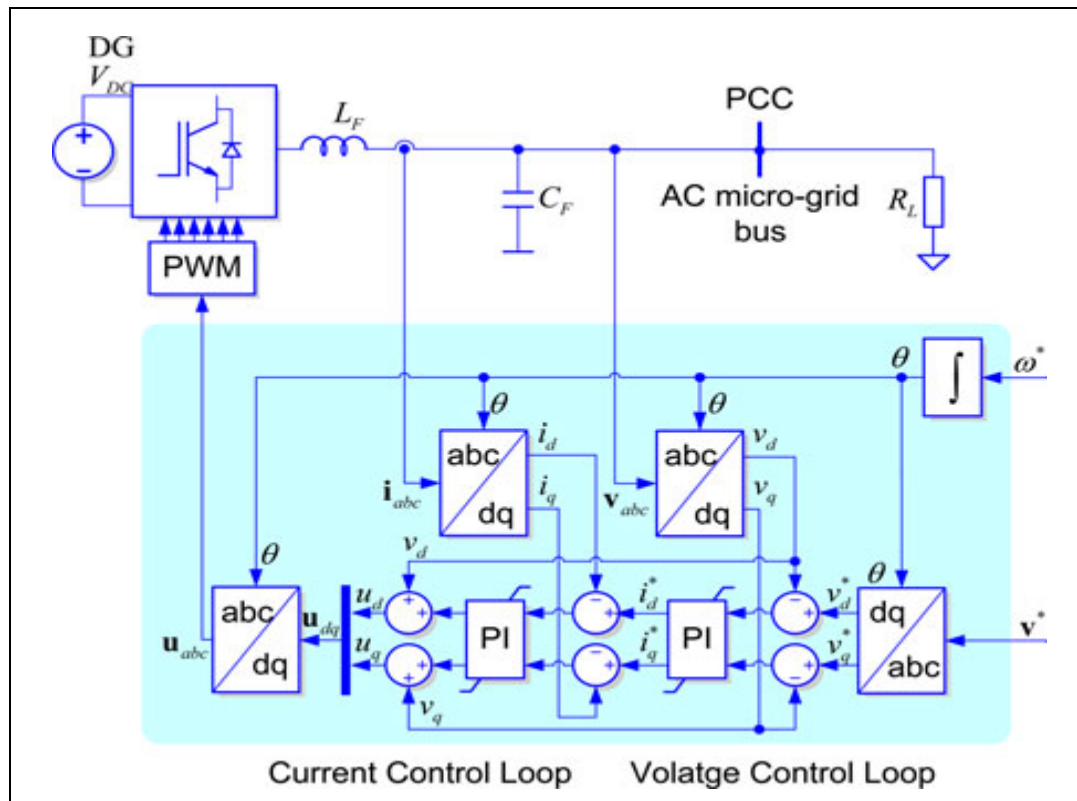


Figure 1.11 Schematic diagram of grid forming power converter

1.5.6.3 Control of Power Converters Supplying a Network

The power converters feeding the network are controlled as a source current which are exhibiting high parallel output impedance. These converters are connected in parallel and are supplying the grid (Bouزيد et al., 2015). Currently, most of the power converters which are fitting to DG systems operate in grid-connected mode, such as in photovoltaic or wind power systems (Bouزيد et al., 2015). These converters can participate in controlling the amplitude and frequency of the microgrid through adjustment of the active and reactive power references, P^* and Q^* . This type of the converter's control cannot operate in the island mode if there is not a power converter to form or support a network, or a local synchronization system for amplitude and voltage adjustment and the frequency of the AC microgrid (Rocabert et al., 2012). Figure 1.12 illustrates a typical control structure of an AC converter which is feeding the grid (Rocabert et al., 2012).

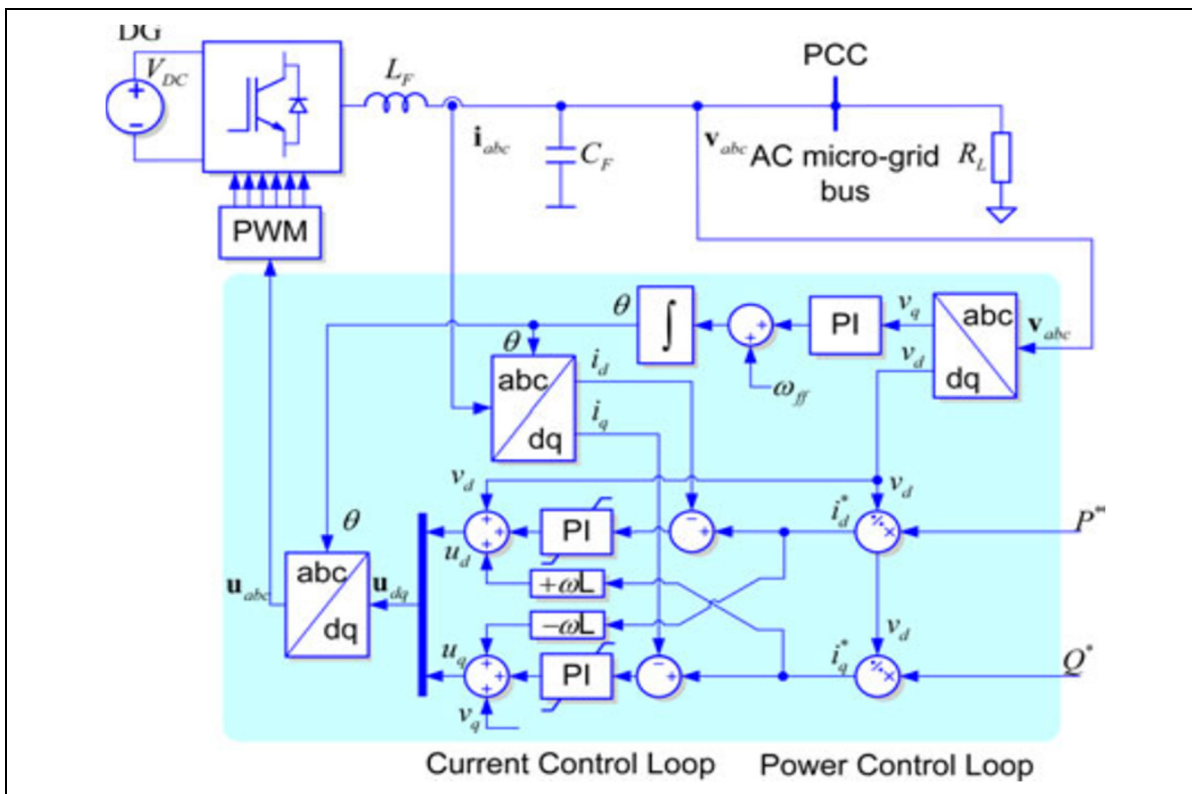


Figure 1.12 Typical control structure in a three-phase grid-feeding power converter

1.5.6.4 Control of Grid Supporting Power Converter

The grid-supporting converter is designed to regulate the AC voltage E and the frequency ω of the grid by controlling the active and reactive power which are injected into the grid (Bouzid et al., 2015). There are two main categories of the grid-supporting power converters, those are controlled as a voltage source converter with a link impedance (Bouzid et al., 2015), as shown in Figure 1.10 (d), or those are controlled as a current source converter with parallel impedance, as shown in Figure 1.10(C) (Rocabert et al., 2012).

1.5.7 Control Technique in Islanded Mode

1.5.7.1 Master-Slave Control

In master-slave control, a strong micro terminal will be selected to work under VF control. The source that takes the place of the electrical network is called main source while the others are called slave sources (Z. Chen, Wang, Li, & Zheng, 2017; Z. Yang & Ho, 2016).

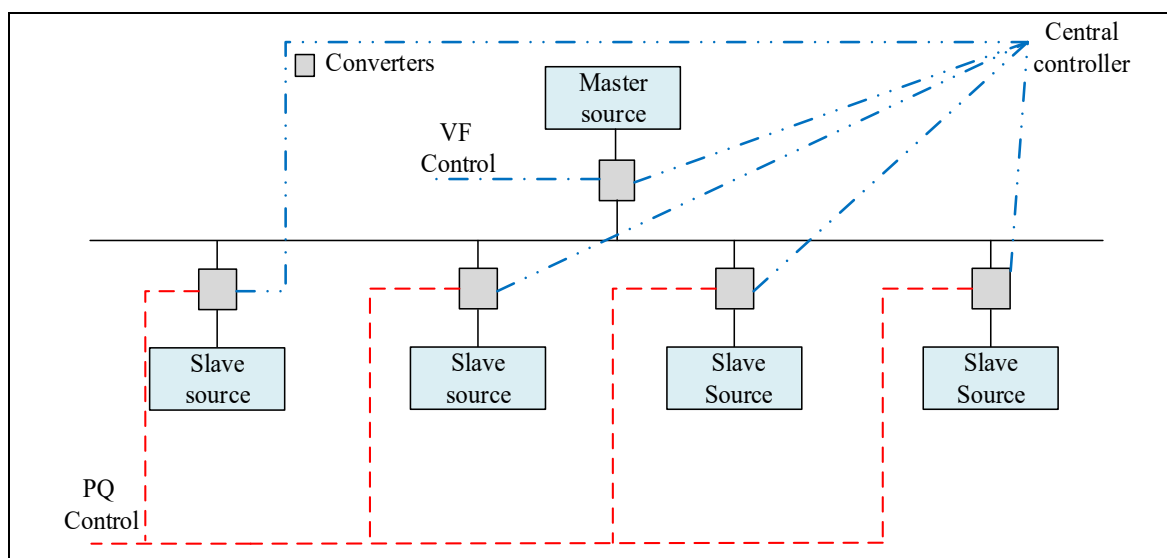


Figure 1.13 Master-slave control designs

1.5.7.2 Peer-to-Peer Control

Peer-to-peer control is a decentralized control strategy. It does not depend on the communication system and the converters are in charge of making decisions only on the basis of the local information (Z. Chen et al., 2017). In this strategy, when a power source is connected or disconnected from the system, the microgrid will continue to operate without any additional reconfiguration. Therefore, “plug and play” functionality is achieved which also increases the system reliability (Z. Yang & Ho, 2016). However, there will be a variation in frequency and voltage which is depending on the characteristic of droop control. Figure 1.14 shows the peer-to-peer control architecture (Rocabert et al., 2012).

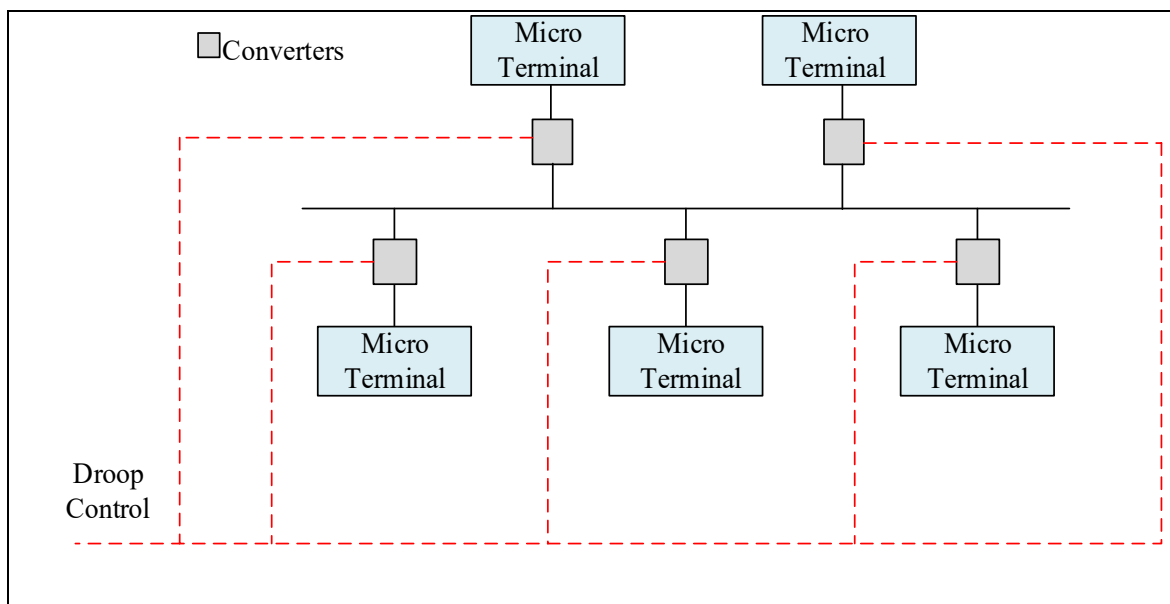


Figure 1.14 Peer-to-peer control architecture

1.5.7.3 Hierarchical Control

This control method contains three levels of control, which are primary control, secondary control, and tertiary control (Z. Yang & Ho, 2016).

1.5.7.4 Control of the Multi-Agent System

The multi-agent system (MAS) is an emerging technology that permits each micro-source or load to be as an agent and can exchange information with neighboring agents to collaborate for a common goal (Niannian & Mitra, 2010; Z. Yang & Ho, 2016). Figure 1.15 shows multi-agent control architecture.

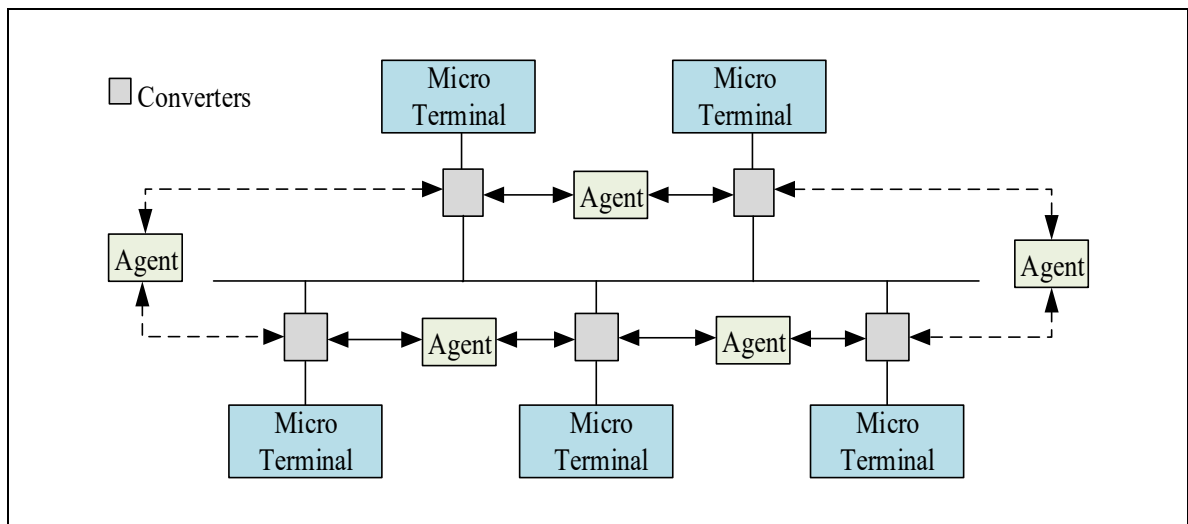


Figure 1.15 Multi-agent control architecture

1.5.8 Microgrid Control Strategy, Power Management and Optimization

In complex MG systems an improved virtual impedance methods have been used to achieve reactive power sharing. However, the realization of this latter is difficult. Hence, hierarchical control strategy has been proposed to guarantee stable and dynamic performance of the current sharing. (Olivares et al., 2014). In order to improve the stability of the MGs and have an efficient shared load power in MG, the hierarchical control structure is used for two modes of operations; grid-connected mode and in island mode (Alsafran, 2018). Figure 1.16 shows the hierarchical control structure contains three levels control: primary control, secondary, and tertiary control (Olivares et al., 2014).

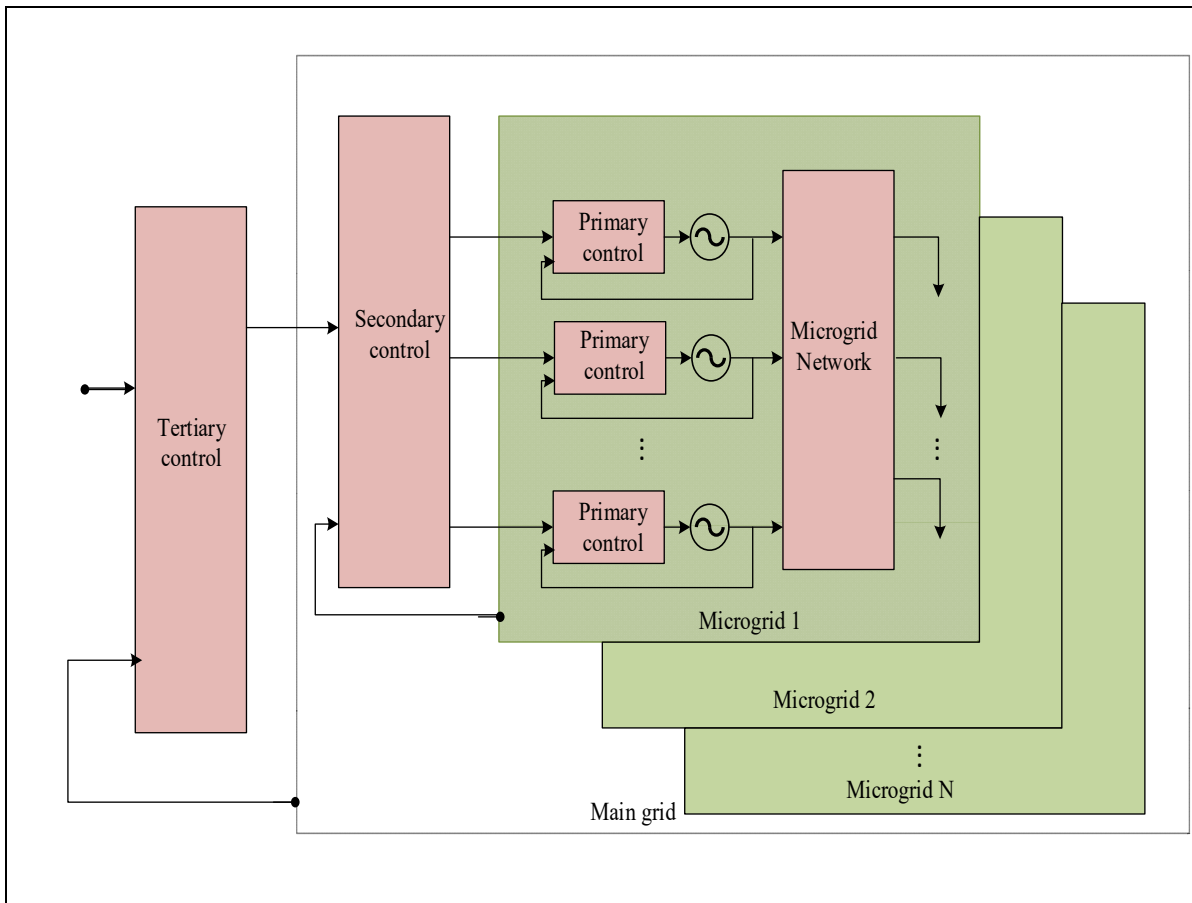


Figure 1.16 Hierarchical control levels

1.5.8.1 Primary Control

Primary control is also known as the local control or internal control which is exclusively based on the local measurements and it does not require any communication (Olivares et al., 2014). The control role is to ensure the stability of the voltage and the frequency. The power sharing is ensured by the droop control which is applied to this level without any communication links (Y. Han, Li, Shen, Coelho, & Guerrero, 2017). Inverter output control and power sharing control are the general methods of the first control level (Brabandere et al., 2007; Dou et al., 2016; Guerrero et al., 2011; Sabzehgar, 2015).

1.5.8.2 Secondary Control

The secondary control which is also named as microgrid energy management system (EMS), is responsible for the reliability, safety and economical operation of the microgrids (Olivares et al., 2014). The secondary control level uses either centralized control (Mehrizi-Sani & Iravani, 2010; Pilo, Pisano, & Soma, 2007) or decentralized control (Dou, Liu, & Guerrero, 2014; Z. Wang, Yang, & Wang, 2011).

1.5.8.3 Tertiary Control

Tertiary control which is the highest level of control, is fixed for the long term and generally optimal, these set points are fixed according to the needs of the main network. The control purpose is to organize the operation of several microgrids which are interacting with each other in the system, and also to communicate the main network needs (Olivares et al., 2014).

1.5.9 Control Strategy of Autonomous Microgrids

The control strategy linked to microgrids intervenes locally in the control of the power electronics interfaces available to each distributed generation unit. Autonomous distributed generation systems are responsible for maintaining a quasi-sinusoidal voltage at the AC bus, which is independent of the inrush currents of the electrical loads. On the other hand, autonomous distributed generation systems are also responsible for the management of power flows and load distribution in the microgrid.

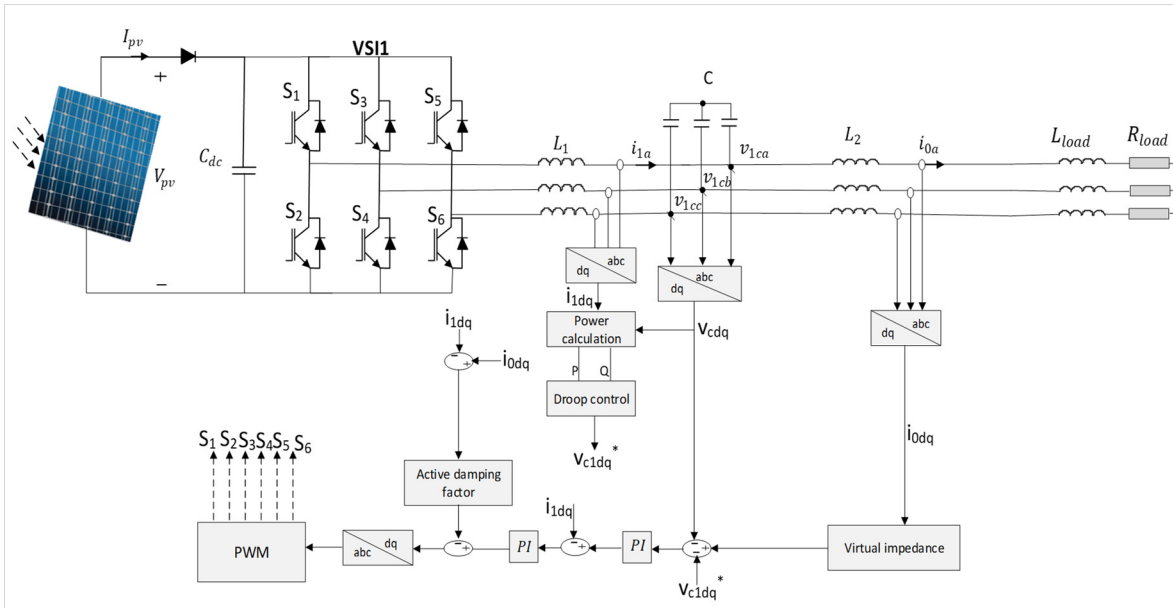


Figure 1.17 Typical structure of the primary control of an autonomous distributed generator

Figure 1.17 shows a typical structure of the primary control of a stand-alone distributed generator for a microgrid application. The inverter has a local controller which contains two control loops; the first concerns the output voltage regulation of the inverter which is measured at the edges of the LC filter capacitor. The second loop is established based on a power control loop (active and reactive), virtual output impedance, an active damping control loop, and a reference voltage generation block. The illustrated control strategy is locally implemented without requiring to the communication links; so, it supports the decentralized nature of these structures.

1.6 Conclusion

This chapter summarizes recent developments in DG control techniques used in MG system. Different definitions and control structures of a MG have been defined. The literature review has been presented in two parts. The first part discusses the power converters with LCL filter for distributed generation, the closed-loop control, and the active damping control methods (lead-leg, Notch filter and capacitor current feedback...). The converters which are connected in parallel to the AC bus in the grid-connected or island modes of operations are then presented.

The second part presents the microgrid; its architect and the different controls for stability, reliability and power management of MG. This thesis will be focusing on the converters which are connected in parallel with LC-LCL filter for microgrid applications. Based on the descriptions and definitions presented in this chapter, and the detailed modeling of the distributed generator with LCL filter which is connected to the grid is well-studied in chapter 2.

CHAPTER 2

LQR CONTROL OF SINGLE-PHASE GRID-TIED PUC5 INVERTER WITH LCL FILTER

Naima Arab ^a, Hani Vahedi ^a, and Kamal Al-Haddad ^a

^a Department of Electrical Engineering, École de Technologie Supérieure,
1100 Notre-Dame West, Montreal, Quebec, Canada H3C 1K3

This chapter has been published in Transactions on industrial Electronics, vol. 67, no. 1, pp. 297-307, January. 2020

Abstract

This chapter presents the current control design procedure of a single-phase grid-tied 5-level Packed U-Cell inverter (PUC5) with LCL output filter. The PUC5 inverter is used as an interface of renewable energy sources like solar applications. The LCL filter is calculated according to the grid-tied operation and converter ratings. An optimal controller, based on linear quadratic regulator with integral action (LQRI), is designed to inject a sinusoidal current with low harmonic distortion at unity power factor. Required to that design, the PUC5 inverter is modelled in D-Q frame. The sensor-less voltage control is incorporated into the switching technique to balance the PUC5 capacitor voltage and generate 5-level waveform at the output. Experimental tests are performed on a laboratory benchmark to confirm the theoretical design. The results prove the efficiency and accuracy of the adopted control strategy in steady state and under transients of grid current, grid inductance, AC and DC voltage amplitudes.

2.1 Introduction

Multilevel converters interfacing with renewable energy sources have received considerable interest in recent years due to their ability to reduce harmonics, proper operation at lower switching frequency and to provide high power at high quality (Sebaaly, Vahedi, Kanaan, Moubayed, & Al-Haddad, 2016). Thus, these technologies have attracted considerable

attention in high-reliability, high-power applications, such as electric vehicles and charging stations (Zongbin et al., 2017), PV inverters and grid-connected converter (Rahim, Chaniago, & Selvaraj, 2011; Trabelsi, Bayhan, Ghazi, Abu-Rub, & Ben-Brahim, 2016; Villanueva, Correa, Rodriguez, & Pacas, 2009).

Multilevel converters are appropriate in energy conversion applications to generate low harmonic waveforms (Vahedi, Labbé, & Al-Haddad, 2016). The 7-level Packed U-Cell (PUC7) inverter was introduced first by Al-Haddad *et al* to produce seven-level output voltage waveform (Vahedi, Kanaan, & Al-Haddad, 2015). The PUC7 holds six switches and a single capacitor and its voltage is fixed to one-third ($1/3$) of an isolated DC source. This converter requires complicated controllers for that capacitor with extra voltage sensor (Ounejjar, Al-Haddad, & Grégoire, 2011). The single phase five-level configuration of that inverter was then proposed by Vahedi to overcome the drawback of PUC7 (Vahedi et al., 2016). The PUC5 is obtained by setting the capacitor voltage at half of the dc source. The sensor-less voltage control of PUC5 inverter has been incorporated in the switching technique. The PUC5 inverter is used in many applications as shunt active power filter in (Vahedi, Shojaei, Dessaint, & Al-Haddad, 2018), stand-alone and grid-connected inverter in (Vahedi et al., 2016).

To incorporate residential solar PV systems and small-scale applications into the grid, a single-phase inverter commonly used between renewable energy sources and the utility grid where the power converters are usually equipped with passive filters (L, LC or LCL) to reject the switching harmonics produced by the grid-connected inverter (Komurcugil, Altin, Ozdemir, & Sefa, 2016). Harmonics attenuation is not very pronounced in case of a series inductor (L) and a large inductance is needed. The LCL filter is becoming popular and attractive for many applications. The use of the LCL filter leads to a low inductance, lower losses, and thus lets a more compact design (Peña-Alzola, Liserre, Blaabjerg, Ordonez, & Yang, 2014a). The harmonic attenuation is higher, and makes it possible to use low switching frequencies to meet the IEEE standards (Reznik, Simões, Al-Durra, & Muyeen, 2014a). Moreover, the low switching frequency allows using multilevel topologies in this application.

In spite of the above-mentioned advantages, LCL filters have their own weaknesses like resonance. Numerous strategies have been proposed to deal with the resonance, including the methods of passive and active damping. The PD (passive damping) consists of adding resistance in parallel or in series with the capacitor or the inductance of the LCL filter (Abdikarimuly, Familiant, Ruderman, & Reznikov, 2016b; Anzalchi, Moghaddami, Moghaddasi, Sarwat, & Rathore, 2016; Liserre, Blaabjerg, & Hansen, 2005; W. Wu, He, & Blaabjerg, 2012; W. Wu et al., 2017). These methods have the advantage of being simple and reliable, on the other hand, the addition of a resistive element increases the losses dissipated by joule effect. Some efficient and more flexible methods have been also presented in (C. Chen, Xiong, Wan, Lei, & Zhang, 2017; Hao, Yang, Liu, Huang, & Chen, 2013). The AD (active damping) method modifies the control strategies of the system without adding passive elements (C. Chen et al., 2017). The virtual impedance has been proposed in (J. He & Li, 2012), where the authors proposed a single loop for the purpose of controlling the inverter output with the addition of virtual impedance in parallel, but uses additional sensors. A lead-lag compensator is added by (T. Liu, Liu, Liu, Tu, & Liu, 2017) in the current loop. Another kind of active damping is a notch filter, which is incorporated in the control path to mitigate the resonance peak by an anti-peak of this latter (Dannehl, Liserre, & Fuchs, 2011b). Another interesting technique to damp the resonance is to add a supplementary feedback of the current or capacitor voltage in the controller. In (Dannehl, Fuchs, Hansen, & Thogersen, 2010), authors have studied different feedback loops to evaluate their performance in damping resonances. Sliding mode control with LCL filter of a grid-tied converter has been reported in (Hao et al., 2013; Komurcugil, Ozdemir, Sefa, Altin, & Kukrer, 2016a). H_∞ has been proposed in (S. Yang et al., 2011), where the controller has a low steady-state error to stabilize the whole system despite grid impedance variations, with low THD of grid current. In the literature, authors also used hybrid damping in (Ricchiuto, Liserre, & Santis, 2012) and (W. Wu et al., 2017) for grid-tied applications.

The optimal control LQR (Huerta, Pizarro, Cobreces, Rodriguez, Giro, et al., 2012; Š, Komrska, Šmídl, Glasbergerová, & Peroutka, 2016) is a good nominee, which will allow insuring fast tracking, robustness to parameter variations, low THD, unit power factor to the

grid, and simplicity in implementation but this controller has some demerits, such as the large number of sensors used to perform full state feedback, and this can be solved by using an observer and estimators. In (Š et al., 2016), authors used multi-harmonic current control based LQ control for UPS application through LCL filter. The work performed in (Huerta, Pizarro, Cobreces, Rodriguez, Giro, et al., 2012) presents UPS inverter based on LQR control using proportional resonant (PR) controllers. On the other hand, the LQR control was used in the discrete time (DLQR) as published in (Maccari, Luiz do Amarai Santini, Coracao de Leao Fontoura de Oliveira, & Foletto Montagner, 2013).

The aim of this paper is to evaluate the feasibility and the effectiveness of the LQRI controller applied for single phase PUC5-LCL connected to the grid. LQR control can guarantee good stability margins and better performance of the control signal by the correct selection of matrices of the LQR control (Maccari, Luiz do Amarai Santini, et al., 2013). This control method offers advantages such as fast dynamic responses and robustness as reported in many works.

The purpose of this article is to develop a new modeling of single phase grid-tied PUC5-LCL inverter for households applications. The main contributions of this work include a control method based on optimal control with the integration of active damping in the control of single-phase system. The paper examines the connectivity and effectiveness of single-phase PUC5-LCL inverter to the grid based on LQR control in terms of energy transfer, adaptability, power quality, etc.

In this study, first the third-order passive filter design for the grid-tied PUC5 inverter is explained. Afterwards, the mathematical model in D-Q reference frame of single-phase grid-tied PUC5-LCL is presented. Then the design of the LQRI controller is provided to have a low THD of grid current and unity power factor mode of operation.

The PUC5 inverter configuration and switching states, the passive filter (LCL) design as well as the D-Q model of the single-phase grid-tied PUC5 inverter are presented in section 2.2.

Then, the design of the adopted controller is provided in section 2.3. The detailed experimental implementation of the controller on a dSpace1103 is described in section 3.4. Moreover, practical results are shown and discussed in that section.

2.2 Grid-Tied PUC5-LCL Inverter

2.2.1 Configuration

The configuration of single-phase grid-tied PUC5-LCL is presented in Figure 2.1. Its function is primarily to inject the generated energy from renewable energy source to the grid.

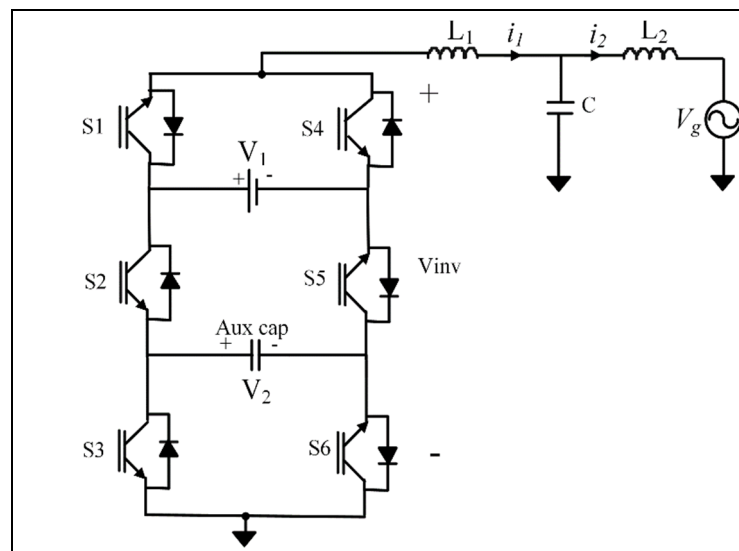


Figure 2.1 Single-Phase PUC5 inverter connected to the grid via LCL filter

Table 2.1 All states of PUC5 Inverter

States	S ₁	S ₂	S ₃	Output Voltage	V_{inv}	Influence on V_2
1	1	0	0	V_1	+2E	No Influence
2	1	0	1	V_1-V_2	+E	Charging
3	1	1	0	V_2	+E	Discharging
4	1	1	1	0	0	No Influence
5	0	0	0	0	0	No Influence
6	0	0	1	$-V_2$	-E	Discharging
7	0	1	0	V_2-V_1	-E	Charging
8	0	1	1	$-V_1$	-2E	No Influence

The single-phase grid-tied PUC5-LCL system is depicted in Figure 2.1. Switching states of the PUC5 inverter are enumerated in Table 2.1. Assuming V_1 equals to $2E$ and V_2 is balanced at E . The PUC5 inverter is controlled by six driving signals (S1 to S6). The sensor-less voltage balancing of the auxiliary capacitor (V_2) has been completely described in (Vahedi et al., 2016). As a brief summary, it could be noted that the auxiliary capacitor of PUC5 inverter is charged during positive half-cycle by switching state 2 and then discharged through switching state 6 at negative half-cycle. Such symmetric charging and discharging process keeps the capacitor voltage fixed and equal to half of the DC voltage (V_1). Consequently, five levels are engendered at the PUC5 inverter output, which forms a 5-level waveform with low THD. Figure 2.2 illustrates the five-level pulse-width modulation (PWM) scheme where four carriers and the reference voltage are presented. This latter is shifted vertically to modulate the reference waveform.

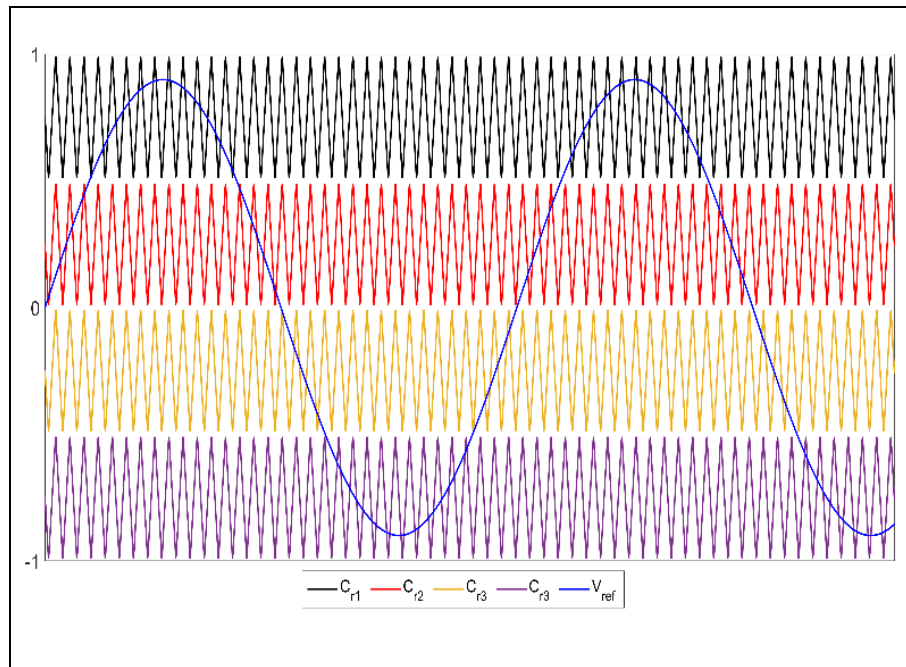


Figure 2.2 Five-level pulse-width modulation (PWM) scheme

2.2.2 LCL Filter Design

The passive LCL filter is composed of inductances L_1 and L_2 as well as the capacitance C . According to the structure under study represented in Figure 2.1, the corresponding transfer function of the third-order passive filter in continuous state is written as follows:

$$G_{i_2}(s) = \frac{i_2}{V_{inv}} = \frac{1}{CL_1L_2 s^3 + (L_1 + L_2)s} \quad (2.1)$$

Equation (2) is used to calculate the resonance frequency:

$$f_{res} = \frac{1}{2\pi} \cdot \sqrt{\frac{(L_1 + L_2)}{CL_1L_2}} \quad (2.2)$$

The value of inverter output inductor L_1 is determined as:

$$L_1 \leq \frac{0.05 \times V \times m}{\Delta i_{out} \times f_{sw}} \leq \frac{0.05 \times 120 \times 1}{1 \times 2 \times 10^3} \leq 3mH \quad (2.3)$$

Where V is the grid voltage, f_{sw} is the switching frequency, and m is the modulation amplitude.

The inverter output inductor value (L_1) is chosen as 2.5mH.

The following equations allow to calculate the value of L_2 inductor (Reznik, Simões, Al-Durra, & Muyeen, 2014b).

$$z_b = \frac{V^2}{P_n} = \frac{120^2}{1200} = 12 \quad (2.4)$$

$$C_b = \frac{1}{\omega z_b} = \frac{1}{377 \times 12} = 221.04\mu F \quad (2.5)$$

C_b and Z_b are the base capacitance and inductance respectively, ω is the angular frequency, V is the grid voltage rms value, P_n is the active power absorbed by the converter.

$$L_2 = \frac{\sqrt{\frac{1}{k_a^2} + 1}}{\alpha C_b \omega_{sw}^2} = \frac{\sqrt{\frac{1}{0.2^2} + 1}}{11.04\mu \times (2 \times \pi \times 2 \times 10^3)^2} = 3.4mH \quad (2.6)$$

The value of L_2 is then taken as 2.5 mH.

k_a is the desired attenuation which is taken as 0.2 (Reznik et al., 2014b).

The value of the capacitor (C) is calculated as:

$$C = \alpha C_b = 0.05 \times 221.04\mu = 11.04\mu F \quad (2.7)$$

α is the percentage of capacitor versus base capacitor where the maximum value of α is taken as 0.05 (Jayalath & Hanif, March 2017; Naima Arab, 2017). The filter capacitor is chosen 15 μ F.

Figure 2.3 illustrates the frequency response of the designed LCL filter. It shows that the resonant frequency at the peak point is around 1.16 kHz, which complies with the theoretical calculation obtained from equation (2.1).

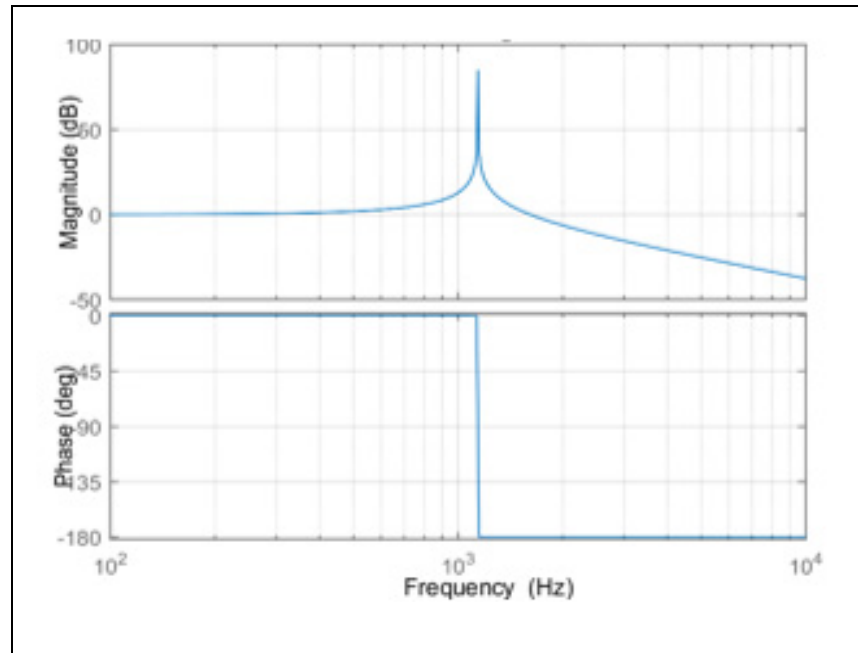


Figure 2.3 Bode plots of the designed LCL filter

Calculation of Voltage Capacitor (V_1)

$$V_1 = 1.2 \times \hat{I}_g = 1.2 \times 170 = 204V \quad (2.8)$$

Hence, the value of V_1 is taken as 200V to inject the current from DC side to the AC grid.

Design of the Auxiliary Capacitor

The auxiliary capacitor is designed as the following:

$$\frac{1}{2} C_{aux} (V_1^2 - V_1^{*2}) = \alpha V I t \quad (2.9)$$

$$\frac{1}{2} C_{aux} (V_1^2 - V_1^{*2}) = 1.2 \times 120 \times 10 \times 0.005 \Rightarrow C_{aux} = 1297.3 \mu F$$

V_1 is the reference DC voltage, V_1^* is the minimum voltage level of V_1 . V and I are voltage and grid current, α is overloading factor and t is the transient time (B. Singh, Chandra, & Al-Haddad, 2015.). The value of C_{aux} is equal to 1297.3 and is taken as 1000 μ F in this work.

2.3 Single-Phase d-q Model

The equation describing single-phase grid-tied PUC5-LCL operations is represented by (2.10):

$$L_1 \frac{di_1}{dt} + R_1 i_1 = v_{inv} - v_c \quad (2.10.a)$$

$$L_2 \frac{di_2}{dt} + R_2 i_2 = v_c - v_g \quad (2.10.b)$$

$$C \frac{dv_c}{dt} = i_1 - i_2 \quad (2.10.c)$$

The inverter output current (i_1), grid current (i_2), and capacitor voltage (v_c) are the real variables of the system. L_1, R_1 and L_2, R_2 are respectively the PUC5 and grid side inductors and parasitic resistors.

Park transformation is generally used in three-phase systems to obtain the d-q model, and in single-phase structures, the imaginary variables (in β axis) should be generated from the real variables (in α axis) (Bahrani, Rufer, Kenzelmann, & Lopes, 2011). Thus

$$i_{1\beta} = i_{1\alpha} e^{-\pi/2}, i_{2\beta} = i_{2\alpha} e^{-\pi/2}, v_{c\beta} = v_{c\alpha} e^{-\pi/2}, v_{g\beta} = v_{g\alpha} e^{-\pi/2} \quad (2.11)$$

The matrix transformation from α - β to d - q components is given in (2.12):

$$T = \begin{bmatrix} \sin(\omega t) & -\cos(\omega t) \\ \cos(\omega t) & \sin(\omega t) \end{bmatrix} \quad (2.12)$$

The T_{inv} transformation is set below:

$$T_{inv} = T^{-1} = \begin{bmatrix} \sin(\omega t) & \cos(\omega t) \\ -\cos(\omega t) & \sin(\omega t) \end{bmatrix} \quad (2.13)$$

After transformation, the PUC5-LCL model in d-q reference frame is illustrated as equation (2.14).

$$\begin{aligned} \frac{di_{2d}}{dt} &= \frac{-R_2}{L_2} i_{2d} + \omega i_{2q} + \frac{1}{L_2} v_{cd} - \frac{1}{L_1} v_{gd} \\ \frac{di_{2q}}{dt} &= -\omega i_{2d} - \frac{R_2}{L_2} i_{2q} + \frac{1}{L_2} v_{cq} - \frac{1}{L_1} v_{gq} \\ \frac{di_{1d}}{dt} &= \frac{-R_1}{L_1} i_{1d} + \omega i_{1q} - \frac{1}{L_1} v_{cd} + \frac{V_1}{L_2} d_d \\ \frac{di_{1q}}{dt} &= -\omega i_{1d} - \frac{R_1}{L_1} i_{1q} + \frac{1}{L_1} v_{cq} + \frac{V_1}{L_2} d_q \\ \frac{dv_{cd}}{dt} &= \frac{-1}{C} i_{2d} + \frac{1}{C} i_{1d} + \omega v_{cq} \\ \frac{dv_{cq}}{dt} &= \frac{-1}{C} i_{2q} + \frac{1}{C} i_{1q} - \omega v_{cd} \end{aligned} \quad (2.14)$$

The model of equation (2.14) is nonlinear, thus a linearization around equilibrium points is needed. The equilibrium points are obtained by putting equation (2.14) equal to zero ($\dot{\mathbf{x}}=0$) and replacing the variables by their steady-state values. The obtained operating points in steady state are then:

$$\begin{aligned} i_{1d} = I_{1d} = 0, i_{1q} = I_{1q} = 0, i_{2d} = I_{2d} = 0, i_{2q} = I_{2q} = 0, v_{gd} = 0, \\ v_{gq} = V\sqrt{2}, v_1 = V_1. \end{aligned} \quad (2.15)$$

Where,

i_{2d} , i_{2q} and i_{1d} , i_{1q} are grid current components and the PUC5 inverter output current respectively, v_{cd} , v_{cq} are the capacitor voltage components, V_1 is the dc voltage, v_{gd} and v_{gq} are the grid voltage components in d-q, and d_d , d_q are the duty cycle components.

The small signal model obtained by a linearization around the operating point obtained previously is presented as:

$$\frac{dx_i}{dt} = Ax_i + Bu_i + Ev_i \quad (2.16)$$

Where, A , B , and E matrices are given as follows:

$$A = \begin{bmatrix} \frac{-R_2}{L_2} & \omega & 0 & 0 & \frac{1}{L_2} & 0 \\ -\omega & \frac{-R_2}{L_2} & 0 & 0 & 0 & \frac{1}{L_2} \\ 0 & 0 & \frac{-R_1}{L_1} & \omega & \frac{-1}{L_1} & 0 \\ 0 & 0 & -\omega & \frac{-R_1}{L_1} & 0 & \frac{-1}{L_1} \\ -\frac{1}{C} & 0 & \frac{1}{C} & 0 & 0 & \omega \\ 0 & -\frac{1}{C} & 0 & \frac{1}{C} & -\omega & 0 \end{bmatrix}, B = \begin{bmatrix} 0 & 0 \\ \frac{V_1}{L_1} & 0 \\ 0 & \frac{V_1}{L_1} \\ 0 & 0 \\ 0 & 0 \\ 0 & 0 \end{bmatrix}, E = \begin{bmatrix} \frac{-1}{L_1} & 0 \\ 0 & \frac{-1}{L_1} \\ 0 & 0 \\ 0 & 0 \\ 0 & 0 \\ 0 & 0 \end{bmatrix}$$

$$x_i = \left[i_{2d}, i_{2q}, i_{1d}, i_{1q}, v_{cd}, v_{cq} \right]^T$$

$$u_i = \left[d_d, d_q \right]^T$$

$$v_i = \left[v_{gd}, v_{gq} \right]^T$$

x_i is the states, u_i is the control input, and v_i is the disturbance vectors of PUC5-LCL inverter.

2.4 Design and Implementation of Optimal Control for Grid-Tied PUC5-LCL

The LQR is realized by designing the state feedback controller where the objective function J is minimized. The linearized model (2.16) is used and the optimal gains are obtained with the good selection of matrices to have fast tracking response and stable system.

The computed LQRI gains are obtained through minimizing the cost function J .

$$J = \int_0^{\infty} (x^T Q x + u^T R u) dt \quad (2.17)$$

Where Q and R are the state and control weighting matrices. The control law that minimizes the cost function is given below:

$$u = -Kx \quad (2.28)$$

Where, u is the controller signal, k is the gain matrix, and x is the state variables. The controller gain k is calculated by:

$$K = R^{-1} B^T P \quad (2.39)$$

P is the result of the Algebraic Riccati Equation. The Riccati equation is given bellow [26]:

$$A^T P + P A - P B R^{-1} B^T P + Q = 0 \quad (2.20)$$

To guarantee zero errors in steady state, additional states must be added in the linearized model shown in (2.16). These two new states are the integral of the currents i_{2d} and i_{2q} .

$$x_{\square} = \left[i_{2d\square} \quad i_{2q\square} \quad i_{1d\square} \quad i_{1q\square} \quad v_{cd\square} \quad v_{cq\square} \quad \int i_{2d\square} \quad \int i_{2q\square} \right]^T \quad (2.21)$$

$$u_{\square} = \left[d_{d\square} \quad d_{q\square} \right]^T, \quad v_{\square} = \left[v_{gd\square} \quad v_{gq\square} \right]^T \quad (2.22)$$

The matrices of the model of PUC5-LCL A , B and E are:

$$A = \begin{bmatrix} \frac{-R_2}{L_2} & \omega & 0 & 0 & \frac{1}{L_2} & 0 & 0 & 0 \\ -\omega & \frac{-R_2}{L_2} & 0 & 0 & 0 & \frac{1}{L_2} & 0 & 0 \\ 0 & 0 & \frac{-R_1}{L_1} & \omega & \frac{-1}{L_1} & 0 & 0 & 0 \\ 0 & 0 & -\omega & \frac{-R_1}{L_1} & 0 & \frac{-1}{L_1} & 0 & 0 \\ -\frac{1}{C} & 0 & \frac{1}{C} & 0 & 0 & \omega & 0 & 0 \\ 0 & -\frac{1}{C} & 0 & \frac{1}{C} & -\omega & 0 & 0 & 0 \\ 1 & 0 & 0 & 0 & 0 & 0 & 0 & 0 \\ 0 & 1 & 0 & 0 & 0 & 0 & 0 & 0 \end{bmatrix} \quad B = \begin{bmatrix} 0 & 0 \\ 0 & 0 \\ \frac{V_1}{L_2} & 0 \\ 0 & \frac{V_1}{L_2} \\ 0 & 0 \\ 0 & 0 \\ 0 & 0 \\ 0 & 0 \end{bmatrix}, \quad E = \begin{bmatrix} \frac{-1}{L_1} & 0 \\ 0 & \frac{-1}{L_1} \\ 0 & 0 \\ 0 & 0 \\ 0 & 0 \\ 0 & 0 \\ 0 & 0 \end{bmatrix} \quad (2.23)$$

The output equation of the system is expressed as

$$y_{\square} = Cx_{\square} \quad (2.24)$$

$$y_{\square} = [i_{2d} \ i_{2q}]$$

The matrix C is given below:

$$C = \begin{bmatrix} 1 & 0 & 0 & 0 & 0 & 0 & 0 & 0 \\ 0 & 1 & 0 & 0 & 0 & 0 & 0 & 0 \end{bmatrix} \quad (2.25)$$

Weighting factors are $Q_{i_{2d}}, Q_{i_{2q}}, Q_{i_d}, Q_{i_q}, Q_{v_{cd}}, Q_{v_{cq}}, Q_{\int 2i_d}, Q_{\int 2i_q}$ and matrix Q is given below:

$$Q = \text{diag} \left(Q_{i_{2d}}, Q_{i_{2q}}, Q_{i_d}, Q_{i_q}, Q_{v_{cd}}, Q_{v_{cq}}, Q_{\int 2i_d}, Q_{\int 2i_q} \right) \quad (2.26)$$

Matrix R is:

$$R = w \begin{bmatrix} 1 & 0 \\ 0 & 1 \end{bmatrix} \quad (2.27)$$

The cost function J is given as:

$$\begin{aligned}
 J = J_x + J_u = & Q_{i_{2d}} (i_{2d})^2 + Q_{i_{2q}} (i_{2q})^2 + Q_{i_d} (i_d)^2 \\
 & + Q_{i_q} (i_q)^2 + Q_{v_{cd}} (v_{cd})^2 + Q_{v_{cq}} (v_{cq})^2 + Q_{\int i_{2d}} \left(\int i_{2d} \right)^2 \\
 & + Q_{\int i_{2q}} \left(\int i_{2q} \right)^2 + W \left[(d_d)^2 + (d_q)^2 \right]
 \end{aligned} \tag{2.28}$$

The weights of the matrices Q and R are chosen to meet the specifications. Basically, choosing a small value for R , the matrix Q should be chosen very large; the system is stabilized with less energy (cheap control). On the other hand, choosing a large value for R and small value of Q ; the system is stabilized with high energy (expensive control) (Xue, Chen, Atherton, Society for, & Applied, 2007). Moreover, the weights of matrix Q must be higher for the current loops, and lower for the voltage loop (Engleitner, Nied, Cavalca, & Costa, 2016).

The optimal weights that insure good responses are set as:

$$\begin{aligned}
 Q_{i_d} &= 1e5 \text{ c.u} / A^2, Q_{i_q} = 1.e5 \text{ c.u} / A^2, Q_{i_{2d}} = 1.e6 \text{ c.u} / A^2, \\
 Q_{i_{2q}} &= 1.e6 \text{ c.u} / A^2. \\
 Q_{v_{cd}} = Q_{v_{cq}} &= 1 \text{ c.u} / V^2, Q_{\int i_{2d}} = Q_{\int i_{2q}} = 1.e9 \text{ c.u} / A^2, \\
 W &= 1 \text{ e1 c.u}.
 \end{aligned}$$

The obtained gains of matrix K have been calculated using the *lqr* function existing in Matlab. This function makes it possible to calculate the controller gains once the matrices of the controller are chosen precisely where the matrix K is separated into two matrices $k_p(2 \times 6)$ and $k_i(2 \times 2)$. The computed gains are:

$$\begin{aligned}
 k_p = & \begin{bmatrix} -0.4749 & 0.0063 & -0.8189 & -0.0025 & 0.0682 & 0.0011 \\ -0.0360 & -1.5260 & 0.0015 & -0.8405 & 0.0050 & 0.1244 \end{bmatrix}
 \end{aligned}$$

$$k_i = \begin{bmatrix} -33.2489 & 2.3246 \\ -4.1562 & -70.809 \end{bmatrix}$$

The block diagram of the designed controller (LQRI) is depicted in Figure 2.4. The measured real variables of single-phase grid-tied PUC5-LCL in α axis are the inverter components ($i_{1\beta}$, $i_{2\beta}$, $v_{c\beta}$). The obtained α - β components are the output current ($i_{1\alpha}$), grid current ($i_{2\alpha}$), and capacitor voltage ($v_{c\alpha}$).

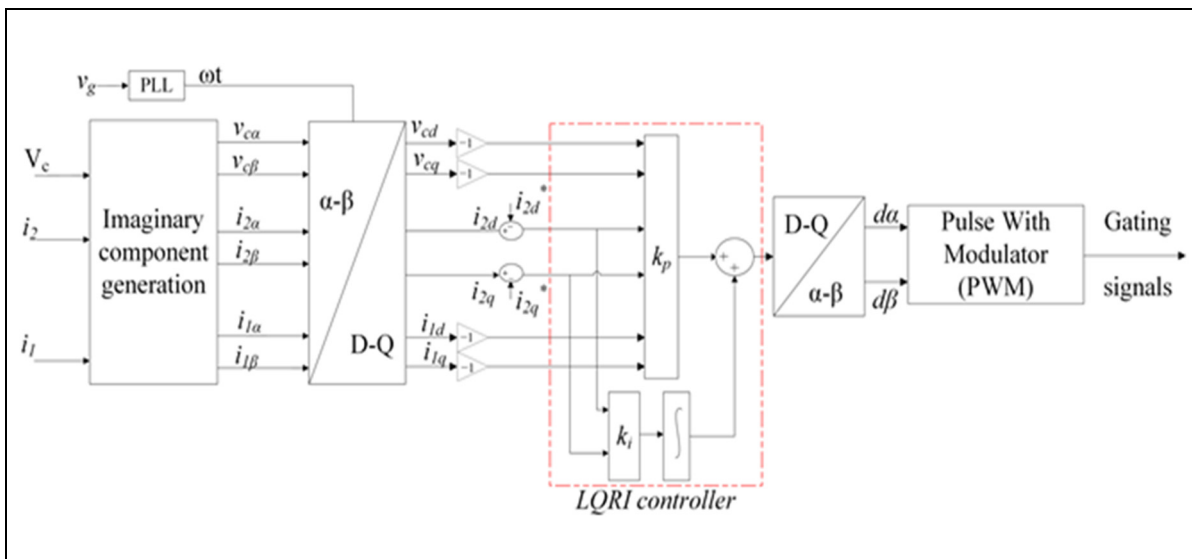


Figure 2.4 Designed controller for single-phase grid-tied PUC5-LCL inverter

These variables are then shifted by 90° to obtain their β component in the D-Q frame in order to obtain (i_{2d} , i_{2q} , i_{1d} , i_{1q} , v_{cd} , v_{cq}) using T transformation. The angle (ωt) is obtained through a PLL on the grid voltage. The current reference in the axis d (i_{2d}^*) is fixed to zero to ensure a unit power factor. The q axis reference current i_{2q}^* is set to a constant value that represents the magnitude of the injected grid current. The current reference components (i_{1d}^*) of the converter is set to zero and the same holds for the capacitor voltage. The comparison of the six references (current and voltage) with the measured values give rise to errors which are subsequently used as input to the LQRI control which makes it possible to have the duty cycle in d-q. It is subsequently converted to α - β coordinates where only the α component is used to engender the

gating signals of the single-phase PUC5 switches.

2.4.1 Comparison between LQR and PI Controller

The principle of conventional vector control method is decoupling d and q axis. The design of the PI controller is done with neglecting the capacitor C of the LCL filter in (2.14) and the model of PUC5-LCL will be simplified to PUC5-L system (Liserre et al., 2005). The model of PUC5-LCL in d-q axis is simplified and given by:

$$\begin{aligned} (L_1 + L_2) \frac{di_{2d}}{dt} + R_2 i_{2d} &= (L_1 + L_2) \omega i_{2q} + V_{inv_d} - v_{gd} \\ (L_1 + L_2) \frac{di_{2q}}{dt} + R_2 i_{2q} &= -(L_1 + L_2) \omega i_{2d} + V_{inv_q} - v_{gq} \end{aligned} \quad (2.25)$$

Where the terms u_d and u_q are used to design the PI controller of the grid current in d-q axis. The model of PUC5-LCL output filter with conventional PI controller has been used to have the direct current control of PUC5-LCL. The control strategy of the PUC5-LCL is illustrated in Figure 2.4, only the current i_2 will be sensed and transformed to d-q frame via the T transformation to obtain the current i_{2d} and i_{2q} . This current will be compared to i_{2d}^* and i_{2q}^* in order to have the pulses of the inverter. The PI controller of the current-loops is designed using open loop of the system and validated with sisotool of Matlab and the tuned controller is shown in Figure 2.5. The results are obtained with optimal phase margin equal to 76.4° and the bandwidth equal to 838 rad/s.

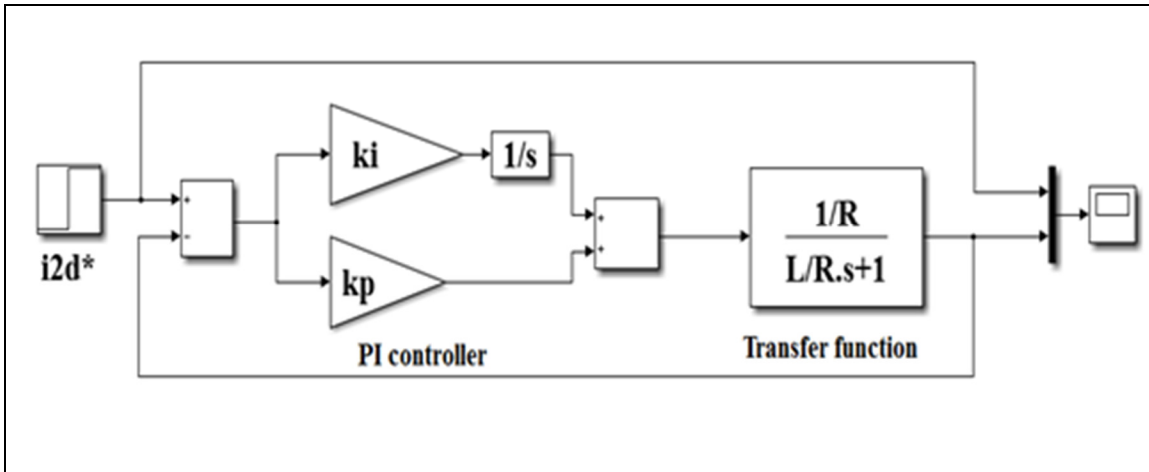


Figure 2.5 Block diagram of the design of the PI controller

Figure 2.6 shows the details of the conventional vector control applied to PUC5-LCL inverter in d - q -axis.

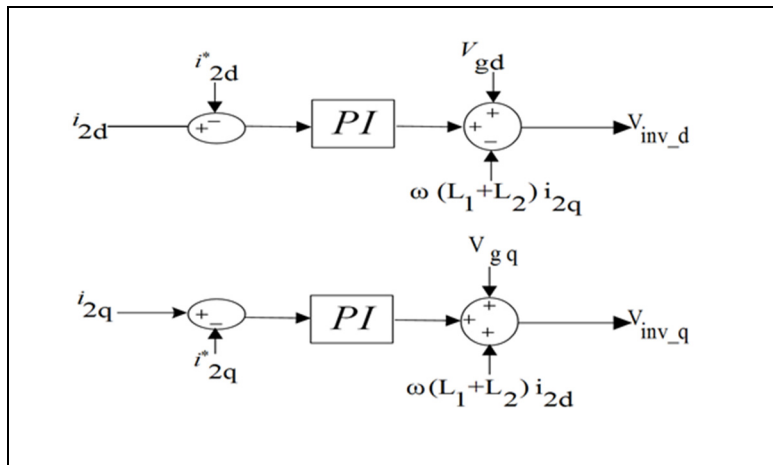


Figure 2.6 Conventional vector control

Furthermore, to compare those two methods, the test of grid current variation was adopted and results are illustrated in Figure 2.7. System parameters have been listed in Table 2.2. Results demonstrate the fast dynamic response in terms of grid current i_2 in d - q frame with the LQRI controller contrary to PI controller. The d - q component of the PUC5-LCL current tracks its reference proving the good tracking of the LQRI controller.

The result obtained with LQRI controller is better than PI controller with good dynamic performance (Figure 2.7b).

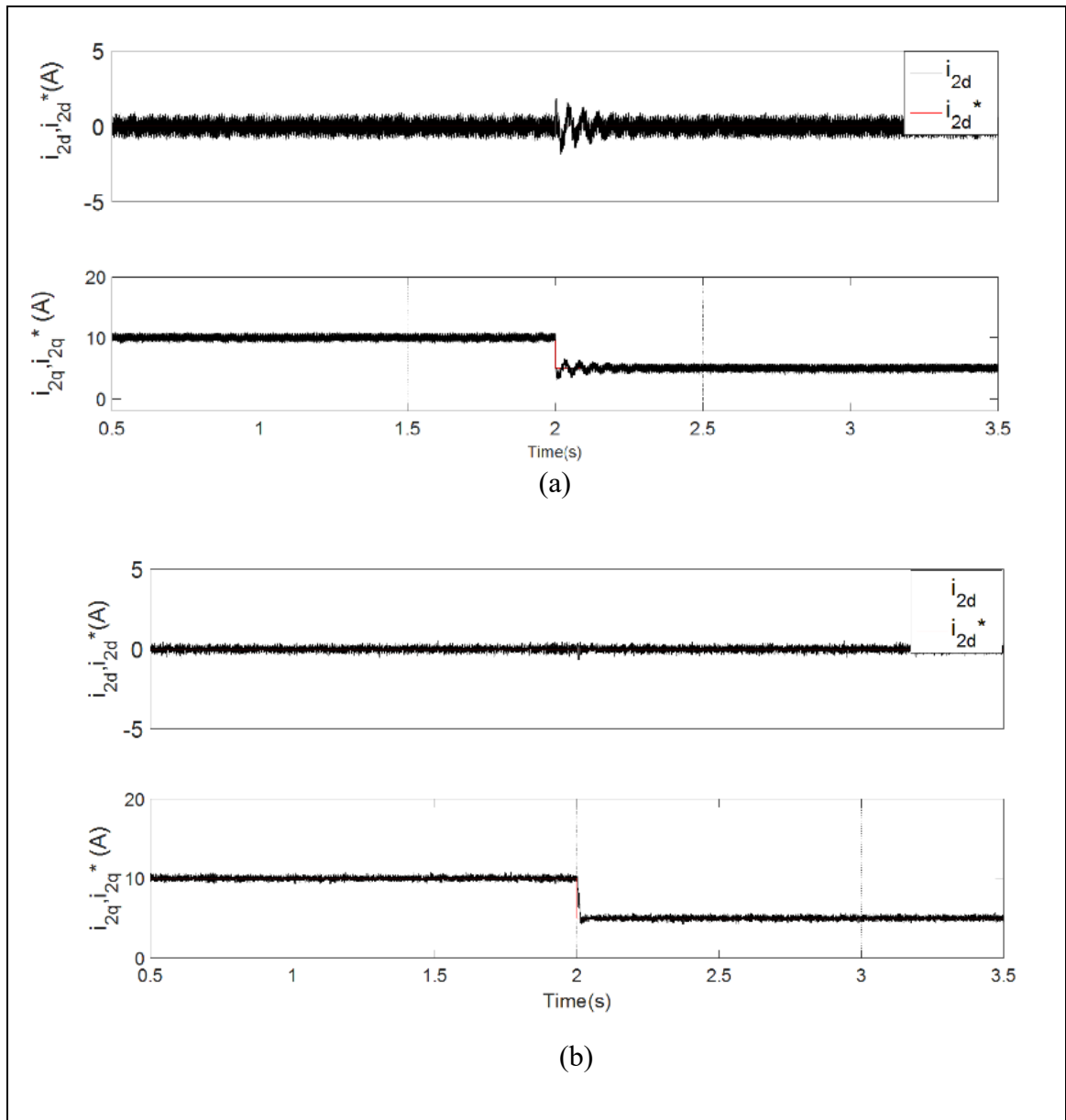


Figure 2.7 Grid current components in D-Q reference frame, (a) with conventional PI control, (b) with LQRI controller

The following Table presents a comparison between PUC5-L with PI controller and PUC5-LCL with LQR controller:

Table 2.2 A comparison between PUC5-L with PI controller and PUC5-LCL with LQR controller

Comparison categories	PUC5-L		PUC5-LCL	
	Controller	PI		LQR
Filter parameters	L=5mH	L=2mH	L1=2.5mH,L2=2.5mH, C=15 μ F	L1=1mH,L2=1mH, C=15 μ F
THD	2.5%	5.27%	1.42%	2.42%

From the table, one can conclude that, PUC5-LCL grid connected converter with LQR controller is desirable for this application where the grid current THD is measured below 1.42% for (L1=2.5mH, L2=2.5mH, C=15 μ F) and 2.42% for (L1=1mH, L2=1mH, C=15 μ F). The LCL filter size was reduced in case of LQR controller whereas, higher inductance value 5mH was required for the PI controller in order to obtain 2.5% THD even if the PI controller gains are optimized for the same switching frequency.

2.5 Experimental Validation

The feasibility and efficiency of the optimal control LQR has been validated on a laboratory experimental setup. The practical parameters are described in Table 2.3. The PUC5-LCL based on LQR controller was implemented in real-time, a dSPACE DS1103 has been used with a sampling time of 20 μ s. Switching signals are sent to the gate drivers to boost and fire the switches of the PUC5 inverter. The setup is depicted in Figure 2.8.



Figure 2.8 Experimental setup. (1) PUC5 inverter, (2) LCL filter, (3) dSPACE 1103 , (4) grid, (5) DC source, (6) oscilloscope

Table 2.3 Experimental tests parameters

Nominal value	Grid voltage	120V RMS
	DC voltage (V_1)	200V
	Grid frequency	60Hz
	Switching frequency	2kHz
	Sampling frequency	50kHz
	Auxiliary Capacitor	1000 μ F
LCL filter	Inverter side inductance	2.5mH
	Grid inductance	2.5mH
	Filter capacitor	15 μ F

The steady state mode of the applied controller has been tested and results are illustrated in Figures 2.9 to 2.12. As depicted in Figure 2.9, the results show the grid current and grid voltage

(i_2 , v_g) respectively, the dc bus voltage V_1 and inverter output voltage V_{inv} . The auxiliary capacitor voltage in PUC5 inverter has been regulated at 100V as half of the DC voltage amplitude. It has been balanced through sensor-less voltage balancing as described in section 2.2. The PUC5 inverter voltage waveform has five identical levels due to an acceptable voltage balancing. The 5-level voltage waveform is formed due to appropriate modulation of the reference signal coming from the controller. Eventually, the grid voltage and grid current are in-phase, which proves the unity power factor operation and confirms the well operation of the LQRI controller.

The grid current and voltage analysis have been performed through AEMC power analyzer. Figure 2.10 shows the acceptable 3.5% THD of the grid current and 1.6% for grid voltage with controlled amplitude of 8A; it is clear that the THD of grid current and grid voltage are lower than the limit accepted by IEEE standards (5%).

Moreover, the power as well as the power factor values are measured as depicted in Figure 2.11. A synchronization with the grid voltage is attained where unit power factor is insured (PF=0.999) and all active power is delivered to the network. Eventually, the α - β current waveforms are captured through dSpace ControlDesk software, which confirm the 90° phase shift and accurate peak amplitude regulation. Note that the grid current reference amplitude is set to 8A.

All those results prove the acceptable performance of the designed controller and installed LCL filter in injecting a pure active power into the grid.

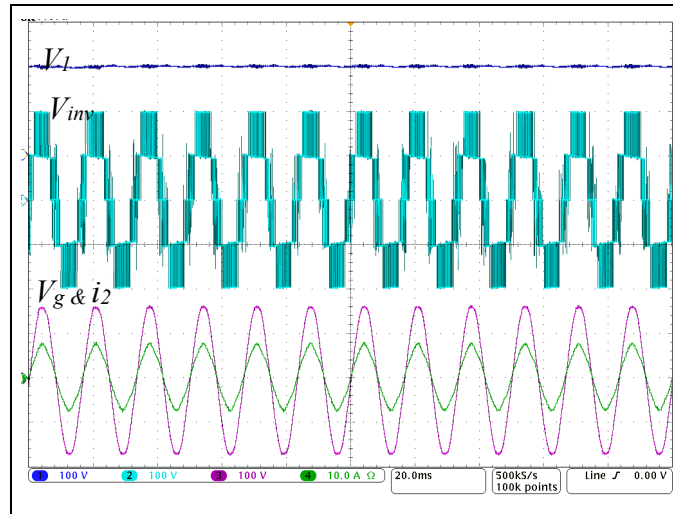


Figure 2.9 Steady state voltage, grid current and DC source voltage waveforms

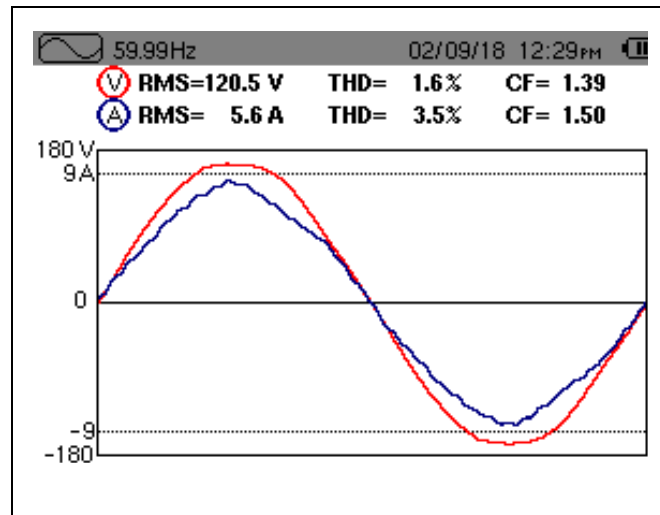
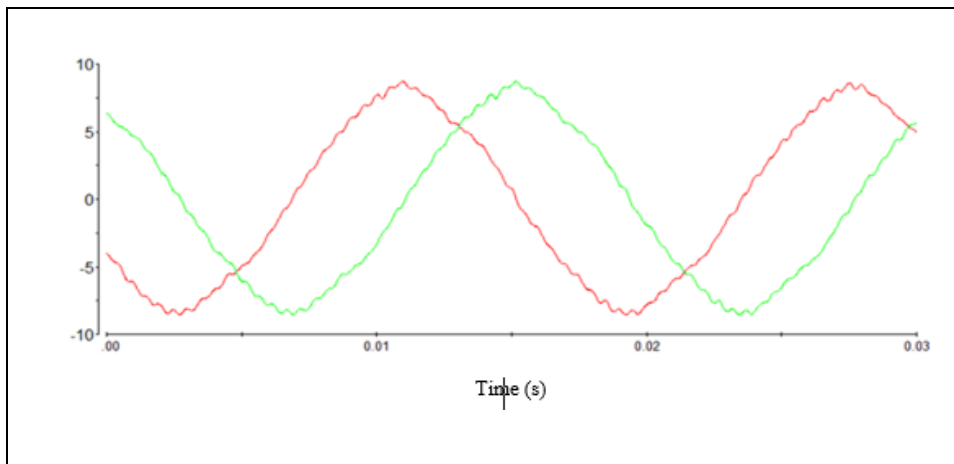


Figure 2.10 Grid current, voltage waveforms, and their Harmonic analysis (THD)

W	+678.8	PF	+0.999
Wh	0000000		
VAR	± 0.3	DPF	+1.000
VARh	€0000000		
	±0000000	Tan	+0.000
VA	679.7	Φ	+000°
VAh	0000000		

Figure 2.11 Power analyzer results

Figure 2.12 Snapshot of grid current in α - β coordinates measured by dSpace ControlDesk software

2.5.1 Performance under Grid Current Variations

The grid current reference amplitude variations has been applied to confirm the high dynamic performance of the proposed controller. Results are presented in Figure 2.13 and 2.14.

As seen in Figure 2.13, the tracking error is measured almost zero during the peak current variations from 4A to 8A. As illustrated in Figure 2.14, the grid current is increased by 100% from 4A to 8A and then decreased to 4A. The controller tracks the reference signal accurately thanks to the integral action, which resulted in injecting a sinusoidal current to the grid at unity power factor and with acceptable THD.

2.5.2 Performance under System Parameter Changes

The grid impedance variation test has been performed to prove the robustness of the controller. The grid current and voltage are presented in Figure 2.15 while the value of grid inductance (L_2) is changed to half of its initial value, as a decrease of 2.5 to 1mH. The grid current amplitude is unaffected by this variation and still in-phase with grid voltage with low THD (3.6% for grid current and 1.6% for grid voltage), A five-level output voltage waveforms is obtained where the capacitor voltage is fixed at half of the DC voltage as shown in Figure 2.15.

The study shows that the LQR controller has a strong ability to adapt under uncertain conditions (large variation in grid inductance), while no other adjustments are required to make in the controller gains which demonstrates the robustness of the designed controller even during change in system-parameter values. It should be noted that such changes happen in real practical systems inevitably.

The power analysis for this decrease of grid inductance is also depicted in Figure 2.17 where the power factor (PF) is still almost 1 insuring a good transfer of active energy to the grid.

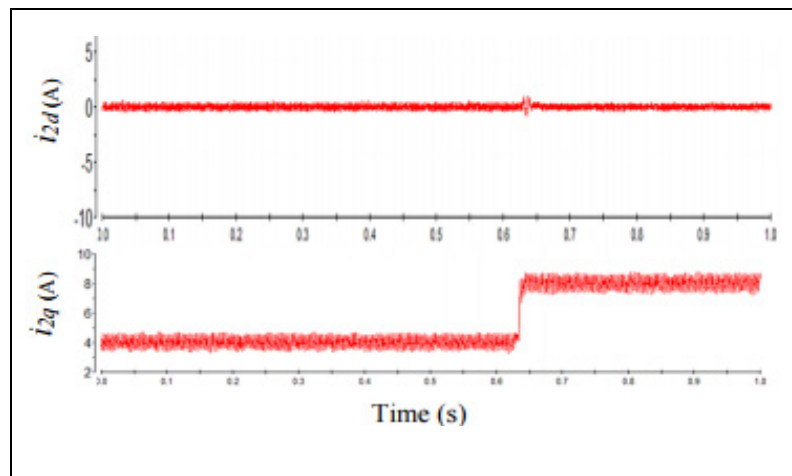


Figure 2.13 Experimental results of the grid current reference variations in d-q frame from 4A to 8A). The upper result is the grid current in d-axis. The lower is the grid current in q-axis

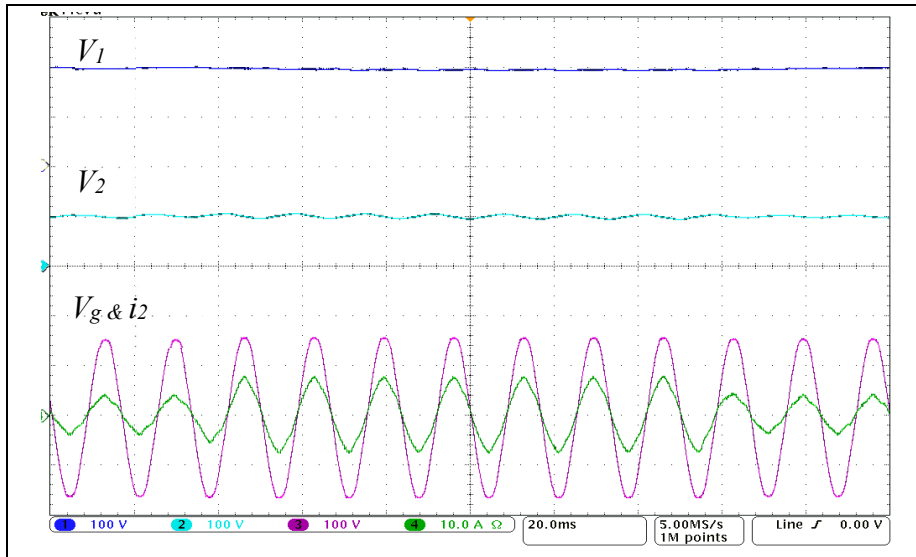


Figure 2.14 Grid voltage, grid current and DC source voltage waveforms for a grid current variations from 4A to 8A and back to 4A

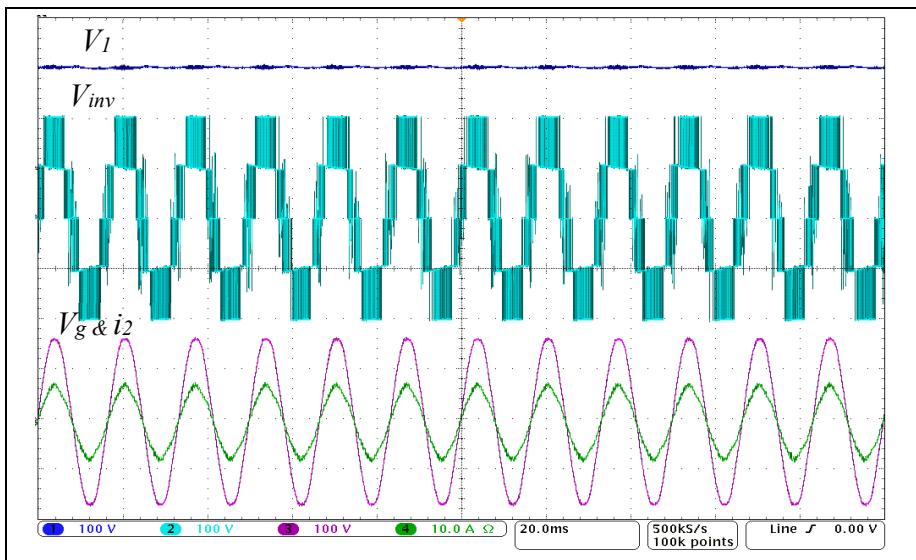


Figure 2.15 Grid voltage and current, inverter output voltage, dc bus voltage for a decrease in grid inductance value

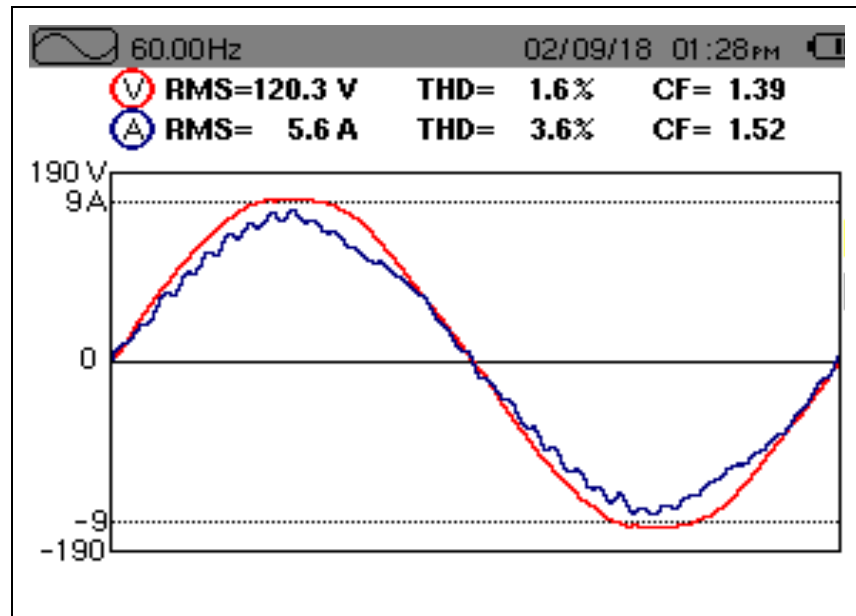


Figure 2.16 Harmonic analysis (THD) of the grid current and voltage for a decrease in grid inductance

W	+677.4	PF	+0.998
Wh	0000000		
VAR	± 0.6	DPF	+1.000
VARh	€0000000	Tan	-0.001
	‡0000000		
VA	678.7	φ	+000°
VAh	0000000		

Figure 2.17 Power analysis results when grid inductance is reduced

2.5.3 Performance under Grid Voltage Sag and Swell

Fig.18 illustrates the results when sudden sag is occurred. One sees that the grid voltage is decreased by 17% of its nominal value. The grid voltage is set to 120V RMS and after a sudden sag, it is decreased to 100V RMS. The grid current remains unchanged and in-phase with the grid voltage despite the grid voltage fluctuation because of accurate performance of the controller.

The system performance under grid voltage swell is shown in Figure 2.19. The grid voltage is increased from the value 120 to 130V RMS. The grid current amplitude is under control acceptably and a synchronization with the grid voltage is observed. The DC voltage V_2 are stabilized and not affected by this disturbance.

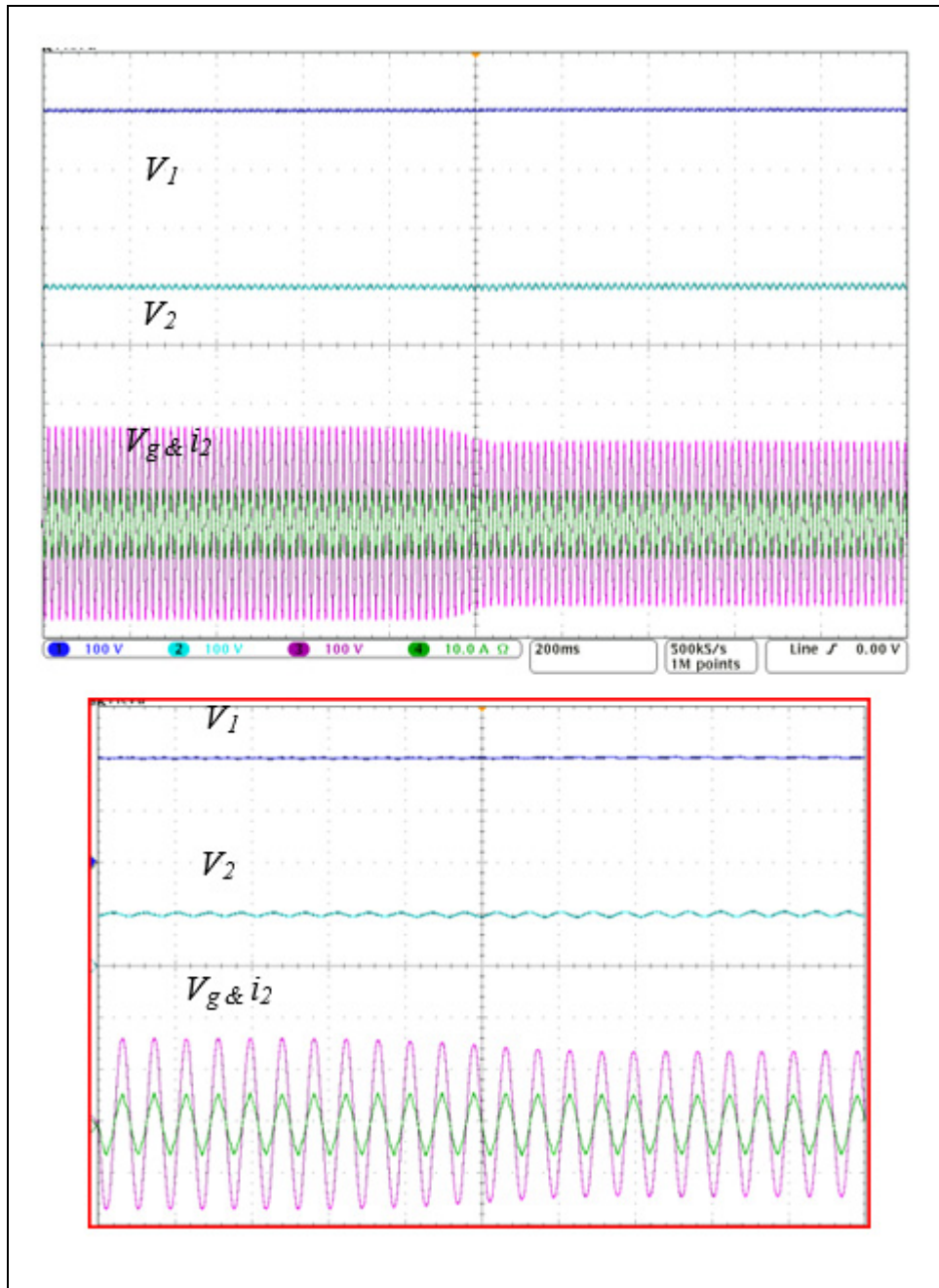


Figure 2.18 Grid voltage and current, DC voltage under grid voltage sag

2.5.4 Performance under DC Voltage Variation

In this test, the performance of the PUC5-LCL was studied under DC voltage variation.

Figure 2.20 shows an increase of 20 V in DC voltage applied to the system, the results show the robustness of the controller with low THD, unit power factor at the grid and lower dc voltage ripples. Furthermore, the sensor-less voltage balancing operated well in order to keep the capacitor voltage at half of the DC voltage. As well, the PUC5-LCL continues to inject a sinusoidal current to the grid due to the robustness of the LQRI controller.

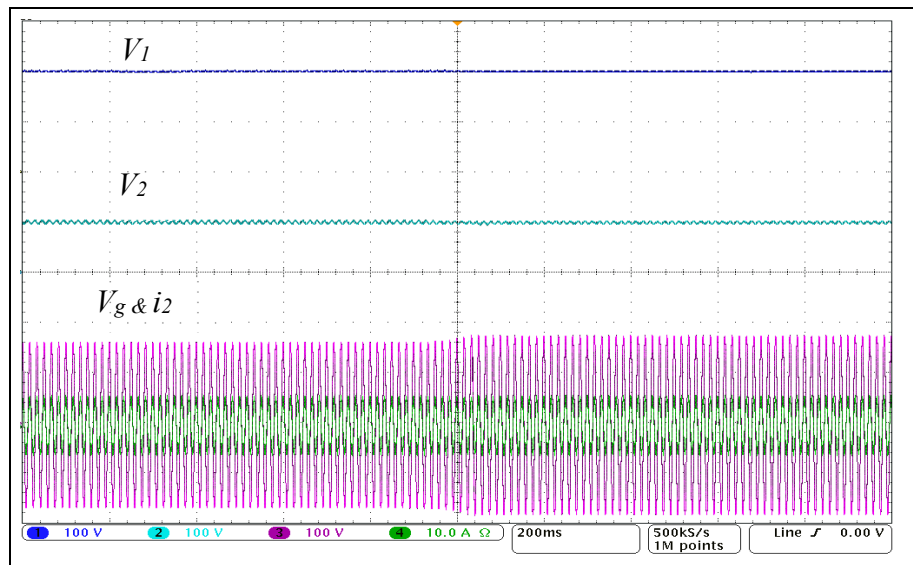


Figure 2.19 Grid voltage and current, DC voltage under grid voltage swell

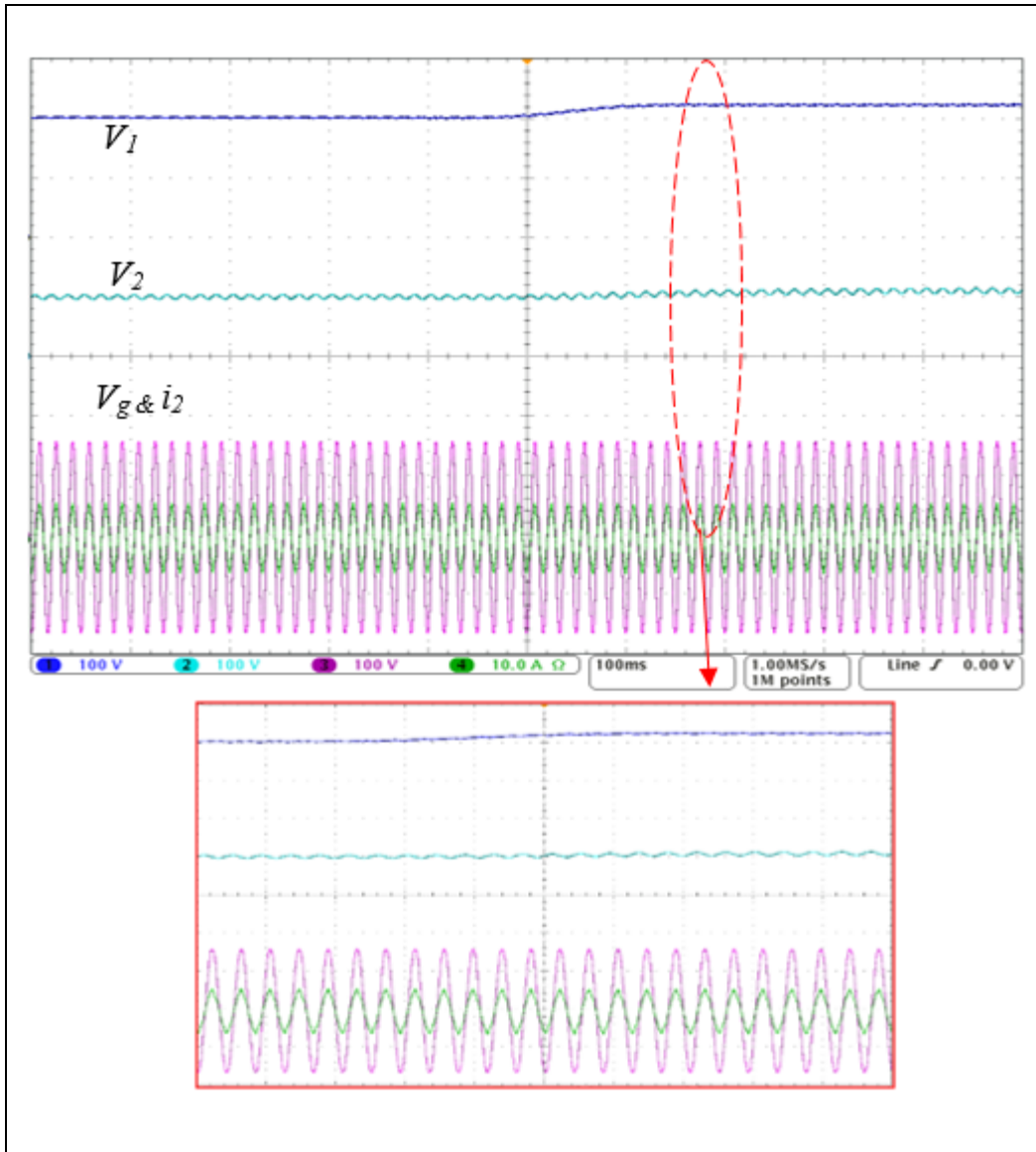


Figure 2.20 Performance under DC voltage variation from 200V to 220

2.6 Conclusion

In this paper, the optimal control of single-phase grid-connected PUC5 inverter with LCL passive filter based on LQRI controller has been proposed. The PUC5-LCL is modelled in d-q frame. Furthermore, the design and practical implementation results of the LQRI controller implemented on a dSPACE ds 1103 to demonstrate and to validate this study. The practical results show acceptable performances of the proposed controller in steady state and transients

with low THD of the grid current and unity power factor operation. The satisfactory dynamic behavior of the controller under grid current variations was also experimentally tested. Moreover, the robustness of the controller has been confirmed during large grid impedance reduction and sudden changes in the AC and DC voltages. Eventually, it can be concluded that the designed LQRI controller operates properly on the PUC5 inverter with LCL filter to inject clean active power into the grid.

CHAPTER 3

A MULTIFUNCTIONAL SINGLE-PHASE GRID-INTEGRATED RESIDENTIAL SOLAR PV SYSTEMS BASED ON LQR CONTROL

Naima Arab^a, Bachir Kedjar^a, Alireza Javadi^a, and Kamal Al-Haddad^a

^a Department of Electrical Engineering, École de Technologie Supérieure, 1100
Notre-Dame West, Montreal, Quebec, Canada H3C 1K3

This chapter has been published in Transactions on industry applications, vol. 55, no. 2,
pp. 2099-2109, March-April 2019

Abstract

This chapter presents a multifunctional single-stage residential photovoltaic power supply based on Linear Quadratic Regulator. The system makes use of a single-phase power converter connected to the grid through an LCL filter. A robust LQRI controller is designed to incorporate added functions such as power line conditioner, active power regulator, and voltage stabilizer. The perturb and observe (P&O) algorithm is used to generate the reference signal for the fluctuating DC bus voltage as well as to extract the maximum power from the solar panels. Full modeling of the converter in the D-Q reference frame is presented. A Linear Quadratic Regulator with added integral action (LQRI) is designed to achieve optimal multifunctionality operation of the residential power supply. Simulation and experimental results confirm the expected performance of the proposed controller for insolation and load variations.

3.1 Introduction

The increasing demand of electric energy in the world has boosted the productivity and the multiple use of renewable energy. The solar photovoltaic (PV) array is among the most important renewable sources used for power generation. Forecasts predict that in 2018 more

than 68.6 GW of the electric power will be provided from solar PV systems (Masson, Orlandi, & Reking, 2014).

Growing interest in grid-integrated PV system is becoming more and more important, where two types of grid connected residential photovoltaic converters are used; the first uses single stage conversion and the second uses a cascaded of two conversion stages (Silva, Sampaio, Oliveira, & Durand, 2017). The two stages topology uses a dc to dc followed by a dc to ac converters; whereas the single stage, PV systems use a direct dc to ac converter which is assumed to have better performance and higher efficiency than the cascaded converters topologies (Barnes, Balda, & Stewart, 2012). Due to the drawbacks of two-stage conversion schemes, the single-stage PV systems attracted the attention of many researchers especially for low-voltage grid applications meant to distribution systems. Single-stage single phase grid integrated PV system based on fuzzy logic controller has been proposed in (Alajmi, Ahmed, Adam, & Williams, 2013); where the control of the active current injected to the grid is realized with a resonant controller (PR). Moreover, in (Meza, Biel, Jeltsema, & Scherpen, 2012) a control scheme based on nonlinear adaptive controller is proposed for single-stage grid integrated PV system; where the study demonstrates similar performance with those obtained using a linear controller. In (Lal & Singh, 2016) an MPPT algorithm is proposed based on modified particle swarm optimization (PSO) associated with additional control schemes in order to improve the usability and performance of single stage grid integrated PV systems. Furthermore, in (Mirhosseini, Pou, & Agelidis, 2015) the authors proposed a control strategy for single-stage and two-stage grid connected inverters with some modifications in the control to improve the system functionalities under abnormal conditions where the dc bus voltage is regulated naturally in single stage, in contrary to two stage conversion scheme. In (Pradhan, Hussain, Singh, & Panigrahi, 2017) a single-stage PV system connected to the grid is proposed with modified variable step size (VSS-LMS) based control to improve the performance of the studied configuration.

Moreover, in order to insure power quality enhancement, solar PV system (SPV) in the distributed generation, active power filters (Rahmani, Al-Haddad, & Kanaan, 2008), and series

compensators (Javadi, Hamadi, Ndtoungou, & Al-Haddad, 2017) are used. However, shunt active power filters are introduced with SPV systems to deal with power quality issues caused by the constant increase of power converters integrated to the distribution systems.

In order to respect grid's connection standards, passive filter is required between the inverter and the network. The passive filter role is to help reduce the amplitude of harmonic currents injected into the grid at the point of common coupling (PCC) (Fang, Xiao, Yang, & Tang, 2017). Despite its benefits, LCL filters have their own drawbacks such as resonance and dependence on network and neighbouring impedances. To overcome these problems, active and passive damping are usually applied to give better performance to the actual passive configuration. Most of these methods are applied to grid connected converters (Houari et al., 2014)-(Komurcugil, Bayhan, & Abu-Rub, 2017), and those that are applied to shunt active power filter (SAPF) are barely mentioned and discussed (Q. Liu et al., 2014), (Fang et al., 2017), (Fujita, 2009).

In most applications targeting SPV connected to the distribution system (Silva et al., 2017),(Tuyen & Fujita, 2015)-(Y. Singh, Hussain, Singh, & Mishra, 2017), where in (Devassy & Singh, 2017) a unified power quality conditioner (UPQC-SPV) with active power filter (APF) capabilities were presented as independent units not integrated into the system functionality as such. Solar PV system grid connected converters can perform the same functions assigned to those performed by shunt active power filters topologies simply by modifying the control algorithm of the SPV systems (Y. Singh, Hussain, Singh, et al., 2017). The active power filter APF functionality is introduced when insolation is unavailable as in (Y. Singh, Hussain, Singh, et al., 2017); an adaptive filter (ALCF) is used in the current control scheme.

To reduce power quality issues in the distribution system, several configurations and control schemes have been proposed in the literature (T.-F. Wu, Nien, Shen, & Chen). Moreover, most of publications were focused on the three-phase systems as in (Agarwal, Hussain, & Singh, 2017; Biricik, Komurcugil, & Basu, 2016) but those dedicated to single phase are rare. As in (Geury, Pinto, & Gyselinck, 2015) the functionalities of SPV systems and APF were combined.

The model in d-q reference frame is carried out to design better controllers (Arab, Kedjar, & Al-Haddad, 2016; Arab, Kedjar, Javadi, & Al-Haddad, 2017; Bahrani et al., 2011; Disha, Prabhu, Chaithra, & Suryanarayana, 2016; Khadkikar & Chandra, 2012; Khadkikar, Singh, Chandra, & Singh, 2010), and the proposed controller is designed in order to eliminate harmonics, and ensure unity power factor at the grid. The LQR controller is a good candidate for this application since it ensures fast dynamic response, robustness, low THD, unit power factor, and simplicity to fine-tune its gains (Arab et al., 2016)-(Kedjar, Kanaan, & Al-Haddad, 2014b). The proposed system encompasses the additional APF capabilities in grid integrated PV systems. A multifunctional grid-interfaced SPV systems operate as APF when the available active power is reduced mainly because of irradiation availability; improving consequently the power quality of the AC distribution system by avoiding possible interaction and coupling between neighbouring installations. Therefore fourth contributions are presented in this work and are as follows:

- The use of linear quadratic regulator to find the optimal controller gains by choosing the optimal values of R and Q matrices in order to minimize the control energy and enhance the stability of the system.
- The integration of active damping in the LQR control allows avoiding the use of damping resistor of LCL filter and improves the quality of the compensation by reducing the current switching ripples in the grid side.
- The proposed LQR control approach eliminates the use of PI controller for DC-link voltage.
- The feed-forward controller is used in the direct current control scheme in order to insure fast dynamic response.

This chapter is organized as follows. After full modeling of the converter, the linearized model of single-phase SPV-APF is presented in section 3.2. The design of the LQR controller with integral action added is presented in detail in section 3.3. In section 3.4, simulation and experimental results obtained using Matlab/Simulink/SPS and the implementation of LQRI

controller in a DS1103 of dSPACE are presented and discussed. Finally, a conclusion along with a discussion is given.

3.2 Modeling OF SPV-APF-LCL

The single-stage solar photovoltaic grid integrated residential systems illustrated by Figure 3.2 consists of SPV panel, a VSI, an LCL filter feeding linear and nonlinear residential loads.

-The single phase inverter with LCL filter (VSI-LCL) is coupled with nonlinear loads, which consist of diode bridges feeding inductive loads and an $R-L$ branches, which represents the linear load.

-The passive filter (LCL) is composed of inductance L_1 , inductance L_2 and capacitance C .

-SPV array and C_{dc} is the dc bus capacitor.

3.2.1 LCL Filter Design

The value of inverter side inductor L_1 is expressed as:

$$L_1 = \frac{mV_{dc}}{4a f_{sw} \Delta i_o} = \frac{200}{4 \times 1.2 \times 10^3 \times 1.35} = 3.08mH. \quad (3.1)$$

Δi_o is the maximum ripple that is expected in the current i_1 , f_{sw} is the switching frequency, and m represents the modulation index.

The value of L_1 is taken as 2.5mH.

The grid side inductance L_2 is calculated in the following:

$$L_2 = r L_1 \quad (3.2)$$

The value of L_2 is taken equal to L_1 .

Filter capacitor value is calculated as:

$$C = \alpha C_b = 0.01 \times 212.2 \mu F = 2.12 \mu F. \quad (3.3)$$

Where:

$$C_b = \frac{1}{\omega z_b} = \frac{1}{377 \times 12.5} = 212.2 \mu F. \quad (3.4)$$

C_b and Z_b are the base capacitance and inductance respectively.

The value of the filter capacitor is taken as $2.5 \mu F$.

In three phase-system Park transformation is generally used to obtain the d-q model that helps designing system controllers using linear or non-linear techniques. In order to apply this concept to single-phase systems the imaginary circuit should be created from the real variables (Figure 3.3) as in (Bahrani et al., 2011). The measured variables represent the real circuit and in order to create the imaginary circuit the variables were shifted by 90° to obtain their equivalent components in the α - β reference frame.

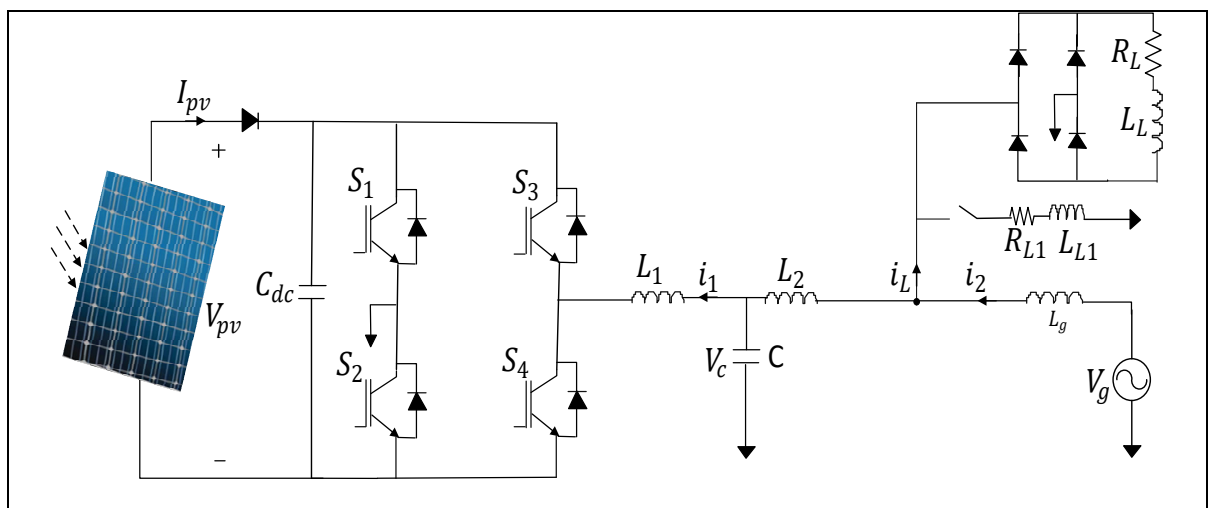


Figure 3.2 Electrical scheme of the system under study

$$\frac{d}{dt} \begin{bmatrix} i_{1d} \\ i_{1q} \\ i_{2d} \\ i_{2q} \\ v_{cd} \\ v_{cq} \\ v_{dc} \end{bmatrix} = \begin{bmatrix} -\frac{R_1}{L_1} & \omega & 0 & 0 & -\frac{1}{L_1} & 0 & 0 \\ -\omega & -\frac{R_1}{L_1} & 0 & 0 & 0 & -\frac{1}{L_1} & 0 \\ 0 & 0 & -\frac{R_2}{L_2+L_g} & \omega & \frac{1}{L_2+L_g} & 0 & 0 \\ 0 & 0 & \frac{R_2}{L_2+L_g} & -\omega & 0 & \frac{1}{L_2+L_g} & 0 \\ \frac{1}{C} & 0 & -\frac{1}{C} & 0 & 0 & \omega & 0 \\ 0 & \frac{1}{C} & 0 & -\frac{1}{C} & -\omega & 0 & 0 \\ \frac{D_d}{C_{dc}} & \frac{D_q}{C_{dc}} & 0 & 0 & 0 & 0 & 0 \end{bmatrix} \begin{bmatrix} i_{1d} \\ i_{1q} \\ i_{2d} \\ i_{2q} \\ v_{cd} \\ v_{cq} \\ v_{dc} \end{bmatrix} + \begin{bmatrix} 0 & 0 \\ 0 & 0 \\ -\frac{V_{dc}}{L_1} & 0 \\ 0 & -\frac{V_{dc}}{L_1} \\ 0 & 0 \\ 0 & 0 \\ \frac{I_d}{C_{dc}} & \frac{I_q}{C_{dc}} \end{bmatrix} \begin{bmatrix} d_d \\ d_q \end{bmatrix} + \begin{bmatrix} \frac{1}{L_1} & 0 \\ 0 & \frac{1}{L_1} \\ 0 & 0 \\ 0 & 0 \\ 0 & 0 \\ 0 & 0 \\ 0 & 0 \end{bmatrix} \begin{bmatrix} v_{gd} \\ v_{gq} \end{bmatrix} \quad (3.7)$$

Where, i_{1d} , i_{1q} and i_{2d} , i_{2q} are the APF output current and grid current components, v_{cd} , v_{cq} are the capacitor voltage in d-q frame, v_{dc} is the dc bus voltage, v_{gd} and v_{gq} are the grid voltage in d-q, d_d , d_q are the duty cycle components.

The linearized small signal model around an operating point is represented by (3.8):

$$\frac{dx_{\square}}{dt} = Ax_{\square} + Bu_{\square} + Ev_{\square} \quad (3.8)$$

A, B, and E are the matrices of the linearized small signal model

which represent respectively the state, control and disturbance matrices of the system.

x , u , and v are the states variables, control input, and disturbance vectors of the system respectively.

$$x = \begin{bmatrix} i_{1d\square} & i_{1q\square} & i_{2d\square} & i_{2q\square} & v_{cd\square} & v_{cq\square} & v_{dc} \end{bmatrix}^T, \quad u = \begin{bmatrix} d_{d\square} & d_{q\square} \end{bmatrix}^T, \quad v_g = \begin{bmatrix} v_{gd\square} & v_{gq\square} \end{bmatrix}^T \quad (3.9)$$

3.3 Controller Design and Implementation

The linear quadrature regulator (LQR) is a well-reputed method that affords the feedback gains by optimizing the control signal $u = -Kx$ which is determined firstly by minimizing the cost

function and secondly by a good selection of the matrices R and Q ; the cost function J is as presented in the following (Arab et al., 2016)-(Kedjar et al., 2014b) :

$$J = \int_0^{\infty} (x^T Q x + u^T R u) dt \quad (3.10)$$

Where $Q \geq 0$ and $R > 0$, are symmetric, definite positive matrices; where these last are the state and control weighting matrices. The Q and R matrices are a tradeoff between the energy of the control law and the controlled output energy (Liebst & Robinson, 1991). As it is well known for the LQR control, the higher the R values, the lower the control effort and the higher the Q values, the shorter the transient regimes for the respective states.(Engleitner et al., 2016; Engleitner, Nied, Cavalca, & Costa, 2018).

The controller optimal gains are calculated by (3.11):

$$K = R^{-1} B^T P \quad (3.11)$$

The cost function J is minimized in order to find the steady-state solution of the Riccati equation shown in (3.12) (Kedjar & Al-Haddad, 2009b):

$$A^T P + PA - PBR^{-1}B^T P + Q = 0 \quad (3.12)$$

Where P is the solution of the Riccati equation which is required to compute the optimal feedback gain K .

In order to insure good performance, the method that consists of adding integral feedback to ensure zero errors in steady state is used. The basic approach of the added integral feedback is to create integral states within the controller to compute the integral of the signal error, and this is why three new states are added in the linearized model of the proposed system. These states are the integral of the currents along d axis (i_{1d}) and q axis (i_{1q}), and dc bus voltage (V_{dc}). Therefore, ten states are obtained as shown by the vector x presented hereafter.

$$\frac{dx_{\square}}{dt} = Ax_{\square} + Bu_{\square} + Ev_{\square} \quad (3.13)$$

$$x_{\square} = \left[i_{1d\square} \ i_{1q\square} \ i_{2d\square} \ i_{2q\square} \ v_{cd\square} \ v_{cq\square} \ v_{dc} \ \int i_{1d} \ \int i_{1q} \ \int v_{dc} \right]^T$$

$$u = \left[d_{d\square} \ d_{q\square} \right]^T, \quad v_g = \left[v_{gd\square} \ v_{gq\square} \right]^T$$

Where the matrices of the linearized model can be expanded as:

$$A = \begin{bmatrix} \frac{-R_1}{L_1} & \omega & 0 & 0 & \frac{-1}{L_1} & 0 & 0 & 0 & 0 & 0 \\ -\omega & \frac{-R_1}{L_1} & 0 & 0 & 0 & \frac{-1}{L_1} & 0 & 0 & 0 & 0 \\ 0 & 0 & \frac{-R_2}{L_2+L_g} & \omega & \frac{1}{L_2+L_g} & 0 & 0 & 0 & 0 & 0 \\ 0 & 0 & -\omega & \frac{-R_2}{L_2+L_g} & 0 & \frac{1}{L_2+L_g} & 0 & 0 & 0 & 0 \\ \frac{1}{C} & 0 & \frac{-1}{C} & 0 & 0 & \frac{-1}{C} & 0 & 0 & 0 & 0 \\ 0 & \frac{1}{C} & 0 & \frac{-1}{C} & -\omega & 0 & 0 & 0 & 0 & 0 \\ \frac{D_d}{C_{dc}} & \frac{D_q}{C_{dc}} & 0 & 0 & 0 & 0 & 0 & 0 & 0 & 0 \\ 1 & 0 & 0 & 0 & 0 & 0 & 0 & 0 & 0 & 0 \\ 0 & 1 & 0 & 0 & 0 & 0 & 0 & 0 & 0 & 0 \\ 0 & 0 & 0 & 0 & 0 & 0 & 1 & 0 & 0 & 0 \end{bmatrix}, B = \begin{bmatrix} 0 & 0 \\ 0 & 0 \\ -\frac{V_{dc}}{L_1} & 0 \\ 0 & -\frac{V_{dc}}{L_1} \\ 0 & 0 \\ 0 & 0 \\ 0 & 0 \\ 0 & 0 \\ 0 & 0 \\ 0 & 0 \end{bmatrix}, E = \begin{bmatrix} \frac{1}{L_1} & 0 \\ 0 & \frac{1}{L_1} \\ 0 & 0 \\ 0 & 0 \\ 0 & 0 \\ 0 & 0 \\ 0 & 0 \\ 0 & 0 \\ 0 & 0 \end{bmatrix} \quad (3.14)$$

The system output equation is as follows:

$$y_{\square} = C x_{\square} \quad (3.15)$$

$$y_{\square} = \left[i_{1d\square} \ i_{1q\square} \ v_{dc} \right]$$

The output matrix is given by (3.16):

$$C = \begin{bmatrix} 1 & 0 & 0 & 0 & 0 & 0 & 0 & 0 & 0 & 0 & 0 \\ 0 & 1 & 0 & 0 & 0 & 0 & 0 & 0 & 0 & 0 & 0 \\ 0 & 0 & 0 & 0 & 0 & 0 & 1 & 0 & 0 & 0 & 0 \end{bmatrix} \quad (3.16)$$

The state weighting matrix is depicted by (3.17)

$$Q = \text{diag}(Q_{i_d}, Q_{i_q}, Q_{i_{2d}}, Q_{i_{2q}}, Q_{v_{cd}}, Q_{v_{cq}}, Q_{v_{dc}}, Q \int i_d, Q \int i_q, Q \int v_{dc}) \quad (3.17)$$

The control weighting matrix R is given by (3.18):

$$R = W \begin{bmatrix} 1 & 0 \\ 0 & 1 \end{bmatrix} \quad (3.18)$$

Moreover, the current approach of selecting the matrices Q and R is carried out by test and error to find the desired response. In this case, the matrices Q and R values are iterated until finding the controller gains that stabilizes the system.

One varies $Q=1, 10, 10^3, 10^5$ until 10^9 and keeping $R=1$. Every variation of Q , the new gains of the controller are calculated.

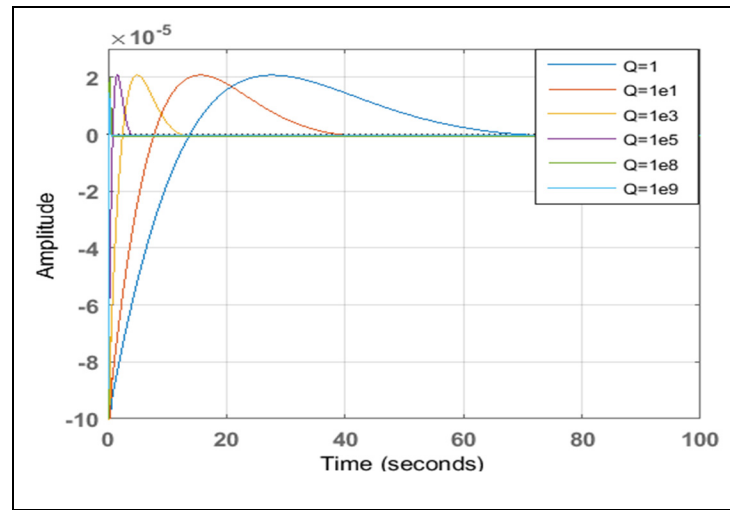


Figure 3.4 Design of LQR control with fixed R and iterating Q

One remark when Q is increased, the step response of the closed system becomes faster, and it reaches very fast the steady state, which means that less energy is needed.

Now varying $R=10^{-3}$, 10^{-2} , 10^{-1} , 1, 10, 10^2 and 10^3 and keeping $Q=10^9$. Every variation of R , the new gains of the controller are also calculated.

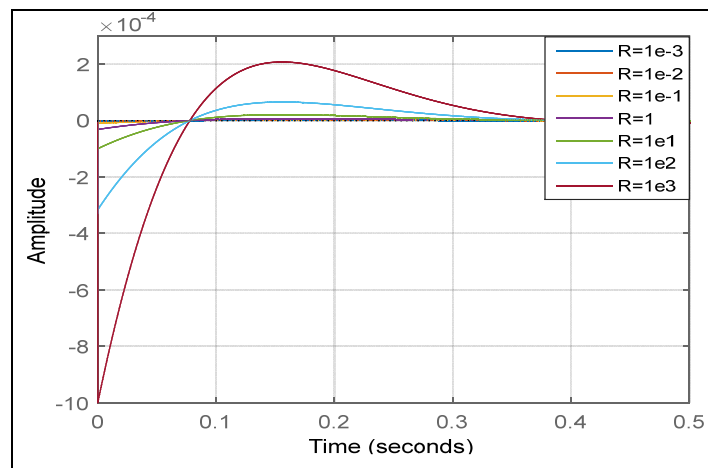


Figure 3.5 Design of LQR control for fixed Q (large value) and iterating R

One remark when R is decreased, the step response of the closed system becomes slower, so for fast response, the value of R is equal to 10^{-3} .

The optimal gains of the controller for all variables of the system (V_{cd} , V_{cq} , i_{1d} , i_{1q} , i_{2d} , i_{2q} , V_{dc}) which satisfy further control specifications such as the output current THD are exposed in the following:

$$Q_{i_{1d}} = Q_{i_{1q}} = 5e6 \text{ c.u.} / A^2, Q_{i_{2d}} = Q_{i_{2q}} = 5e6 \text{ c.u.} / A^2,$$

$$Q_{v_{cd}} = Q_{v_{cq}} = Q_{v_{dc}} = 1e3 \text{ c.u.} / V^2, Q \int i_{1d} = Q \int i_{2d} = 1e9 \text{ c.u.} / A^2,$$

$$Q \int V_{dc} = 1e9 \text{ c.u.} / V^2, W = 1 \text{ c.u.}$$

$$k_p = 1.0e+03 *$$

$$-0.4207 \ 0.0001 \ -1.0002 \ -0.0000 \ 0.0429 \ 0.0000 \ -0.4691$$

$$-0.0002 \ -0.4188 \ -0.0000 \ -1.0002 \ 0.0000 \ 0.042 \ -0.0134$$

$$k_i = 1.0e+04 *$$

$$0.0000 \ 0.2020 \ -0.7068$$

$$0.0004 \ -7.0682 \ -0.0202$$

The stability of the closed-loop feedback system is determined primarily by the location of the eigenvalues of the matrix $(A - BK)$, which are equal to the closed-loop poles.

Figure 3.6 shows the pole placement of the closed loop eigenvalues.

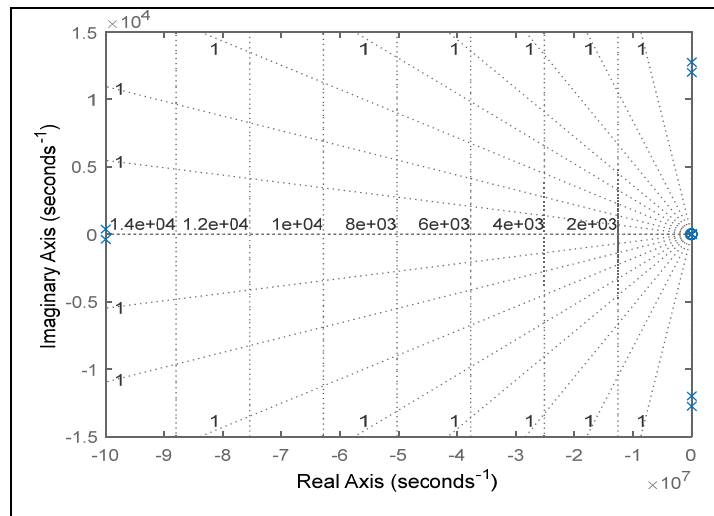


Figure 3.6 Placement of the closed-loop eigenvalues

One can observe that the poles of the closed loop, lie in left-half plane and therefore, the system is stable.

Supposing that the VSC is an ideal converter where the losses are neglected, therefore the obtained steady state current components can be computed and are given as follows:

$$I_{1d}, I_{2d} \neq 0, I_{1q}, I_{2q} = 0.$$

This allows obtaining the static duty cycles as follows:

$$D_d = \frac{V\sqrt{2}}{V_{dc}}, D_q = 0.$$

The feed-forward term is used in order to have fast response (Silva et al., 2017). In this work, the similar feed-forward proposed in (Biricik et al., 2016) with the direct current control scheme based on LQR control is used.

The active current of the PV injected to the grid is estimated as (Luo, Chen, Shuai, & Tu, 2013):

$$I_f = \frac{2P_{pv}}{V_m} \quad (3.19)$$

Where,

P_{pv} : power of SPV.

V_m : the peak amplitude of grid voltage.

V_m is calculated as,

$$V_m = \sqrt{V_d^2 + V_q^2} \quad (3.20)$$

The implementation scheme of the proposed controller in Matlab/Simulink is shown in Figure 3.3. Grid current, converter output current and filter capacitor voltage are measured and phase shifted by 90° using equation (3.5) in order to obtain their corresponding values in α - β frame;

where the equation (3.5) is implemented in dSPACE1103 to obtain 90-degree shift uses a delay input; for 90° corresponds to $1/(4*60)$. To shift a signal with 90° , a delay block Z^{-n} is used ($n=100$). Thereafter, a second transformation on the same variables to $d-q$ components is applied using the T matrix transformation. The phase-locked loop outputs (ωt) signal (Figure 3.7) is used in the T transformation to obtain the components in $d-q$ reference frame. The generation of the shunt active filter reference current i_{ld}^* is obtained by adding both the active current i_{ff} generated by the PV using (3.19), to the extracted oscillating component of the load current i_L . The optimal variation of the DC bus voltage as to ensure maximum power extraction from the PV is realized with the help of perturb and observe algorithm P&O. Therefore, the measured dc bus voltage signal V_{dc} is compared to a precomputed V_{dc}^* obtained from the output of MPPT block as shown in Figure 3.3. The errors signals that are resulting from the comparison of all measured variables (V_{cd} , V_{cq} , i_{ld} , i_{lq} , i_{2d} , i_{2q} , V_{dc}) with their corresponding references in $d-q$ frame are sent to the input of the LQRI controller. Moreover, in order to generate the duty cycle components in $\alpha-\beta$ coordinates, the outputs of the LQRI found in $D-Q$ frame, are then transformed to $\alpha-\beta$ and just the first one is used as input of the PWM block to generate the gating signals of the inverter.

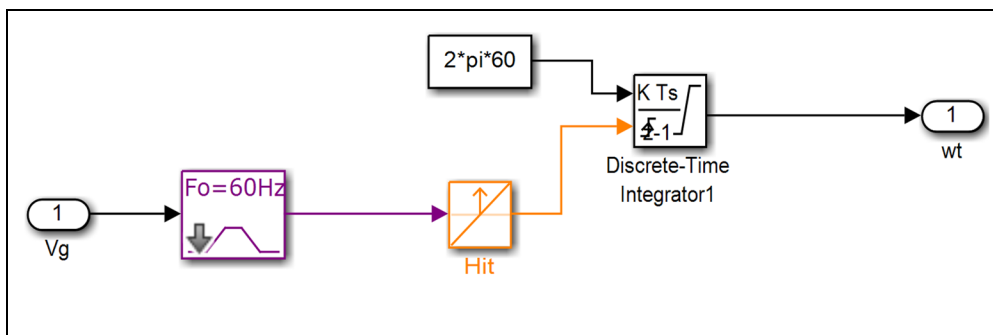


Figure 3.7 The phase-locked loop (PLL)

3.4 Simulation and Experimental Results

3.4.1 Simulation Results

The parameters used for the simulations of the power converter and the electrical system are given in Table 3.1 and Table 3.2.

Table 3.1 System parameters

Parameters	Simulation	Hardware
Grid voltage	120V	110V
DC bus voltage	250V	200V
DC bus capacitance	1200 μ F	1200 μ F
Frequency	60Hz	60Hz
Switching frequency	10kHz	10kHz
LPF cut-off frequency	30Hz	30Hz
Inverter side inductance(L_1)	2.5mH	2.5mH
Grid side inductance (L_2)	2.5mH	2.5mH
Filter capacitor (C)	2.5 μ F	2.7 μ F
Nonlinear Load (L_L)	80mH	60mH
Nonlinear load (R_L)	20 Ω	20 Ω
Linear load (L_{L1})	30mH	
Linear load (R_{L1})	30 Ω	

Table 3.2 Pv array parameters

Parameters	Value
$P_{max}(W)$	250
$V_{oc}(V)$	37.7
$I_{MP}(A)$	8.20
$V_{MP}(V)$	30.5
$I_{sc}(A)$	8.85

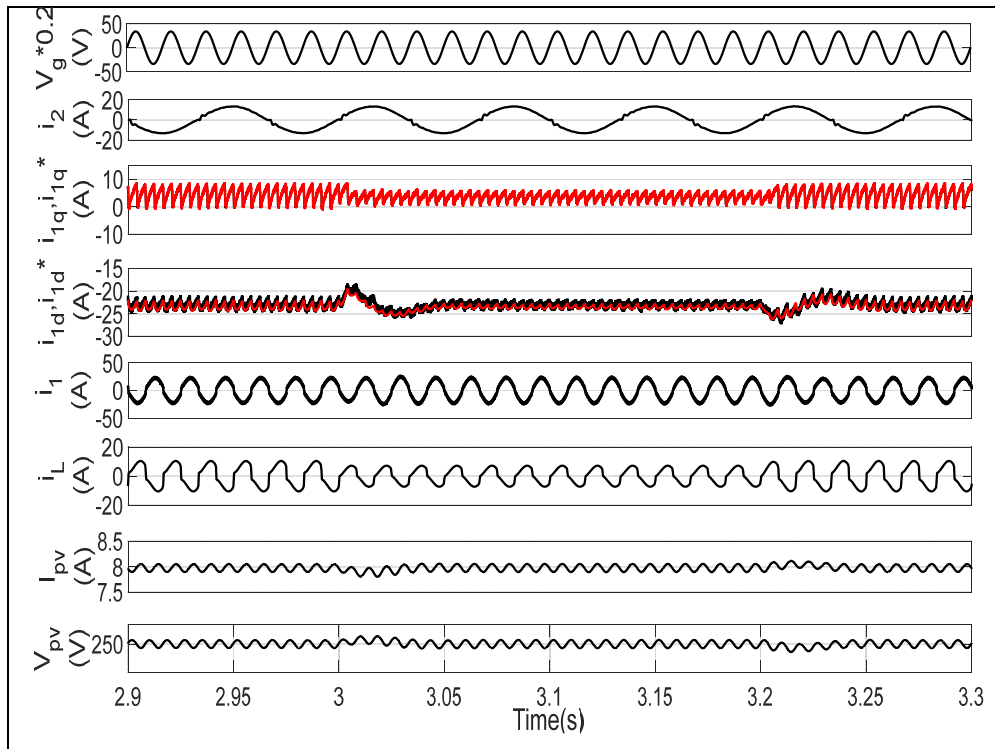


Figure 3.8 System response under load power variations

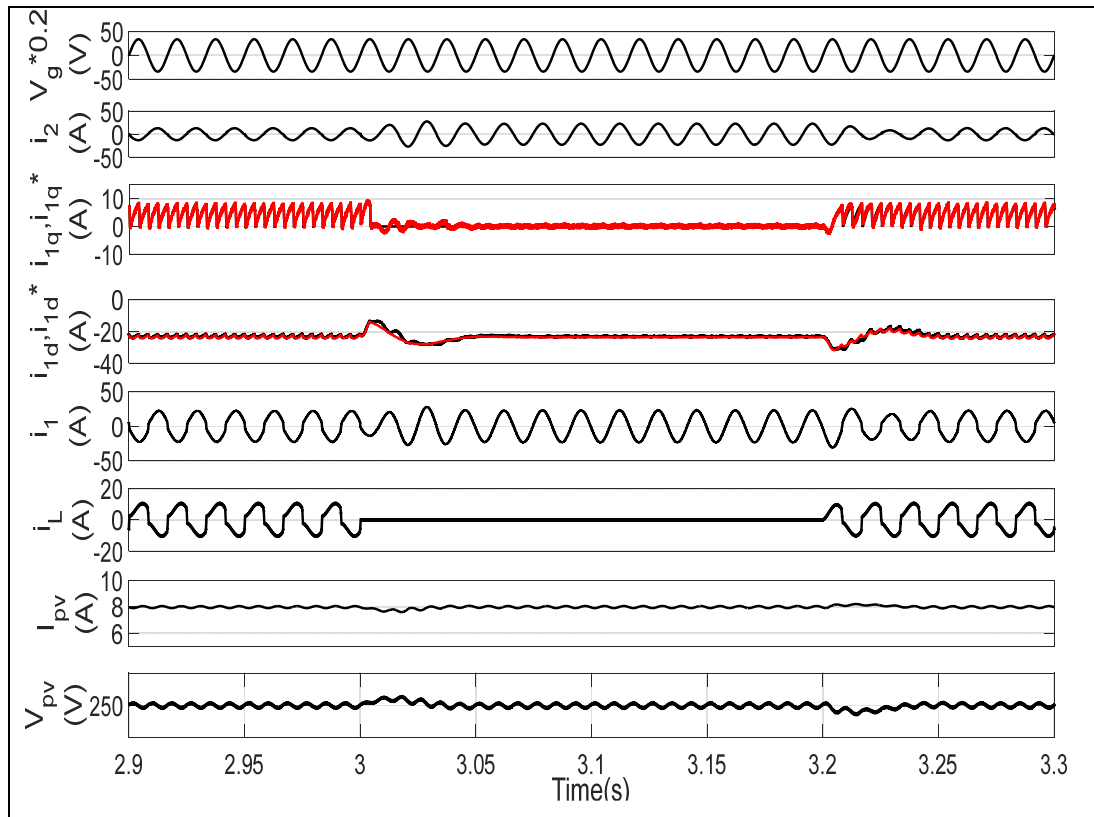


Figure 3.9 System response when load is switched on/off and off/on

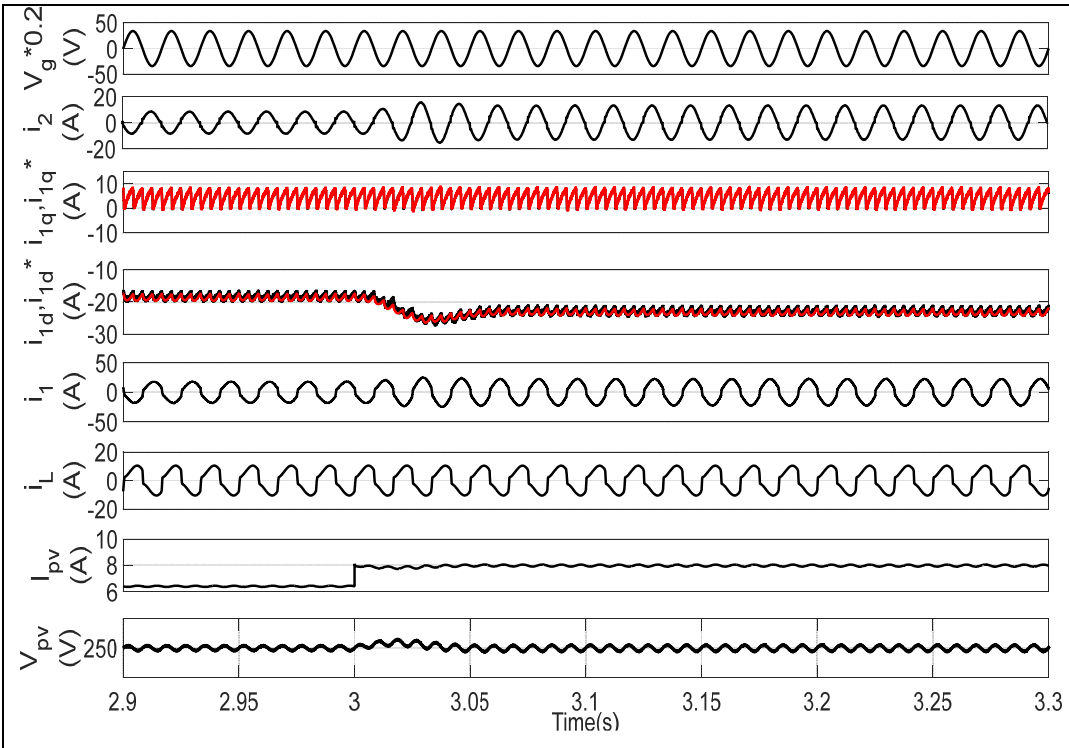


Figure 3.10 System response under insolation variations

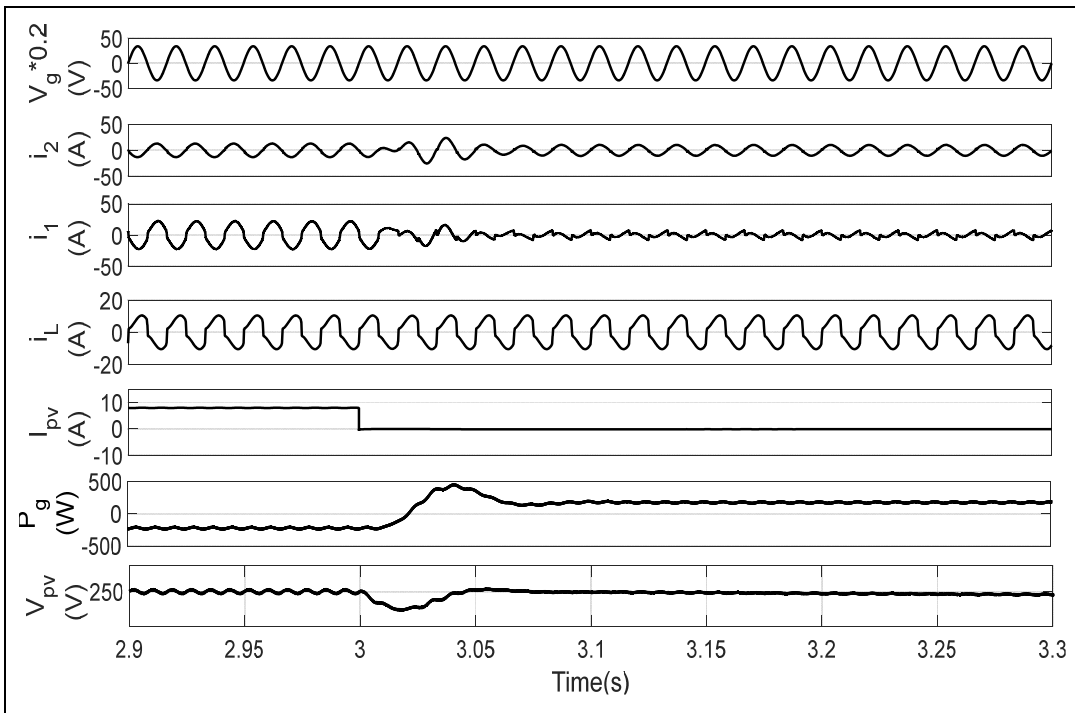


Figure 3.11 System response when insolation is switched on/off

The simulation results of single phase grid integrated solar PV systems shows different observed variables namely grid current i_2 , grid voltage v_g , converter current components (i_{ld}, i_{lq}), load current (i_L), converter current (i_l), DC bus voltage V_{dc} , SPV array current (I_{pv}) and grid power (P_g).

Four tests under linear and nonlinear load were carried out namely (load power variation, insolation variation, load switching on/off and off/on, and SPV-APF to APF transition mode). Figure 3.8 to Figure 3.11 show the obtained simulation results.

3.4.1.1 Controller Performance under Load Power Changes

The first test was carried out for optimal irradiation and different load steps. Therefore, the load power is decreased from 100 to 50% and thereafter is increased from 50% to 100% of its nominal value respectively at $t=3s$ and $t=3.2s$ as shown in Figure 3.8. The grid current is maintained sinusoidal ensuring therefore unity power factor operations of the grid converter. The exceeding P_{pv} power, which is the difference between generated and consumed power is injected into the grid.

Figure 3.9 shows the load switched on/off and then off/on at $t=3s$ and $t=3.2s$ at fixed nominal irradiation (1000 W/m^2) where all the power generated from the PV goes to the network when the load is disconnected. The inverter current components follow thoroughly their references during power variations and when the load is connected and disconnected from the PCC where the settling time is $0.03s$ demonstrating therefore the good dynamic performance of the implemented LQRI robust controller.

3.4.1.2 Controller Performance under Change in Insolation

The insolation level is increased from 800 W/m^2 to 1000 W/m^2 at $t=3s$ (Figure 3.10) and consequently it increases the magnitude of SPV current (I_{pv}) which subsequently increases SPV

power (P_{pv}). The grid current (i_2) is also increased and it is maintained sinusoidal and 180° phase shifted with the grid voltage insuring reactive powerless generator operation mode. The current components (i_{1d} and i_{1d}^*) and (i_{1q} and i_{1q}^*) follow thoroughly their references during the transient variations of insolation.

The SPV-APF to APF transition mode occurred at $t=3s$ is shown in Figure 3.11. One can observe that prior to $t=3s$, the grid current and voltage out of phase, consequently the generated power goes from the SPV to the grid. The SPV-APF feeds the loads and the excess power is automatically transferred to the grid. After $t=3s$ APF capabilities is insured when insolation is unavailable or SPV power is switched off ($P_{pv}=0$) where the DC link voltage is kept constant at its minimum reference value. The grid power (P_g) goes from negative to positive as seen well by the synchronization of grid current and voltage.

3.4.2 Comparison between proposed control and conventional p-q /d-q control

Figure 3.12 shows the comparative performance of the proposed controller with conventional vector $d-q/p-q$ control under insolation variations from 800 to 1000 W/m^2 for the same specifications and parameters.

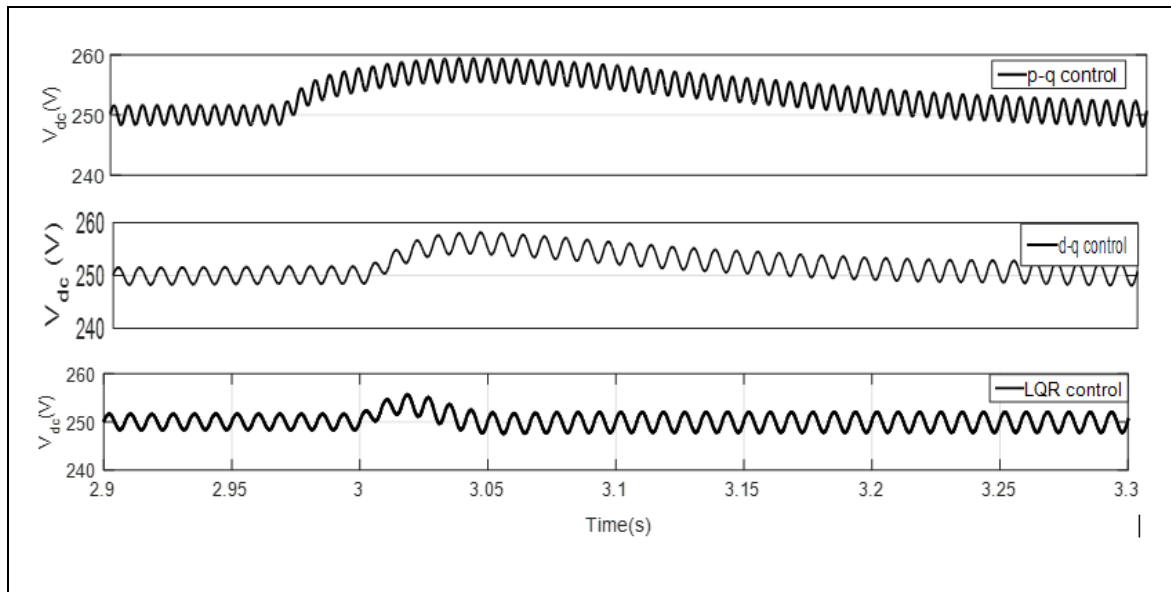


Figure 3.12 Dynamic response under insolation variations

One can see that the response of the LQR controller is accurate and fast compared to p-q and d-q control which reaches the steady state with a time response of 0.03 s. It can be clearly observed that the fastest dynamic response belonged to the LQR control and d-q control method and p-q control is the slowest control method. A comparative evaluation and analysis of both controls are shown in Table 3.3. This table clearly shows the benefits of the proposed LQR control over conventional p-q/ d-q control where a fast response is observed.

Table 3.3 Comparative study of the proposed control with d-q/p-q control

Parameter	LQR control	d-q control	p-q control
PLL	Yes	Yes	No
Complexity	Average	High	Less
Rapidity	Good	Less	Less
Accuracy	Better	Poor	Good
Time response	0.03s	0.1s	0.25s
Overshoot	2%	3%	4%
THD	3%	4.5	5

3.5 Experimental Results

A laboratory experimental setup of the presented SPV-APF-LCL for residential solar application has been built. A 1.2 kVA prototype development using a single-phase converter with LCL filter. The DS1103 of dSPACE was used for the implementation of the LQRI controller in real time. The performance of the system is evaluated during both transients and steady state operations. The gating signals are obtained using dSPACE PWM module. Figure 3.13 shows the experimental setup and its parameters are described in Table 3.1. The sampling time T_s of the controller is set to 42 μ s.

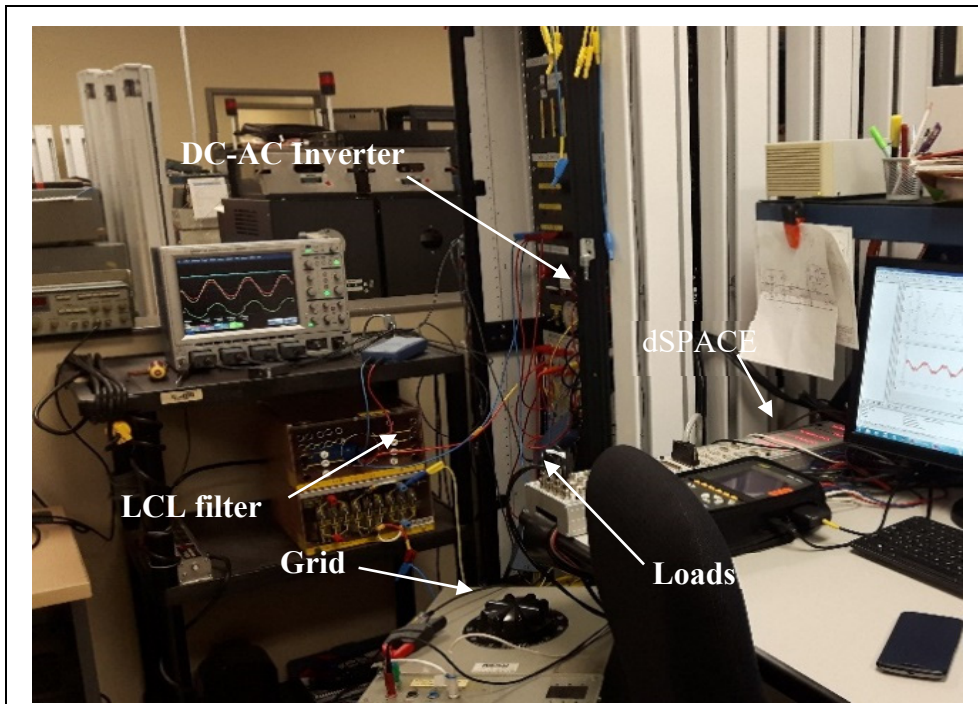


Figure 3.13 Laboratory setup

The steady state operation of the SPV-APF mode obtained with the implemented controller is shown in Figure 3.14. These results illustrate the grid voltage v_g , grid current i_2 , the dc bus voltage and inverter output current i_l . It can be observed that the grid current and voltage waveforms are 180 degrees phase shifted.

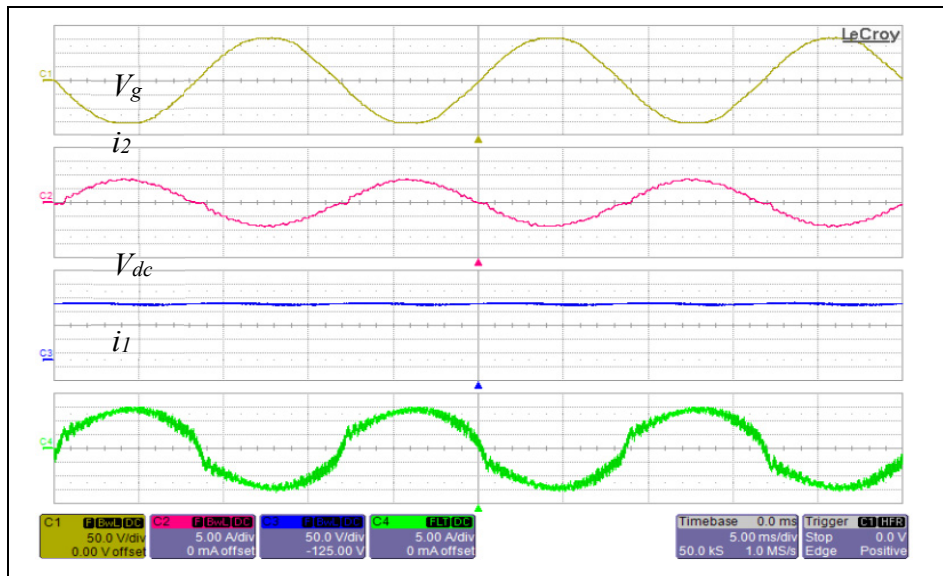


Figure 3.14 Steady state waveforms in presence of load

Figure 3.15 shows the passage from total absence of irradiation to full insolation. During this test, it can be seen that when the insolation is unavailable the inverter works as compensator as seen by the zoom and during insolation phase the grid current and voltage are out of phase. The APF to SPV-APF soft transition mode is confirmed.

Figure 3.16 shows another likely to happen insolation variations where the active current i_{ff} changed from 15A to 8A.

Figure 3.17 shows the system response for load variations. The load power has been increased from 50% to 100% and then decreased from 100% to 50% where low THD and compensation is kept under control.

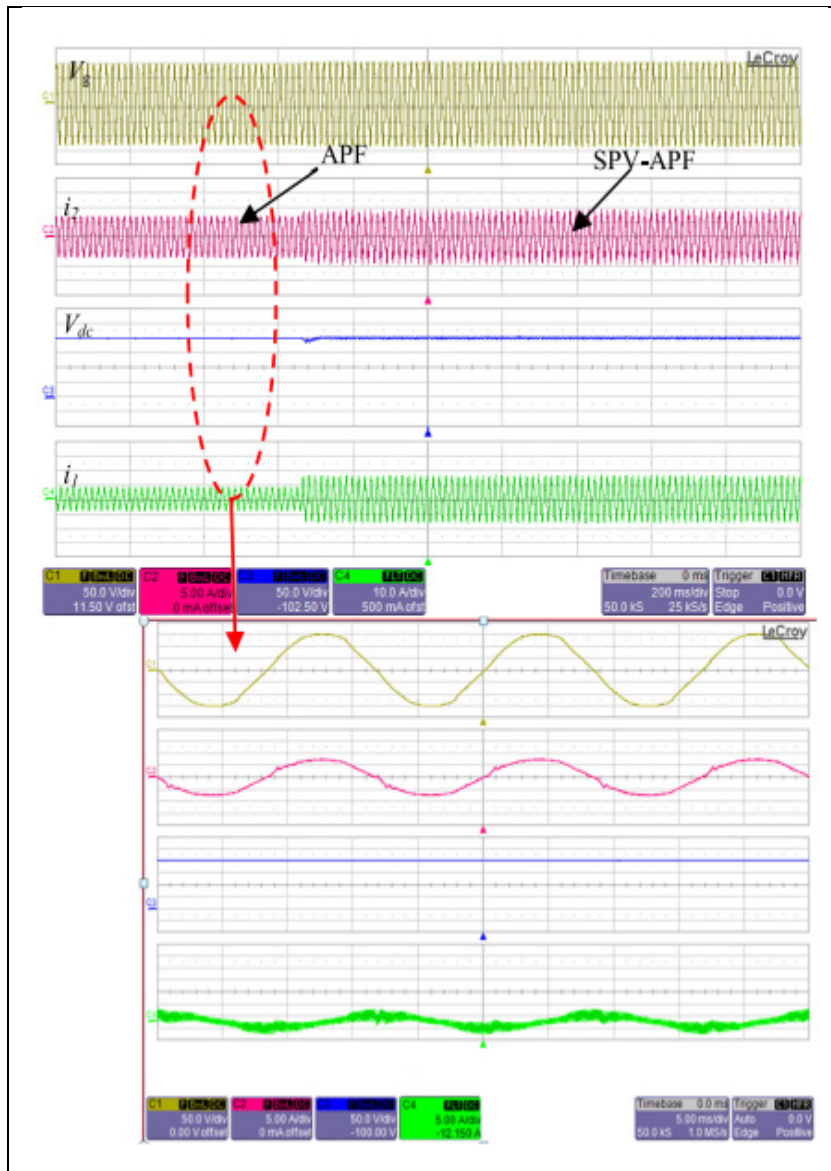


Figure 3.15 System response in the presence of load when insolation is switched on

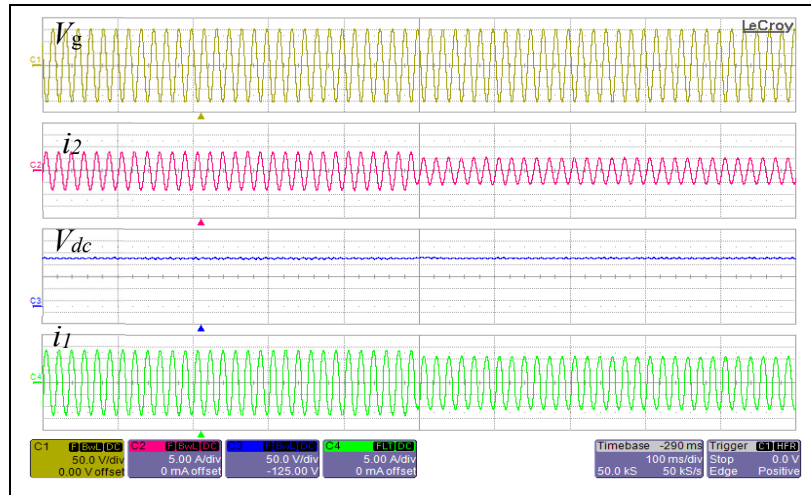


Figure 3.16 System response under insulation variations in presence of load

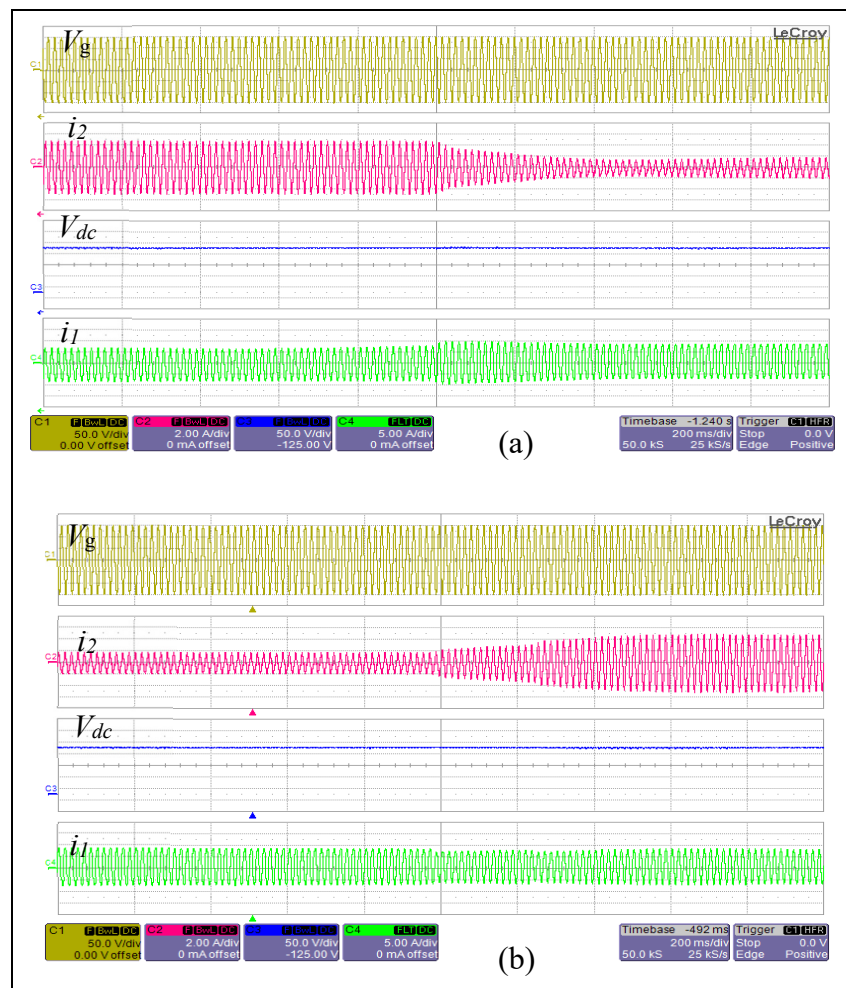


Figure 3.17 Waveforms during load variations (a) increase and (b) decrease

The THD of grid current and voltage are evaluated as 4.5% (Figure 3.18) and 2.1% respectively. The measured load current THD is 28.2% as shown in Figure 3.19. The grid current contains low THD and is still below the accepted limit of the IEEE-519 standards ("IEEE Recommended Practice and Requirements for Harmonic Control in Electric Power Systems - Redline," 2014). These results prove the good capability in terms of harmonic compensation by SPV-APF-LCL structure demonstrating therefore robustness of the proposed controller and its capability of making the system operating at unity power factor during normal mode.

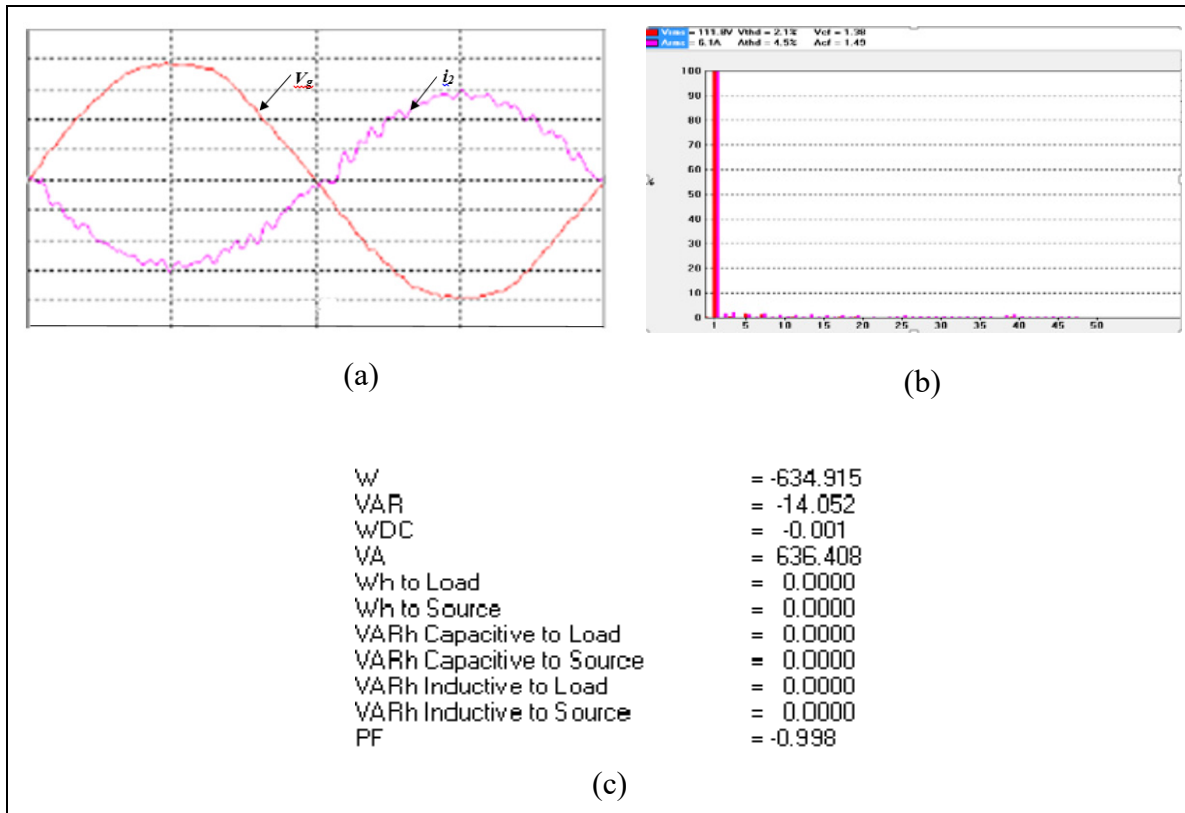


Figure 3.18 Grid voltage and current waveforms (a), harmonic spectra of grid current and grid voltage (b), numerical data of grid power and power factor (c)

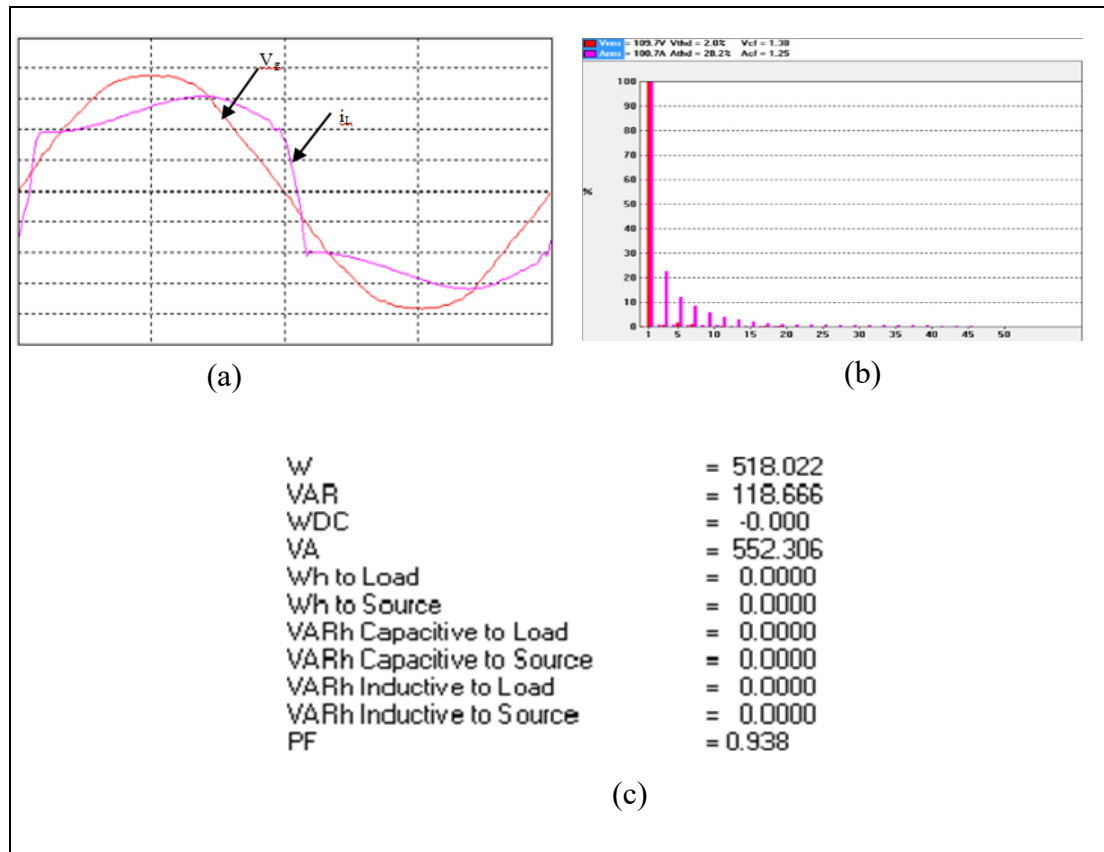


Figure 3.19 Grid voltage and load current waveforms (a), harmonic spectra of load current and grid voltage (b), numerical data of load power and power factor (c)

3.5.1 Comparison between proposed control scheme and with others existing in the literature

The proposed control scheme for grid integrated SPV system is compared with other control scheme existing in the literature (Sun et al., 2017), (Tsai-Fu, Hung-Shou, Chih-Lung, & Tsung-Ming, 2005), (Y. Singh, Hussain, Singh, et al., 2017) and are provided in Table 3.4. One can conclude from Table 3.4 that the proposed control is better and has important characteristics compared to other controllers. The proposed controller guarantees the global stability of the closed loop system, a fast dynamic response and eliminates the transient oscillations.

Table 3.4 Comparison of the proposed system with the existing work in the literature

Comparison categories	(Sun et al., 2017)	(Tsai-Fu et al., 2005)	(Luo et al., 2013)	Proposed controller
Number of stage	Two	Single	Two	Single
APF function	Not included	Included	Not included	Included
Type of coupling	LCL	L	LC	LCL
Type of damping	Active	Not reported	Passive	Active
Implementation complexity	Complicate	Moderate	Moderate	Simple
VDC ripples	High	Not reported	Not reported	Less
THD of grid current	3.67%	5%	5.2%	3%
Overshot and oscillation	Exists	Not reported	Exists	None
Stability	Not reported	Not reported	Guaranteed	Guaranteed
Dynamic response	Slow	Not reported	Fast	Fast
DC bus controller	PI controller	PI controller	PI controller	LQR controller
MPPT	IC	P&O	P&O	P&O
Model	d-q	Natural	p-q	d-q

3.6 Conclusion

This chapter presents the design and implementation of a robust Linear Quadratic Regulator scheme for a single stage multifunctional SPV-APF-LCL. The proposed robust controller is suitable for single-phase residential solar photovoltaic system applications. Under the smart grid initiative, it is demonstrated the efficiently managing the active power generated by the

solar panels, this single stage configuration can compensate current that could be harmonic generated by distorted supply voltage, and nonlinear loads found in a single-phase AC distribution system. Experimental and simulation tests show the good performance of the proposed controller in steady state and dynamic response where a low THD of grid current and small settling time and overshoot are obtained. The SPV-APF to APF mode transition is experimentally implemented and proved its effectiveness. Consequently, the results carried out, confirmed the suitability and effectiveness of the LQRI as a robust type of controller which is an excellent candidate for single stage SPV-APF-LCL single phase connected to an AC distribution system.

CHAPTER 4

A ROBUST STABILIZER FOR POWER SHARING BASED ISLANDED AC MICROGRID

Naima Arab ^a, Kamal Al-Haddad ^a, Fellow, IEEE, and Abdelhamid Hamadi ^a.

^a Department of Electrical Engineering, École de Technologie Supérieure, 1100 Notre-Dame West, Montreal, Quebec, Canada H3C 1K3

This chapter has been submitted to the Journal of Emerging and Selected Topics in Power Electronics, February 2021.

Abstract

This chapter presents a new droop control based on robust stabilizer to enhance power sharing performance between DGs connected to the AC bus bar as well as to enhance stability issues while using high droop gains, and to dampen the low frequency oscillation mode. Moreover, the additional signals of the stabilizer are added to the conventional droop control scheme and its impact is quantified and analyzed. The model of the system is realized in d-q reference frame without communication links between the converters. Thereafter, the voltage and current control loops are designed using LQR controller to regulate and track the references signals in the presence of uncertainties and instabilities. The stability analysis of the proposed droop control is done using dynamic phasor model and the eigenvalues of the system are presented. The simulation results of the AC microgrid with the proposed control are presented and evaluated. Furthermore, a hardware-in-the-loop (HIL) of the AC microgrid system was used as real time validation tool using real time (RT-Lab) of the OPAL-RT technologies along with dSPACE control platform. The achieved results prove the effectiveness and accurateness of the implemented control scheme.

4.1 Introduction

Modern electrical distribution systems are nowadays facing great defies like social demands, guaranteeing electrical reliability while maximizing environmental profits (Dou et al., 2016). Therefore, the concept of microgrid is evolving as a hopeful alternative to address these mentioned defies.

The distributed microgrid is commonly containing different distributed generators (DGs), storage devices and loads, and easily interconnected to other AC sources that can function in grid-connected or in islanded mode (Dou et al., 2016).

However, the issues of controlling the power sharing between several DGs pose a direct challenge and perhaps a threat to the stability of the microgrid (Y. Chen et al., 2016). For that reason, the way to ensure a precise power sharing between connected multi-parallel inverters has since become an important issue to be addressed (Y. Chen et al., 2016).

Furthermore, the droop control is the most used to achieve power sharing among inverters connected in parallel. This control focuses on the stability of both voltage and frequency of the MG. This latter is also used to reach active and reactive power sharing (Y. Han, Li, et al., 2017). The classical droop control presents some defects like low power sharing accuracy, poor dynamic performance, and voltage and frequency deviations (Imran et al., 2019).

The X/R ratio in microgrids is low, where the droop coefficients must be increased to avoid instabilities (Golsorkhi & Lu, 2015). However, the high droop gains causes the low frequency mode to move towards the right half-plane, which my exhibit instability (Sharma, Mishra, & Pullaguram, 2020).

A modified droop control has been developed in literature in order to enhance the power-sharing performance and to improve stability of the MG. In (Joung et al., 2019), a modified decoupled voltage and frequency controller for DGs is presented, which can keep the frequency and voltage amplitude of MG constant, whereas a frequency restore loop is added to the

classical droop control for efficient power sharing and stabilization of the frequency response. A voltage-current droop control has been used in (Y. Li & Fan, 2017) for a precise power sharing among connected inverters. However, the active and reactive powers show oscillations for lower droop coefficients values. In (Das et al., 2017), a d-q voltage droop control is presented, and the performance of the system with this technique does not depend on the line parameters. Though, the control is tested only in case of equal power sharing. A washout filter is added in the classical droop control to restore the voltage and frequency without communication links presented in (Y. Han et al., 2018; Yazdanian & Mehrizi-Sani, 2016), but the design of the washout filter was unspecified. On the other hands, a virtual capacitor technique to reduce steady state reactive power sharing error in MG is presented in (Xu et al., 2019). Despite, a conventional droop control is used and the low frequency mode for lower droop gains was not presented. Moreover, a control scheme based on V-I characteristics to obtain fast dynamics and flexibility of the distributed generator was presented and discussed in (Golsorkhi & Lu, 2015).

An additional active damping controller is used in (Kahrobaeian & Mohamed, 2014) for MG with dynamic loads (induction motor). In (Majumder et al., 2010) a supplementary loop based on PSS is added to the conventional control in order to insure the system stability when large values of droop angle are used. Nevertheless, the design of the stabilizer was not generalized; an optimization method was used. Furthermore, a cascade lead compensators was proposed in (Dheer, V, Kulkarni, & Doolla, 2019) to increase the stability margin of the system. However, the design procedure of the compensators are not presented. In (Firdaus & Mishra, 2020), a supplementary loop are added to the classical droop control for stability improvement of the MG. However, the effect of disturbances were not considered. A summarized comparison of some reviewed droop control and the proposed controller is presented in Table 4.1.

Table 4.1 Comparison of the proposed controller with others existing in literature

Comparison categories	(Kahrobaeian & Mohamed, 2014)	(Majumder et al., 2010)	(Dheer et al., 2019)	(Firdaus & Mishra, 2020)	Proposed controller
Implementation complexity	Medium	Medium	Simple	Medium	Simple
Power sharing performance	Medium	Good	Medium	Good	Very good
Dynamic response	Slow	Fast	Slow	Not reported	Fast
Voltage and current control loop	PI controller	Not reported	Not reported	Not reported	LQR controller
Design of the stabilizer	Not reported	Not reported	Not reported	Reported	Reported
Stability analysis for high droop gains	Guaranteed	Guaranteed	Not reported	Guaranteed	Guaranteed
Overshot and oscillation at low frequency mode	Exists	None	Exists	Exists	None
Unequal power sharing	Not reported	Not reported	Not reported	Not reported	Reported

In response to the aforementioned issues, the authors present in this paper a new droop control based on robust stabilizer for robust power sharing without communication links. An additional control loop is inserted in the classical droop control to insure stability of the system while using high droop gains and guaranteeing proper power sharing. Moreover, the dynamic phasor model is used for stability analysis of the system under study. Furthermore, the voltage and current control loops are designed using LQR controller.

The chapter is planned as follows: Section 4.2 provides the mathematical modeling of the microgrid. The proposed droop control is depicted in section 4.3. In Section 4.4, the LQR control is designed for voltage and current control loops. The stability analysis of MG with dynamic phasor is shown in Section 4.5. In Section 4.6, two interconnected converters are presented to illustrate a negative interaction and discussing the performance of the suggested

control, which is supported by simulation and HIL experimental validation. Finally, concluding remarks are presented.

4.2 Microgrid Model

The studied microgrid system is presented in Figure 4.1. It consists of two distributed generators (represented by three phase voltage source types of converters) connected to a three-phase load through LCL filter. The global control scheme contains a power calculation block, the proposed droop control structure and the voltage and the current control loops.

The model in the synchronous reference frame d-q is described by the thereafter 6 differential equations:

$$\begin{aligned}
 \frac{d i_{1d}}{dt} &= \frac{-R_1}{L_1} i_{1d} + \omega i_{1q} + \frac{1}{L_1} (d_d V_{dc1} - v_{1cd}) \\
 \frac{d i_{1q}}{dt} &= \frac{-R_1}{L_1} i_{1q} - \omega i_{1d} + \frac{1}{L_1} (d_q V_{dc1} - v_{1cq}) \\
 \frac{d v_{1cd}}{dt} &= \omega v_{1cq} + \frac{1}{C_1} (i_{1d} - i_{01d}) \\
 \frac{d v_{1cq}}{dt} &= -\omega v_{1cd} + \frac{1}{C_1} (i_{1q} - i_{01q}) \\
 \frac{d i_{01d}}{dt} &= \frac{-R_2}{L_2} i_{01d} + \omega i_{01q} + \frac{1}{L_2} (v_{1cd} - v_{pccd}) \\
 \frac{d i_{01q}}{dt} &= \frac{-R_2}{L_2} i_{01q} - \omega i_{01d} + \frac{1}{L_2} (v_{1cq} - v_{pccq})
 \end{aligned} \tag{4.1}$$

Where:

i_{1d} , i_{1q} and i_{01d} , i_{01q} are the inverter currents and the output currents components respectively. v_{1cd} and v_{1cq} are the d-q components of the capacitor C voltage, v_{pccd} and v_{pccq} are the d-q components of PCC voltage, and d_d , d_q are the switching function in d-q frame respectively.

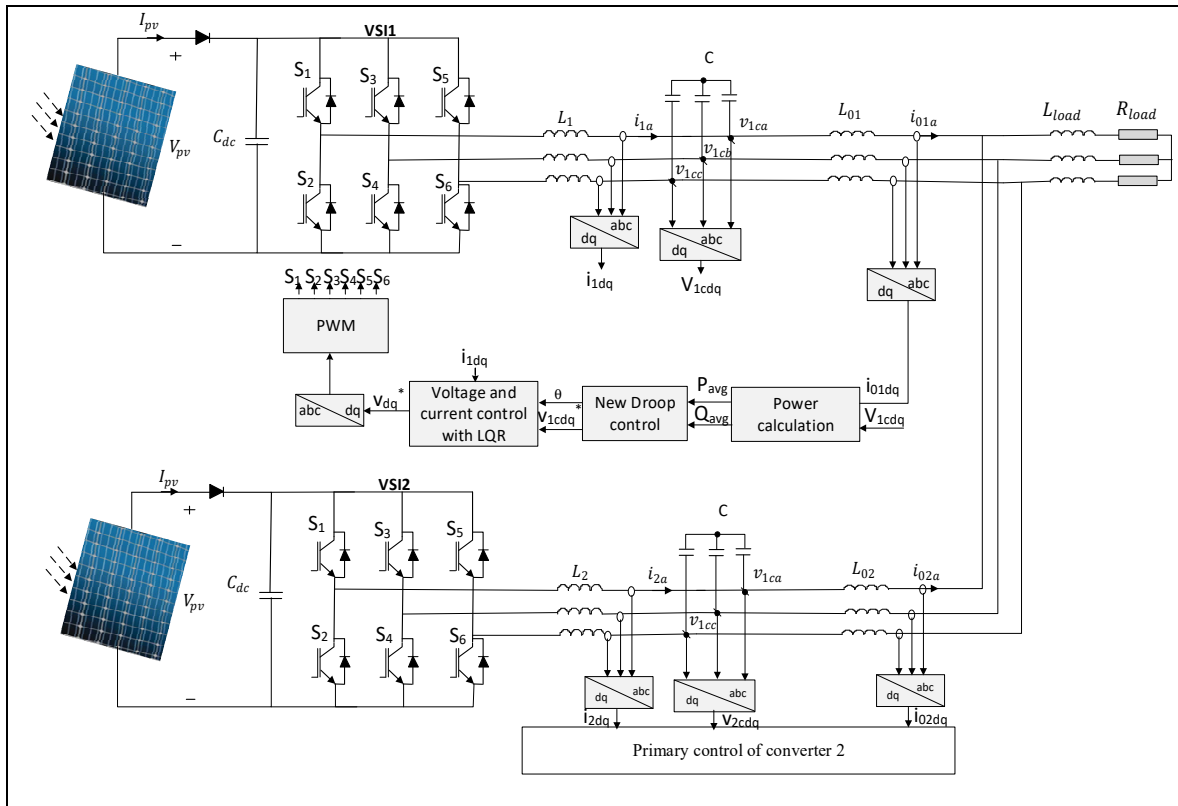


Figure 4.1 The Bloc diagram of AC microgrid

4.3 New Droop Control

An autonomous microgrid is considered in this work, which has two DGs connected in parallel to an AC bus supplying loads as shown in Figure 4.1. Each DG consists of a three-phase inverter VSI connected through LCL filter.

The conventional droop control given by (4.2) has been modified and a new droop control with stabilizing signals added has been used for voltage and frequency regulation, and to insure power sharing. The voltage and frequency droop control equations are given as follows (Brabandere et al., 2007; Conti, Nicolosi, Rizzo, & Zeineldin, 2012), (Pasha, Zeineldin, Al-Sumaiti, Moursi, & Sadaany, 2017):

$$\begin{aligned}\omega^* &= \omega_n - k_p P \\ V_{cd}^* &= V_n - k_q Q, \quad V_{cq}^* = 0\end{aligned}\tag{4.2}$$

Where ω_n and V_n are the rated frequency and the rated voltage of the droop control correspondingly, k_p and k_q are the droop control gains. P , Q are the active and reactive powers, correspondingly.

The injected instantaneous active and reactive power components d-q reference frame are given by (4.3):

$$\begin{aligned}P &= v_{1cd} i_{01d} + v_{c1q} i_{01q} \\ Q &= v_{1cd} i_{01q} - v_{c1q} i_{01d}\end{aligned}\tag{4.3}$$

The average active and reactive powers are achieved using low pass filter as:

$$\begin{aligned}P_{avg} &= \frac{\omega_c}{1 + \omega_c s} P \\ Q_{avg} &= \frac{\omega_c}{1 + \omega_c s} Q\end{aligned}\tag{4.4}$$

Where ω_c is the filter cutoff frequency.

The modified droop control is obtained by adding a stabilizer to generate the stabilization signals of the voltage (δV) and frequency ($\delta \omega$). These additional signals are added to the reference signals of frequency and voltage which are achieved from the classical droop control, as presented in Figure 4.2.

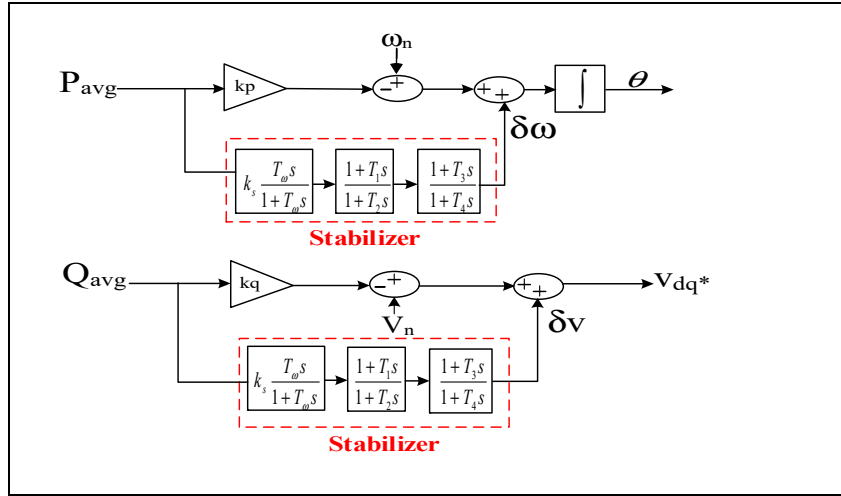


Figure 4.2 The proposed droop control details for DG#1

The stabilizer used in this work is set by (4.5), where k_{stab} is the compensator gain and the second term presents the washout filter which functions as a high-pass filter. The third and fourth terms represent the two-stage lead-lag compensator (Hasan, Salman, & El-Hawary, 2016).

The stabilizer is described by the equation hereafter:

$$H(s)_{stabilizer} = k_{stab} \frac{T_{\omega} s}{1 + T_{\omega} s} \frac{1 + T_1 s}{1 + T_2 s} \frac{1 + T_3 s}{1 + T_4 s} \quad (4.5)$$

Where

k_{stab} is the compensator coefficient, T_1 , T_2 , T_3 , and T_4 are the time constants of the lead-leg compensators. The parameters (T_1, T_3) and (T_2, T_4) are considered equal.

4.3.1 Stabilizer Design

Lead-Leg Block

The lead-lag compensator is used to improve steady state and transient response.

The low-pass filter transfer function is obtained by (4.6) as:

$$\frac{P}{p_{avg}} = \frac{\omega_c}{1 + \omega_c s} \quad (4.6)$$

As reported in the literature, the system with conventional droop control uses high droop coefficients in order to have faster and better power sharing performance, but a high droop coefficient, results in a large frequency deviation in steady state (Kahrobaeian & Mohamed, 2014; Sharma et al., 2020). Moreover, to design the lead-leg compensator the classical droop control is used in order to determine the critical mode where the system becomes marginally stable as shown in Figure 4.3.

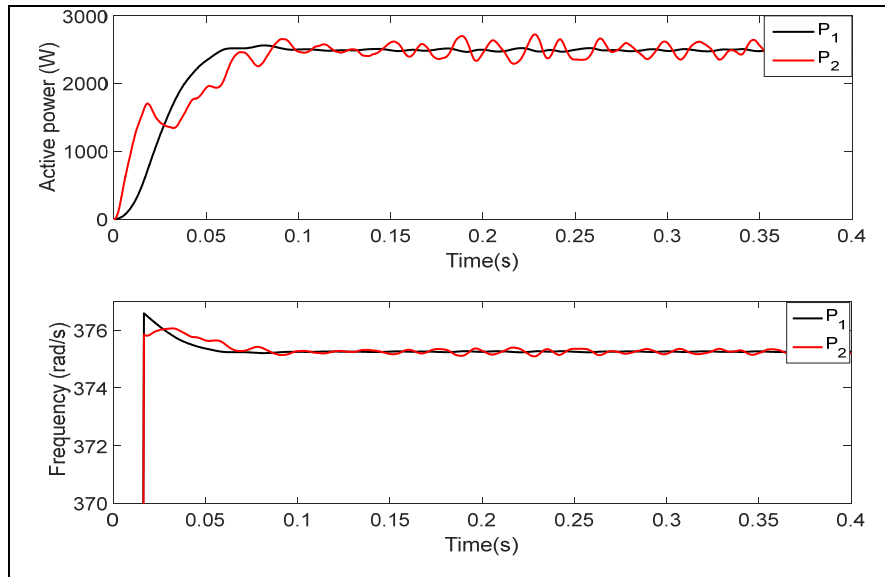


Figure 4.3 Active power sharing and frequency with conventional droop at critical droop coefficient

One can conclude that the system is although stable, but has a poor dynamic performance. The rise time is $T_r=0.07s$ as can be seen from Figure 4.3, and the oscillating frequency of the low-frequency mode is approximately equal to 43 rad/s and the lag of the transfer function given in (9) at this frequency is -26.5° . The lead compensator of the stabilizer presented in Figure 4.4 should compensate this lag by providing 26.5° lead in P_{avg} . Then the time constants are

calculated using equation (4.8)-(4.9) (Ayres, Kopcak, Castro, Milano, & da Costa, 2010; Cook, 2013).

$$\alpha = \frac{1 - \sin\left(\frac{\varphi_m}{2}\right)}{1 + \sin\left(\frac{\varphi_m}{2}\right)} \quad (4.7)$$

$$T_2 = \frac{1}{\omega_m \sqrt{\alpha}} \quad (4.8)$$

$$T_1 = \alpha T_2 \quad (4.9)$$

φ_m is the peak phase shift, n ($n=2$) is the number of the lead-lag blocks, and ω_m is the frequency of the critical mode.

The time constant (T_2), is chosen equal to 0.018s and T_1 is equal to 0.011s.

Washout Block

A washout filter is a high-pass filter that discards the DC component and allows to pass the transitory part of the signal (Sharma et al., 2020; Yazdanian & Mehrizi-Sani, 2016). The transfer function of the washout filter is given by (4.10).

$$G_{washout} = \frac{sT_w}{1 + sT_w} = \frac{s}{s + \omega_w} \quad (4.10)$$

T_w is time constant of the washout filter.

The washout filter should pass the attenuated oscillatory signal at the lowest frequency, which is approximately 43 rad/s, but the filter cut-off frequency, $\omega_w < 43$ rad/s and it is chosen equal to 2 rad/s (Kundur, 2013; Yazdanian & Mehrizi-Sani, 2016).

Gain K_{stab}

The stabilizer gain k_{stab} , has an important effect on damping oscillations. The gain k_{stab} is fixed at a value which results in a damping as high as the critical system (Kundur, 2013) and it is chosen equal to 0.0001.

4.4 Voltage and Current Control Loop Design

A robust inner and outer control loop based on LQR controller is used, to regulate and track the references and to achieve stability and robustness versus perturbations.

The purpose of the LQR controller design is to determine the optimal control law u .

$$u = -k \cdot x \quad (4.11)$$

Where the gain k is determined by minimizing the cost function J presented in the following (Arab et al., 2016)-(Kedjar et al., 2014b).

$$J = \int_0^{\infty} (x^T Q x + u^T R u) dt \quad (4.12)$$

The first step to design the LQR controller is to select the Q and R weighting matrices. Then, the gain k can be computed using *lqr* function in Matlab.

The details of the LQR controller design has been studied in our previous work (Arab, Kedjar, Javadi, & Al-Haddad, 2019; Arab, Vahedi, & Al-Haddad, 2019).

4.5 Stability Analysis with Dynamic Phasor Model (DPM)

In this part of the paper, the dynamic phasor model is used to model an island microgrid as shown in Figure 4.1. This concept is used for stability analysis of the proposed control scheme.

The active and reactive output power of the inverter can be written according to Figure 4.1 as below (Guo et al., 2014):

$$P = 3 \frac{Ls + R}{(Ls + R)^2 + (\omega L)^2} (V_c^2 - V_c V_{pcc} \cos \delta) + 3 \frac{\omega L}{(Ls + R)^2 + (\omega L)^2} V_c V_{pcc} \sin \delta \quad (4.13)$$

$$Q = 3 \frac{\omega L}{(Ls + R)^2 + (\omega L)^2} (V_c^2 - V_c V_{pcc} \cos \delta) - 3 \frac{Ls + R}{(Ls + R)^2 + (\omega L)^2} V_c V_{pcc} \sin \delta \quad (4.14)$$

Where

V_c and V_{pcc} are the capacitor C voltage and the PCC voltage correspondingly. δ is the power angle.

Using (4.13) and (4.14), a linearized multi-variable transfer function matrix around operating points is obtained as (Mohamed & El-Saadany, 2008; Sharma et al., 2020):

$$\begin{bmatrix} \Delta P(s) \\ \Delta Q(s) \end{bmatrix} = \begin{bmatrix} H^{\omega \rightarrow P}(s) & H^{v \rightarrow P}(s) \\ H^{\omega \rightarrow Q}(s) & H^{v \rightarrow Q}(s) \end{bmatrix} \begin{bmatrix} \Delta \omega(s) \\ \Delta V_c(s) \end{bmatrix} \quad (4.15)$$

Where

$$H^{\omega \rightarrow P}(s) = \frac{\Delta P}{s \Delta \delta} = 3 \frac{(Ls + R) \sin \delta^0}{(Ls + R)^2 + (\omega L)^2} V_c^0 V_{pcc}^0 \frac{1}{s}$$

$$H^{v \rightarrow P}(s) = \frac{\Delta P}{\Delta V_c} = 3 \frac{(Ls + R)(2V_c^0 - V_{pcc}^0 \cos \delta^0 + \omega L V_{pcc}^0 \sin \delta^0)}{(Ls + R)^2 + (\omega L)^2}$$

$$H^{\omega \rightarrow Q}(s) = \frac{\Delta Q}{s \Delta \delta} = -3 \frac{(Ls + R) \cos \delta^0 - \omega L \sin \delta^0}{(Ls + R)^2 + (\omega L)^2} V_c^0 V_{pcc}^0 \frac{1}{s}$$

$$H^{v \rightarrow Q}(s) = \frac{\Delta Q}{\Delta V_c} = 3 \frac{2\omega L V_c^0 - V_{pcc}^0 (\omega L \cos \delta^0 + (Ls + R) \sin \delta^0)}{(Ls + R)^2 + (\omega L)^2}$$

The multivariable transfer function matrix of MG with the proposed stabilizer obtained from Figure 4.2 is given as:

$$H(s) = \frac{H^{\omega, v \rightarrow P, Q}(s) \times H_{LPF}(s)}{1 - (k_{pq} \times H^{\omega, v \rightarrow P, Q}(s) \times H_{LPF}(s) \times H_{stab}(s))} \quad (4.16)$$

To have desired power sharing with conventional droop control, higher gains are needed. To overcome this problem the stabilizer is designed to ensure system stability even with high gains. Figure 4.4 shows the eigenvalues of the DPM model of the closed loop system when the stabilizer is used for k_p variations.

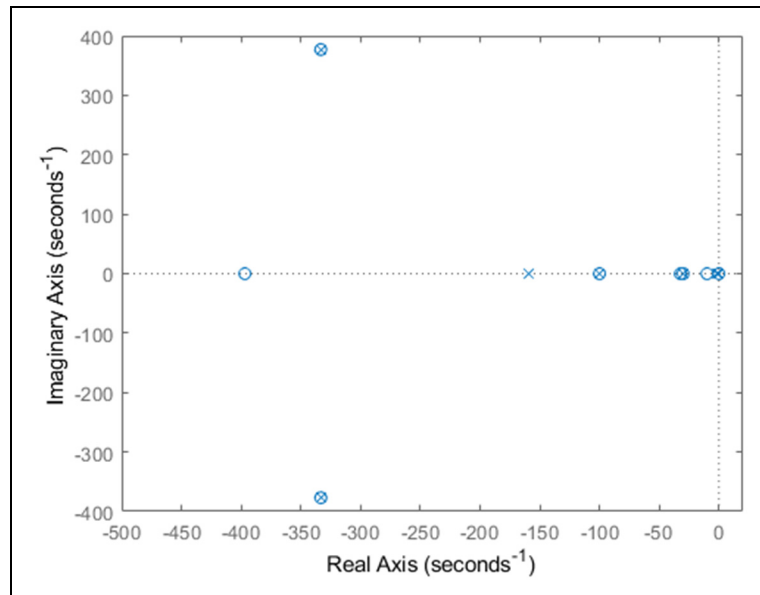


Figure 4.4 Dominant eigenvalues for k_p variation with DPM method

Figure 4.4 shows that all the poles of the system are in the left half-plane, indicating stable operation of the system.

4.6 Simulation and Experimental Results

Experimental and simulation tests are performed in order to prove the effectiveness of the proposed stabilizer in AC microgrid.

4.6.1 Simulation Results

The model of the proposed system presented in Figure 4.1 in d-q frame is realized in Matlab/Simulink/sim power systems, and the obtained results are presented hereafter in case of balanced nonlinear load and unbalanced load with higher droop gains during all the simulations. The system parameters used in simulations are shown in Table 4.2.

Table 4.2 System parameters

Parameters	Values
DC bus voltage	650V
DC bus capacitance	1200 μ F
Frequency	60Hz
Switching frequency	10kHz
Inverter side inductance(L_l)	1.5mH
Inverter side inductance (L_o)	0.5mH
Filter capacitor (C)	25 μ F

First case under higher and lower droop gains

As seen in Figure 4.3, when the stabilizer is disconnected, the system is marginally stable at its critical limit ($k_p=1*10^{-4}$). In this case, the system with the stabilizer on is tested by increasing the droop coefficient value and then decreased beyond its critical limit at $t=0.15$ s. Figure 4.5 shows that the stabilizer provided a damping to the system. The system is stable and a fast desired power sharing have been obtained for higher and lower droop gains without any oscillations.

Therefore, it is not necessary to increase the droop coefficients to have a precise power sharing without frequency deviation when the stabilizer is included in the control of AC microgrid.

Second case under reduced system

In this case, the system with the proposed stabilizer is tested for reduced system, where DG#2 is disconnected at $t=0.15s$. One can see from Figure 4.6 that a proper power sharing is obtained with stable operation of the system, which proves the effectiveness of the proposed supplementary controller.

Third case under balanced nonlinear load variations

The simulation results are obtained using the proposed supplementary controller shown in Figure 4.2 under nonlinear load variations where this latter is composed of a diode bridge feeding capacitive load in parallel. The load power is decreased and then increased (Figure 4.7) respectively at $t=0.15s$ and $t=0.2s$. One can see that case where the additional controller is included in the droop control, the active power (P_1 and P_2) are equal and well shared, the frequency of both converter is well superimposed, and the three-phase output current of converter 1 remains stable without overshoot with the use of the proposed stabilizer. The voltage at the PCC remains unchanged. The power sharing is well distributed as desired when the stabilizer is included in the control of the AC microgrid.

As an illustration of the usefulness of the proposed stabilizer, the same two parallel inverters are used but with unbalanced load. In this case (Figure 4.8), the load power is decreased at $t=0.15s$ and then increased at $t=0.2s$. The active powers (P_1 and P_2) and the inverters currents are shared equally and precisely between the two DGs while stable voltages are conserved. The frequency regulation is insured.

The stabilizer does not introduced any frequency and voltage deviations and transients under load changes while high droop gains are used. The power sharing is faster and well distributed as desired when the stabilizer is included in the control of AC microgrid for higher droop gains.

Fourth case load switched on/off and then off/on

Figure 4.9 illustrates the load connected and then disconnected at $t=0.15\text{s}$ and $t=0.2\text{s}$ respectively. For both tests, the microgrid quickly reaches steady state with desired power sharing and stable voltage on the AC bus. It can be seen that the frequency regulation of the MG system is ensured. The inverters currents are shared equally and precisely between the two DGs.

In summary, it can be concluded from various tests that are performed, the proposed stabilizer is more suitable in AC microgrid applications in order to distribute a desired power sharing.

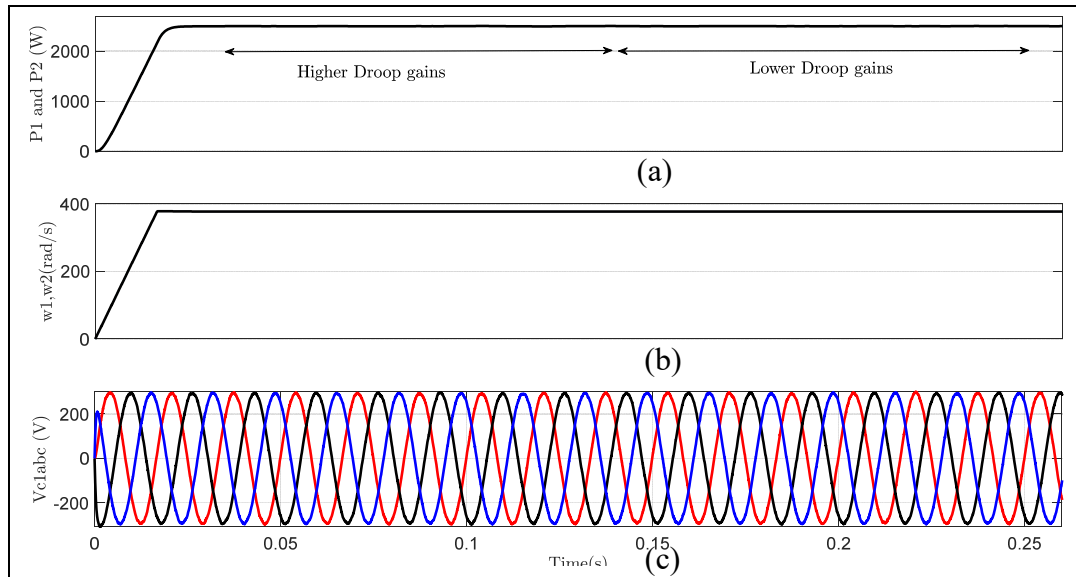


Figure 4.5 Stabilizer under higher droop gains, (a) the active power of converter 1 and converter 2, (b) frequency of converter 1 and converter 2, (c) PCC voltage

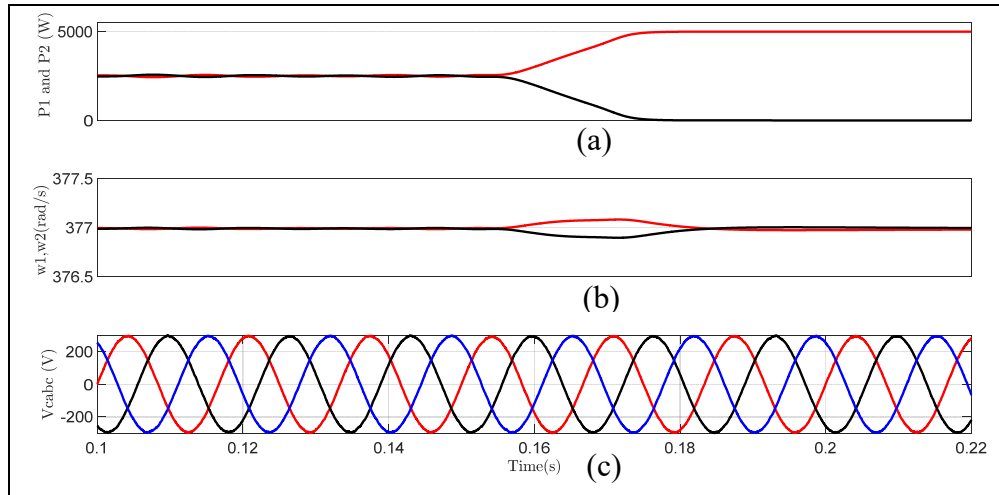


Figure 4.6 Stabilizer under reduced system, (a) the active power of converter 1 and converter 2, (b) frequency of converter 1 and converter 2, (c) PCC voltage

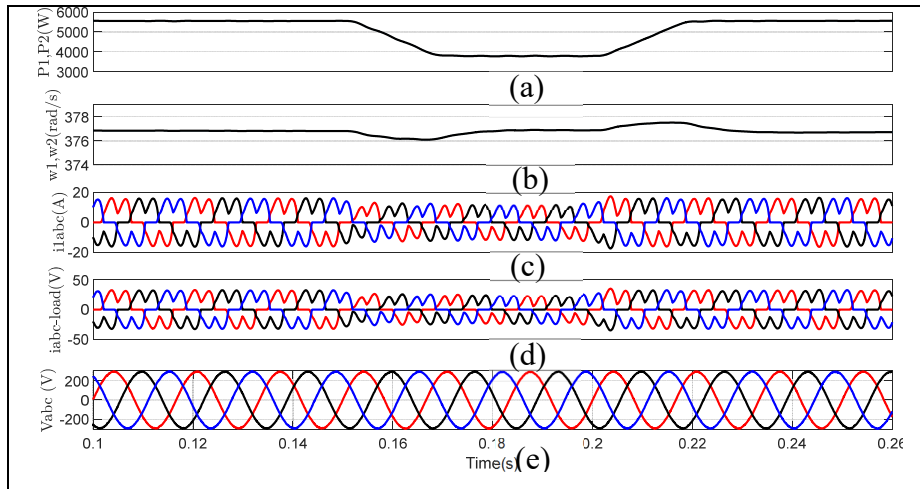


Figure 4.7 Stabilizer under nonlinear load variations, (a) the active power of converter 1 and converter 2, (b) frequency of converter 1 and converter 2, (c) current of converter 1, (d) load current, (e) PCC voltage

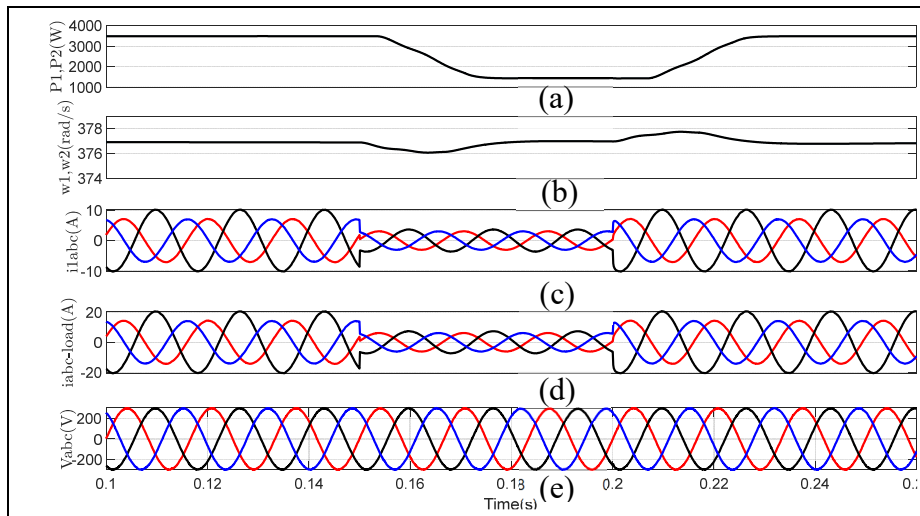


Figure 4.8 Stabilizer under unbalanced load variations, (a) the active power of converter 1 and converter 2, (b) frequency of converter 1 and converter 2, (c) current of converter 1, (d) load current, (e) PCC voltage

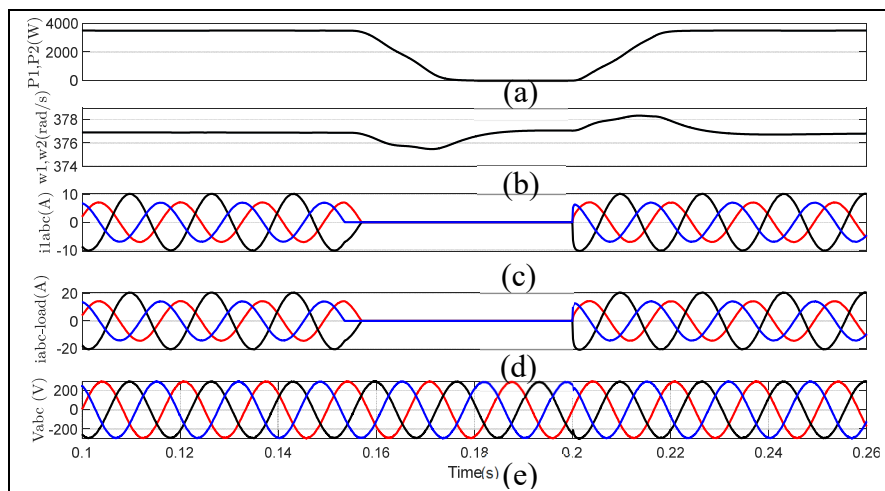


Figure 4.9 Stabilizer when the unbalanced load is switched on/off and then off/on, (a) the active power of converter 1 and converter 2, (b) frequency of converter 1 and converter 2, (c) current of converter 1, (d) load current, (e) PCC voltage

4.6.2 Experimental Results

In this section, the studied AC microgrid system presented in Figure 4.2 is implemented using a real time simulator HIL (RT-Lab) of the OPAL-RT technologies, where the electrical system

is implemented on the Opal-RT simulator OP4510 and the proposed control scheme is performed on the dSPACE DS1103 (Javadi, Abarzadeh, Grégoire, & Al-Haddad, 2019) as shown in Figure 4.10.

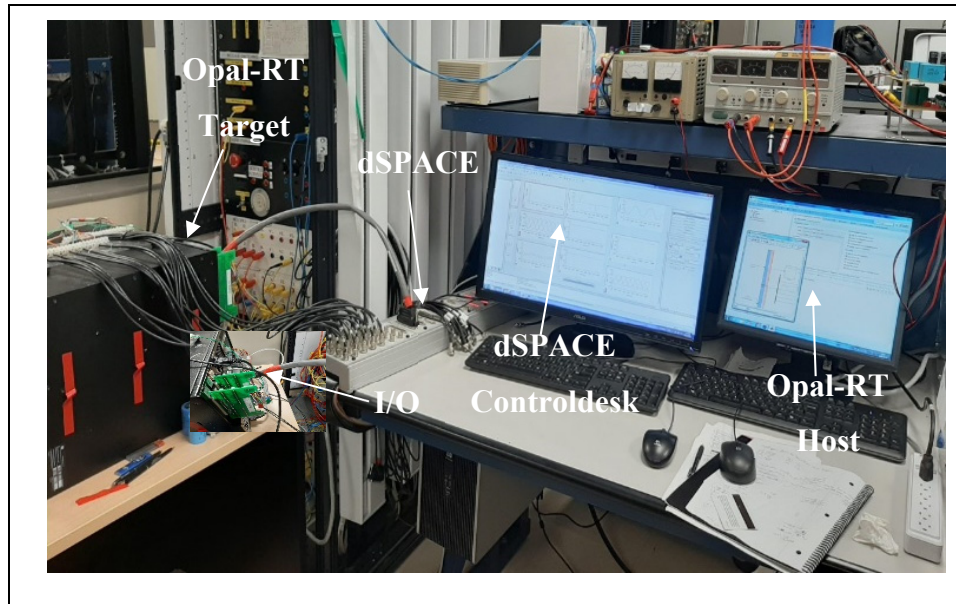


Figure 4.10 Experimental setup used for HIL implementation

The DGs use the suggested droop control, and initially supply a balanced and unbalanced linear load. The power sharing of the load between the two DGs is insured according to their droop controller.

The experimental results under different scenarios are presented in Figure 4.11 to Figure 4.16. In some tests, the waveforms (currents and voltages) of DG2 are the same as those of DG1 so are not shown in this paper to avoid redundancy.

Steady State with Lower Droop Gains

The proposed controller is tested under balanced and unbalanced load with lower droop gains as presented in Figure 4.11 and Figure 4.12. One can see the equal power sharing between the two DGs, the inverters share same power thus, the same currents. The output voltage of DG1

remains unchanged. As illustrated, the voltage and frequency signals meet their nominal values and the power-sharing has good precision.

As it can be seen, the suggested droop control for the AC microgrid works well. Eventually, one can conclude that the proposed control scheme responds well to provide desirable voltage and frequency regulation and to have a desired power sharing in presence of balanced and unbalanced load when lower droop gains are used.

Load Power Variations with Higher Droop Gains

From Figure 4.13 and Figure 4.14, it is clearly shown that when the load changes (increased and then decreased), the output voltage of DG1 remains unchanged, while the output currents of DG1 (i_{abc1}) have the constant proportional variation which proves that the power sharing is satisfactory as expected. It implies that the proposed stabilizer is able to track the loading transition speedily and exactly without oscillations when high droop gains are used.

Unequal Power Sharing

This case aims to examine the power-sharing performance of the stabilizer when the parallel inverters have different rated power. The results of the output current (i_{abc1}) and the active power (P_1, P_2) are shown in Figure 4.15 and Figure 4.16 under balanced and unbalanced load. The obtained results show a proper power sharing as expected.

Clearly, the suggested droop control demonstrates proper power sharing performance, and good dynamic response while higher and lower droop gains are used.

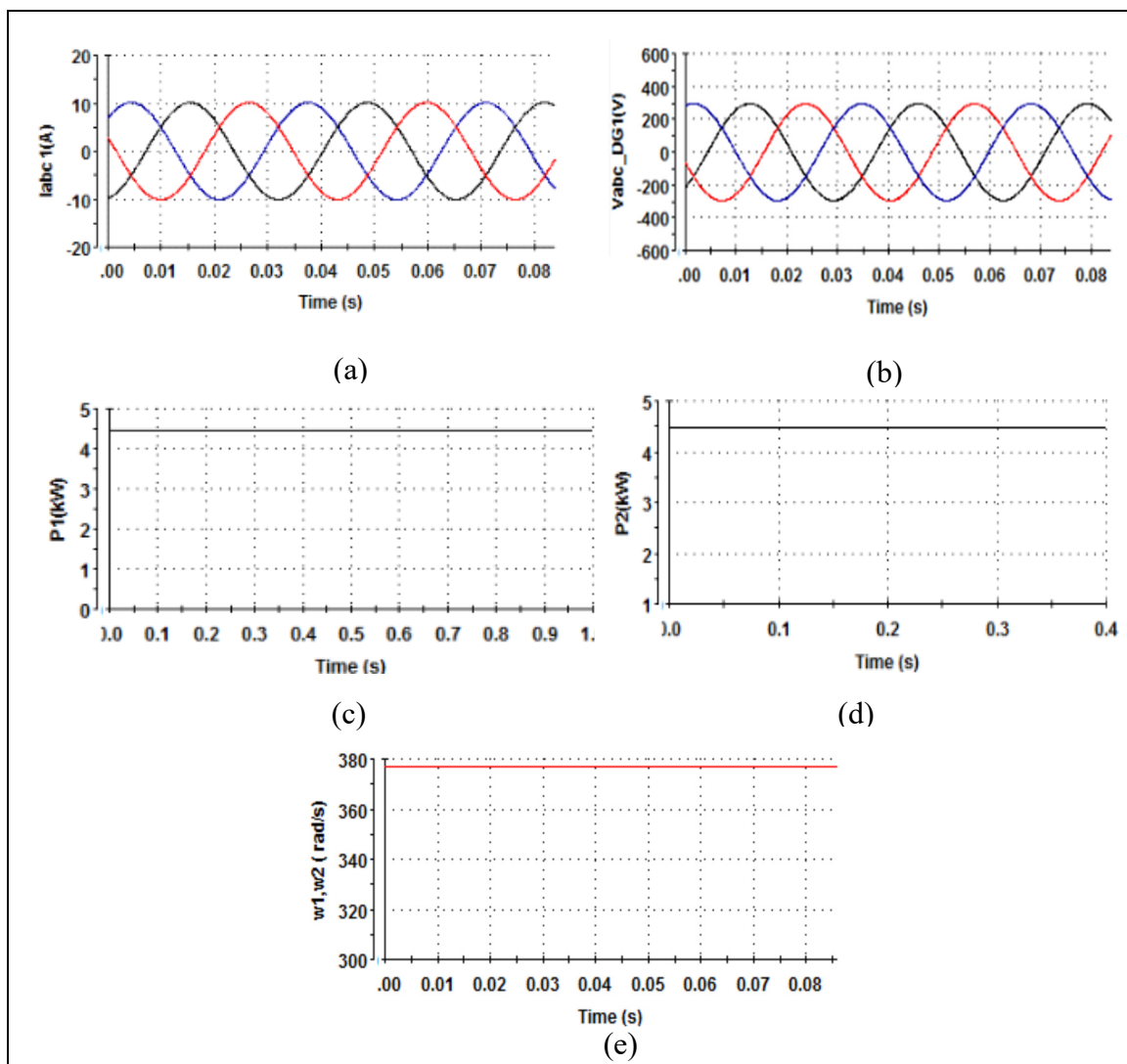


Figure 4.11 Experimental results of AC microgrid with the proposed droop control under balanced equal power sharing

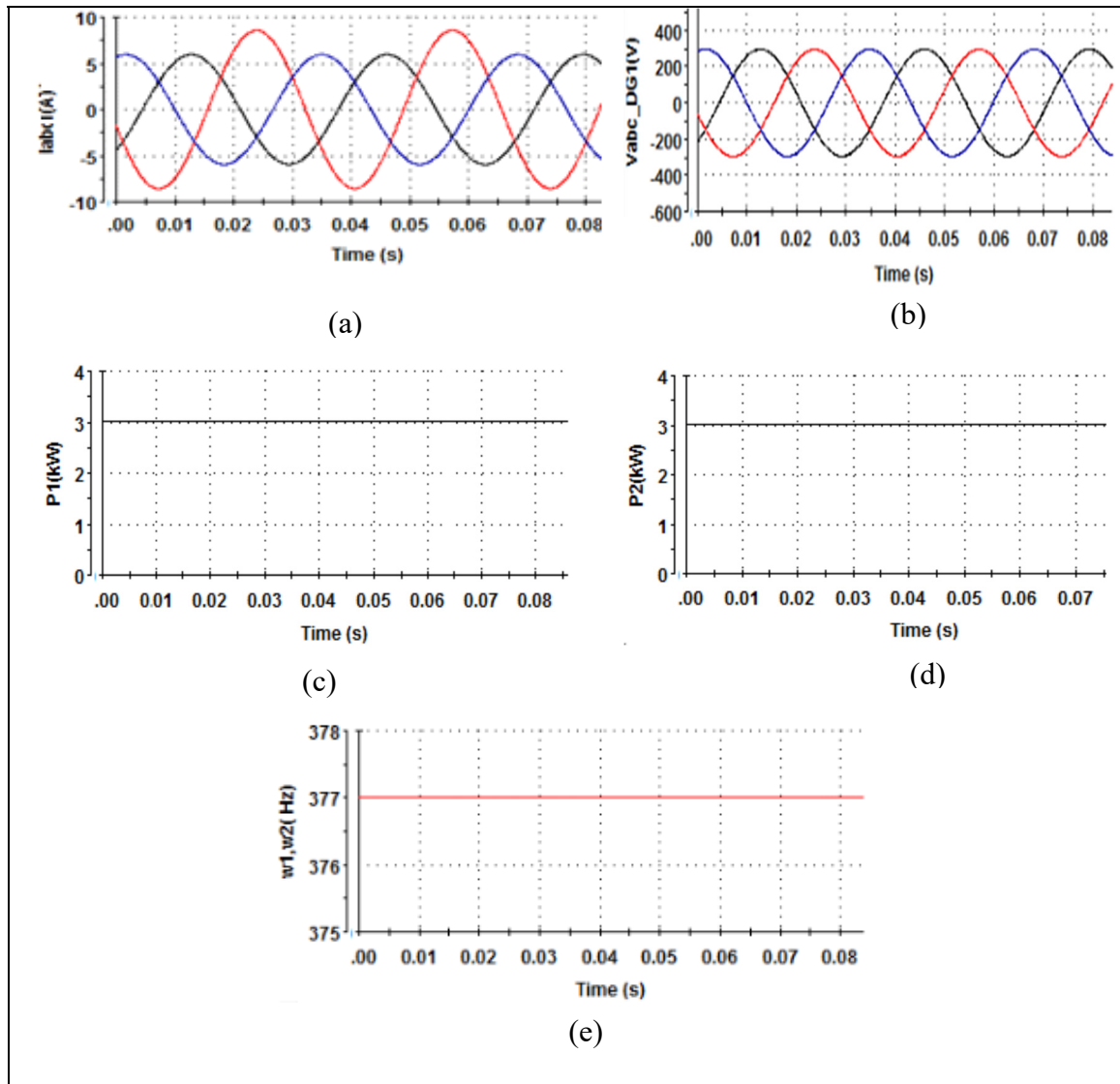


Figure 4.12 Experimental results of AC microgrid with the proposed droop control under unbalanced equal power sharing

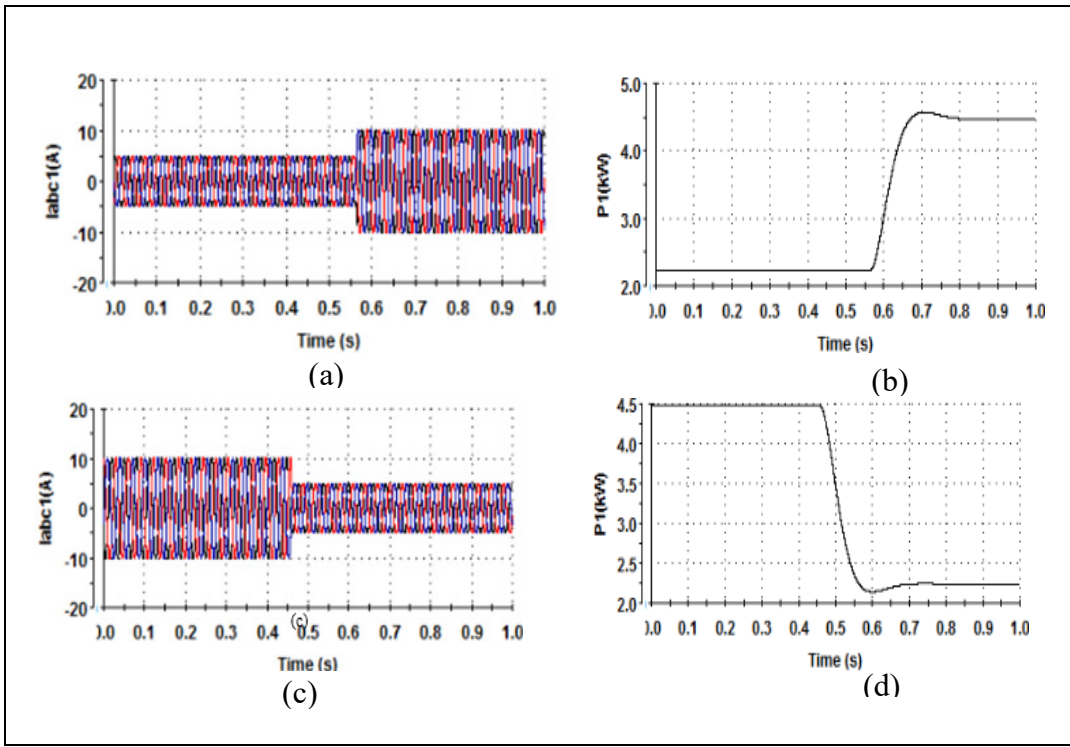


Figure 4.13 Waveforms of the proposed droop control during balanced load variations, (a, b) increase and (c, d) decrease

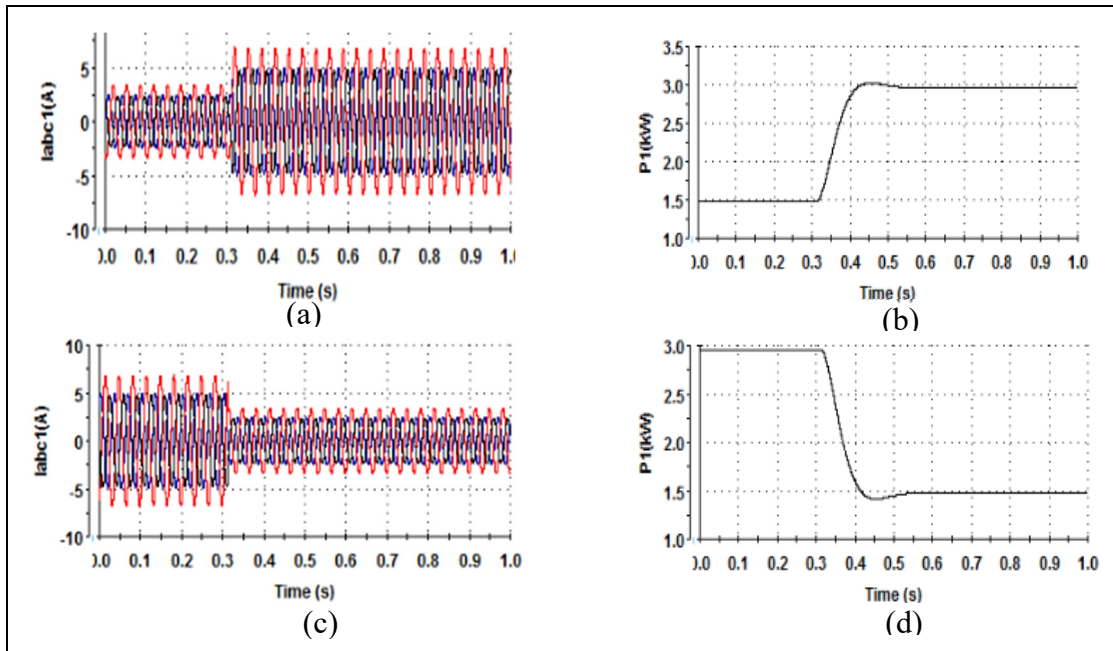


Figure 4.14 Waveforms with the proposed droop control during unbalanced load variations, (a, b) increased and (c, d) decreased

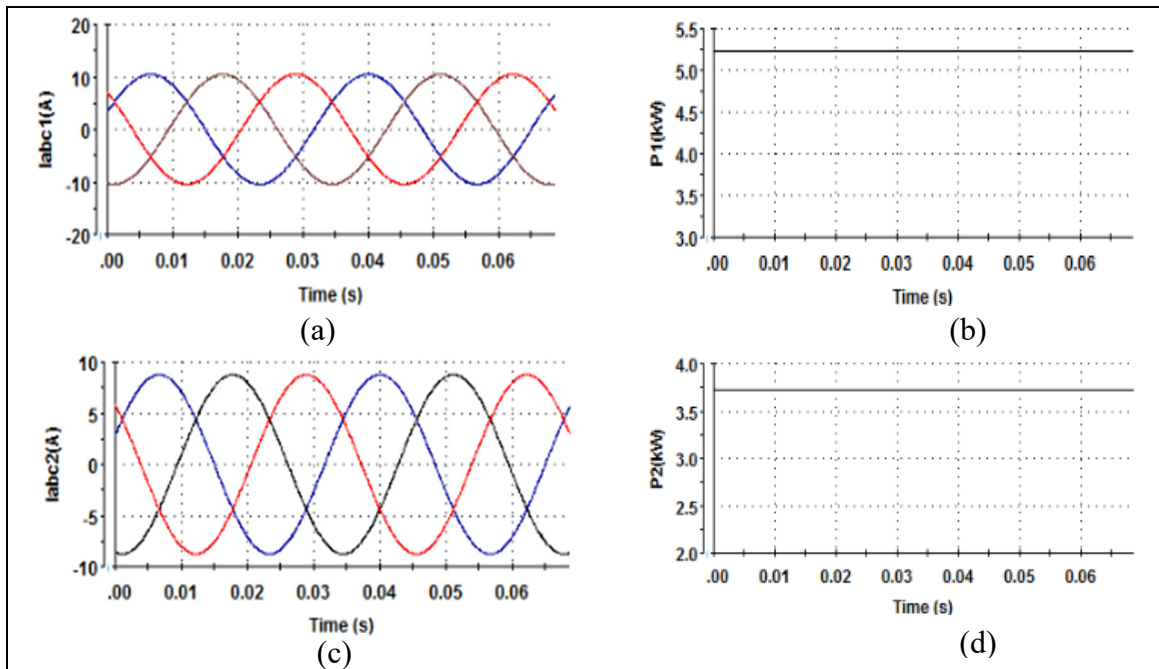


Figure 4.15 Waveforms with the proposed droop control during balanced unequal power sharing

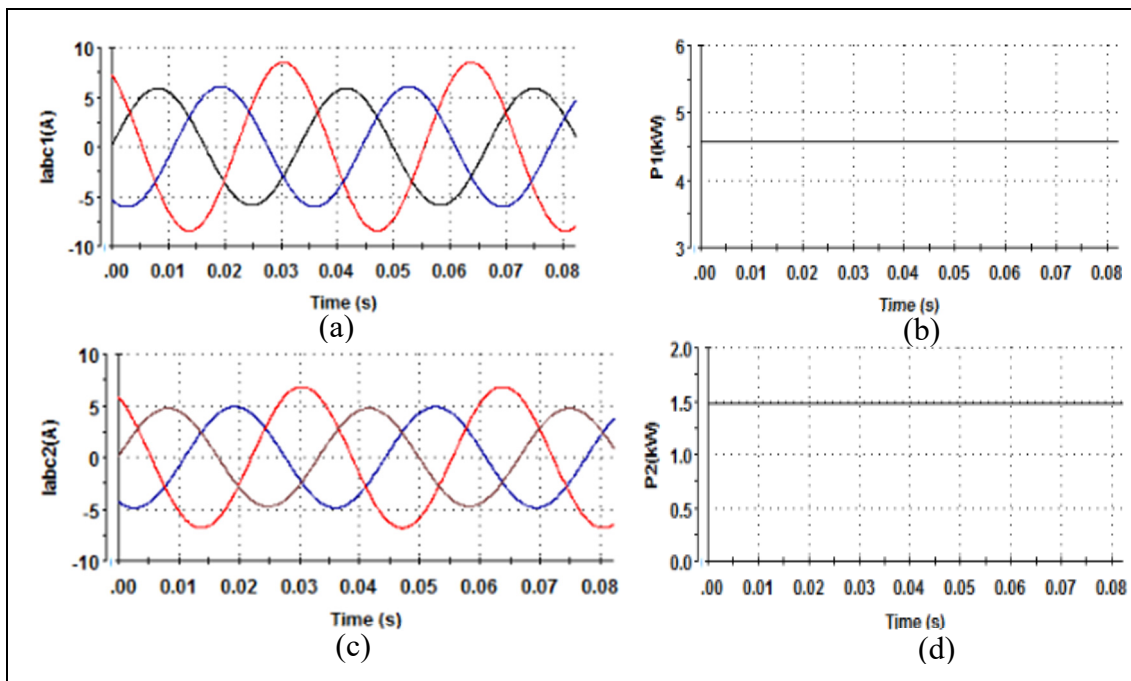


Figure 4.16 Waveforms with the proposed droop control during unbalanced unequal power sharing

4.7 Conclusion

In this chapter, a new droop control based on robust stabilizer to improve transient power sharing was developed for two DGs operating in parallel without communication links, and to improve system stability while higher and lower droop gains are used. The stabilizer has been designed by correctly selecting the parameters in order to dampen the low frequency mode. The stability analysis was carried out and the eigenvalues are obtained using DPM. The voltage and current loops were designed with LQR controller to regulate and track the references signals in the presence of uncertainties and disturbances. Experimental and simulation results are given in order to approve the validity of the suggested control that contributes to preserving microgrid stability. Subsequently, robust power sharing performance are obtained in steady state and transients. The proposed droop control was validated experimentally on an HIL platform.

CONCLUSION AND FUTURE WORK

The conclusions of the thesis are presented and the contributions which are aimed to provide new solutions for improving the distributed generators robustness. The future work that could be done using the knowledge from this study is also presented.

One of the main objectives of this work is around the control of the converters intended for distributed generation systems in microgrid applications. The research work aims to develop and solve certain problems related to the modeling and control of a voltage source inverter. Therefore, the robustness and stability of the microgrid system is ensured while an optimal power sharing is guaranteed among the inverters which are connected in parallel. In order to achieve this research objective, several control algorithms are offered at the distributed generator and MG.

In the first step, the work is devoted to the study of a distributed generator connected to the grid through LCL filter. In the second step, an autonomous microgrid which is established by several distributed generators units is well-studied. The structures objective is to meet the electrical energy needs of the connected loads while ensuring power quality; particularly the voltage at the connection point is ensured. In this thesis, it is mainly focused to develop the effective control strategies which are aimed to ensure that the system is operating according to the standards.

The most important conclusions of this research work are briefly summarized as follows:

A comprehensive literature review has been done on distributed generators and their control methods which are operating in the grid-connected mode or the islanded mode. Mainly, this review focuses on active damping control that allows achieving the complexity of the model and the resonance problems by adding the LCL filter. This review also allows knowing the connection impact of multiple parallel converters on the AC bus. A comprehensive state of the art on MG has been presented, accordingly.

A distributed generator based on multilevel PUC5 inverter connected to the grid through LCL filter is proposed. The proposed system is controlled using linear quadratic controller (LQR) to maximize disturbance rejection performance in the distributed generator. In order to test the robustness of the control system, an equivalent circuit is modeled in d-q frame. The performed experimental results prove the effectiveness of the suggested control system under uncertainties and the rejection of disturbances. The proposed controller is compared to the classical PI controller in terms of power quality, good tracking performance and disturbance rejections. A comparative analysis was done to show the advantages of the proposed LQRI controller over the conventional controller. Experimental and simulation results under various critical scenarios demonstrated the good performance of the proposed control strategy. The proposed strategy significantly improves the voltage and current THD at the same time.

A multifunctional single-stage residential photovoltaic power supply is proposed for power quality enhancement, especially in the presence of the non-linear loads. The proposed system consisted of the single-stage single-phase inverter which is connected to the grid under loads. An LQR controller was developed based on the description of the active filter. This technique offers satisfactory performance. Furthermore, it prevents the unpredictability of electrical charges and parameters variations. The proposed configuration makes it possible to improve the power factor, to prevent current harmonic distortions, and to improve the quality of the voltage waveform at the output of the distributed generator.

A robust stabilizer-based droop control is proposed and developed to improve the dynamic response and stability of MGs. The droop control based stabilizer aims to develop decentralized and distributed control system which improves robustness, and reliability and power quality. The proposed primary control provides the improved dynamic performance, the minimized power sharing errors, and the high reliability and robustness. The principle and effectiveness of the droop control method are widely discussed. Voltage and current control loops use the LQRI method to track reference voltage and current. The performance of the closed loop system has been analyzed to illustrate the capabilities of this technique. The obtained results confirm the effectiveness of the proposed strategy.

The experimental and simulation results obtained are presented and discussed in the chapters to confirm the validity of the developed control strategies. The performance of the developed controllers is extensively verified over several operating conditions.

In order to continue this research work, different perspectives open up:

- The study of the virtual synchronous generator (VSG) in a microgrid for its function of inertia support.
- The single phase 5-level Packed U-Cell inverter (PUC5) has been used in grid connected inverter with LCL filter, it will be interesting to use it in autonomous microgrid applications with the proposed stabilizer.
- The microgrids are unbalanced due to the integration of single-phase generators, unbalanced loads and faults, for this reason, the study of the possibility and constraints linked to an unbalanced configuration of autonomous microgrids will be very interesting.

LIST OF REFERENCES

- Abdikarimuly, R., Familiant, Y. L., Ruderman, A., & Reznikov, B. (2016). *Calculation of current total harmonic distortion for a single-phase multilevel inverter with LCL-Filter*. Paper presented at the IEEE International Power Electronics and Motion Control Conference (PEMC), Varna.
- Agarwal, R. K., Hussain, I., & Singh, B. (2017). Implementation of LLMF Control Algorithm for Three-Phase Grid-Tied SPV-DSTATCOM System. *IEEE Transactions on Industrial Electronics*, 64(9), 7414-7424. doi:10.1109/TIE.2016.2630659
- Agorreta, J. L., Borrega, M., J, L., xF, pez, & Marroyo, L. (2011). Modeling and Control of -Paralleled Grid-Connected Inverters With LCL Filter Coupled Due to Grid Impedance in PV Plants. *IEEE Transactions on Power Electronics*, 26(3), 770-785. doi:10.1109/TPEL.2010.2095429
- Al-Saedi, W., Lachowicz, S. W., Habibi, D., & Bass, O. (2011, 13-16 Nov. 2011). *Power quality improvement in autonomous microgrid operation using particle swarm optimization*. Paper presented at the 2011 IEEE PES Innovative Smart Grid Technologies.
- Alajmi, B. N., Ahmed, K. H., Adam, G. P., & Williams, B. W. (2013). Single-Phase Single-Stage Transformer less Grid-Connected PV System. *IEEE Transactions on Power Electronics*, 28(6), 2664-2676. doi:10.1109/TPEL.2012.2228280
- Alsafran, A. (2018, 21-25 Oct. 2018). *Literature Review of Power Sharing Control Strategies in Islanded AC Microgrids with Nonlinear Loads*. Paper presented at the 2018 IEEE PES Innovative Smart Grid Technologies Conference Europe (ISGT-Europe).
- Anzalchi, A., Moghaddami, M., Moghaddasi, A., Sarwat, A. I., & Rathore, A. K. (2016). A New Topology of Higher Order Power Filter for Single-Phase Grid-Tied Voltage-Source Inverters. *IEEE Transactions on Industrial Electronics*, 63(12), 7511-7522. doi:10.1109/TIE.2016.2594222
- Arab, N., Kedjar, B., & Al-Haddad, K. (2016, 12-14 Oct. 2016). *D-Q frame optimal control of single phase grid connected inverter with LCL filter*. Paper presented at the 2016 IEEE Electrical Power and Energy Conference (EPEC).
- Arab, N., Kedjar, B., Javadi, A., & Al-Haddad, K. (2017, 1-5 Oct. 2017). *Power quality enhancement in single phase energy distribution systems using DQ optimal control*. Paper presented at the 2017 IEEE Industry Applications Society Annual Meeting.

- Arab, N., Kedjar, B., Javadi, A., & Al-Haddad, K. (2019). A Multifunctional Single-Phase Grid-Integrated Residential Solar PV Systems Based on LQR Control. *IEEE Transactions on Industry Applications*, 55(2), 2099-2109. doi:10.1109/TIA.2018.2883551
- Arab, N., Vahedi, H., & Al-Haddad, K. (2019). LQR Control of Single-Phase Grid-Tied PUC5 Inverter with LCL Filter. *IEEE Transactions on Industrial Electronics*, 1-1. doi:10.1109/TIE.2019.2897544
- Ayres, H. M., Kopcak, I., Castro, M. S., Milano, F., & da Costa, V. F. (2010). A didactic procedure for designing power oscillation dampers of FACTS devices. *Simulation Modelling Practice and Theory*, 18(6), 896-909. doi:<https://doi.org/10.1016/j.simpat.2010.02.007>
- Bahrani, B., Rufer, A., Kenzelmann, S., & Lopes, L. A. C. (2011). Vector Control of Single-Phase Voltage-Source Converters Based on Fictive-Axis Emulation. *IEEE Transactions on Industry Applications*, 47(2), 831-840. doi:10.1109/TIA.2010.2101992
- Balanuta, C., Vechiu, I., & Gurguiatu, G. (2012, 12-14 Oct. 2012). *Improving micro-grid power quality using three-phase four-wire active power conditioners*. Paper presented at the 2012 16th International Conference on System Theory, Control and Computing (ICSTCC).
- Banerji, A., Sen, D., Bera, A. K., Ray, D., Paul, D., Bhakat, A., & Biswas, S. K. (2013, 23-24 Aug. 2013). *Microgrid: A review*. Paper presented at the 2013 IEEE Global Humanitarian Technology Conference: South Asia Satellite (GHTC-SAS).
- Barnes, A. K., Balda, J. C., & Stewart, C. M. (2012, 5-9 Feb. 2012). *Selection of converter topologies for distributed energy resources*. Paper presented at the 2012 Twenty-Seventh Annual IEEE Applied Power Electronics Conference and Exposition (APEC).
- Beres, R., Wang, X., Blaabjerg, F., Bak, C. L., & Liserre, M. (2014, 16-20 March 2014). *A review of passive filters for grid-connected voltage source converters*. Paper presented at the 2014 IEEE Applied Power Electronics Conference and Exposition - APEC 2014.
- Beres, R. N., Wang, X., Blaabjerg, F., Liserre, M., & Bak, C. L. (2016). Optimal Design of High-Order Passive-Damped Filters for Grid-Connected Applications. *IEEE Transactions on Power Electronics*, 31(3), 2083-2098. doi:10.1109/TPEL.2015.2441299
- Beres, R. N., Wang, X., Liserre, M., Blaabjerg, F., & Bak, C. L. (2016). A Review of Passive Power Filters for Three-Phase Grid-Connected Voltage-Source Converters. *IEEE Journal of Emerging and Selected Topics in Power Electronics*, 4(1), 54-69. doi:10.1109/JESTPE.2015.2507203

- Biricik, S., Komurcugil, H., & Basu, M. (2016). Photovoltaic supplied grid-tie three-phase inverter with active power injection and reactive harmonic current compensation capability. *IECON 2016* 3087-3092.
- Blasko, V., & Kaura, V. (1997). A novel control to actively damp resonance in input LC filter of a three-phase voltage source converter. *IEEE Transactions on Industry Applications*, 33(2), 542-550. doi:10.1109/28.568021
- Borup, U., Blaabjerg, F., & Enjeti, P. N. (2001). Sharing of nonlinear load in parallel-connected three-phase converters. *IEEE Transactions on Industry Applications*, 37(6), 1817-1823. doi:10.1109/28.968196
- Boulâam, K., & Boukhelifa, A. (2014, 21-24 Sept. 2014). *Fuzzy sliding mode control of DFIG power for a wind conversion system*. Paper presented at the 2014 16th International Power Electronics and Motion Control Conference and Exposition.
- Bouزيد, A. M., Guerrero, J. M., Cheriti, A., Bouhamida, M., Sicard, P., & Benghanem, M. (2015). A survey on control of electric power distributed generation systems for microgrid applications. *Renewable and Sustainable Energy Reviews*, 44, 751-766. doi:<https://doi.org/10.1016/j.rser.2015.01.016>
- BP. (2015). energy outlook 2035.
- BP. (2016). energy outlook 2035.
- Brabandere, K. D., Bolsens, B., Keybus, J. V. d., Woyte, A., Driesen, J., & Belmans, R. (2007). A Voltage and Frequency Droop Control Method for Parallel Inverters. *IEEE Transactions on Power Electronics*, 22(4), 1107-1115. doi:10.1109/TPEL.2007.900456
- Chen, C., Xiong, J., Wan, Z., Lei, J., & Zhang, K. (2017). A Time Delay Compensation Method Based on Area Equivalence For Active Damping of an LCL -Type Converter. *IEEE Transactions on Power Electronics*, 32(1), 762-772. doi:10.1109/TPEL.2016.2531183
- Chen, J., & Song, Y. (2016). Dynamic Loads of Variable-Speed Wind Energy Conversion System. *IEEE Transactions on Industrial Electronics*, 63(1), 178-188. doi:10.1109/TIE.2015.2464181
- Chen, J., Yue, D., Dou, C., Chen, L., Weng, S., & Li, Y. (2020). A Virtual Complex Impedance based P — V Droop Method for Parallel-connected Inverters in Low-voltage AC Microgrids. *IEEE Transactions on Industrial Informatics*, 1-1. doi:10.1109/TII.2020.2997054

- Chen, Y., Guerrero, J. M., Shuai, Z., Chen, Z., Zhou, L., & Luo, A. (2016). Fast Reactive Power Sharing, Circulating Current and Resonance Suppression for Parallel Inverters Using Resistive-Capacitive Output Impedance. *IEEE Transactions on Power Electronics*, 31(8), 5524-5537. doi:10.1109/TPEL.2015.2493103
- Chen, Z., Wang, K., Li, Z., & Zheng, T. (2017, 6-9 June 2017). *A review on control strategies of AC/DC micro grid*. Paper presented at the 2017 IEEE International Conference on Environment and Electrical Engineering and 2017 IEEE Industrial and Commercial Power Systems Europe (EEEIC / I&CPS Europe).
- Chi, Z., Dragicevic, T., Vasquez, J. C., & Guerrero, J. M. (2014, 13-16 May 2014). *Resonance damping techniques for grid-connected voltage source converters with LCL filters — A review*. Paper presented at the 2014 IEEE International Energy Conference (ENERGYCON).
- Cobreces, S., Bueno, E. J., Rodriguez, F. J., Pizarro, D., & Huerta, F. (2010, 4-7 July 2010). *Robust loop-shaping H_∞ control of LCL-connected grid converters*. Paper presented at the 2010 IEEE International Symposium on Industrial Electronics.
- Conti, S., Nicolosi, R., Rizzo, S. A., & Zeineldin, H. H. (2012). Optimal Dispatching of Distributed Generators and Storage Systems for MV Islanded Microgrids. *IEEE Transactions on Power Delivery*, 27(3), 1243-1251. doi:10.1109/TPWRD.2012.2194514
- Cook, M. V. (2013). Chapter 11 - Command and Stability Augmentation. In M. V. Cook (Ed.), *Flight Dynamics Principles (Third Edition)* (pp. 293-351): Butterworth-Heinemann.
- Dannehl, J., Fuchs, F. W., Hansen, S., Th, x00F, & gersen, P. B. (2010). Investigation of Active Damping Approaches for PI-Based Current Control of Grid-Connected Pulse Width Modulation Converters With LCL Filters. *Industry Applications, IEEE Transactions on*, 46(4), 1509-1517. doi:10.1109/TIA.2010.2049974
- Dannehl, J., Liserre, M., & Fuchs, F. W. (2011). Filter-Based Active Damping of Voltage Source Converters With LCL Filter. *IEEE Transactions on Industrial Electronics*, 58(8), 3623-3633. doi:10.1109/TIE.2010.2081952
- Das, P. P., Chattopadhyay, S., & Palmal, M. (2017). A d-q Voltage Droop Control Method With Dynamically Phase-Shifted Phase-Locked Loop for Inverter Paralleling Without Any Communication Between Individual Inverters. *IEEE Transactions on Industrial Electronics*, 64(6), 4591-4600. doi:10.1109/TIE.2017.2674607
- Devassy, S., & Singh, B. (2017). Control of solar photovoltaic integrated UPQC operating in polluted utility conditions. *IET Power Electronics*, 10(12), 1413-1421.

- Dheer, D. K., V, A. S., Kulkarni, O. V., & Doolla, S. (2019). Improvement of Stability Margin of Droop-Based Islanded Microgrids by Cascading of Lead Compensators. *IEEE Transactions on Industry Applications*, 55(3), 3241-3251. doi:10.1109/TIA.2019.2897947
- Dirscherl, C., Fessler, J., Hackl, C. M., & Ipach, H. (2015, 21-23 Sept. 2015). *State-feedback controller and observer design for grid-connected voltage source power converters with LCL-filter*. Paper presented at the 2015 IEEE Conference on Control Applications (CCA).
- Disha, Prabhu, N., Chaithra, L., & Suryanarayana, K. (2016, 20-21 May 2016). *Synchronous reference frame based transformerless single phase grid tie inverter for DC bus power evacuation*. Paper presented at the 2016 IEEE International Conference on Recent Trends in Electronics, Information & Communication Technology (RTEICT).
- Donghua, P., Xinbo, R., Chenlei, B., Weiwei, L., & Xuehua, W. (2014). Capacitor-Current-Feedback Active Damping With Reduced Computation Delay for Improving Robustness of LCL-Type Grid-Connected Inverter. *Power Electronics, IEEE Transactions on*, 29(7), 3414-3427. doi:10.1109/TPEL.2013.2279206
- Dou, C., Li, N., Yue, D., & Liu, T. (2016). Hierarchical hybrid control strategy for micro-grid switching stabilisation during operating mode conversion. *IET Generation, Transmission & Distribution*, 10(12), 2880-2890. doi:10.1049/iet-gtd.2015.1256
- Dou, C., Liu, B., & Guerrero, J. M. (2014). Event-triggered hybrid control based on multi-agent system for microgrids. *IET Generation, Transmission & Distribution*, 8(12), 1987-1997. doi:10.1049/iet-gtd.2013.0869
- Engleitner, R., Nied, A., Cavalca, M. S. M., & Costa, J. P. d. (2016, 20-23 Nov. 2016). *Small wind turbine operating points and their effect on the DC-link control for frequency support on low power microgrids with high wind penetration*. Paper presented at the 2016 12th IEEE International Conference on Industry Applications (INDUSCON).
- Engleitner, R., Nied, A., Cavalca, M. S. M., & Costa, J. P. d. (2018). Dynamic Analysis of Small Wind Turbines Frequency Support Capability in a Low-Power Wind-Diesel Microgrid. *IEEE Transactions on Industry Applications*, 54(1), 102-111. doi:10.1109/TIA.2017.2761833
- Fang, J., Xiao, G., Yang, X., & Tang, Y. (2017). Parameter Design of a Novel Series-Parallel-Resonant LCL Filter for Single-Phase Half-Bridge Active Power Filters. *IEEE Transactions on Power Electronics*, 32(1), 200-217. doi:10.1109/TPEL.2016.2532961
- Farrell, J. (2011, 25 Nov 2017). *The challenge of reconciling a Centralized v. Decentralized Electricity system*.

- Firdaus, A., & Mishra, S. (2020). Mitigation of Power and Frequency Instability to Improve Load Sharing Among Distributed Inverters in Microgrid Systems. *IEEE Systems Journal*, 14(1), 1024-1033. doi:10.1109/JSYST.2019.2920018
- Fujita, H. (2009). A Single-Phase Active Filter Using an H-Bridge PWM Converter With a Sampling Frequency Quadruple of the Switching Frequency. *IEEE Transactions on Power Electronics*, 24(4), 934-941. doi:10.1109/TPEL.2008.2009302
- Geury, T., Pinto, S., & Gyselinck, J. (2015). Current source inverter-based photovoltaic system with enhanced active filtering functionalities. *IET Power Electronics*, 08(12), 2483-2491.
- Golsorkhi, M. S., & Lu, D. D. C. (2015). A Control Method for Inverter-Based Islanded Microgrids Based on V-I Droop Characteristics. *IEEE Transactions on Power Delivery*, 30(3), 1196-1204. doi:10.1109/TPWRD.2014.2357471
- Guerrero, J. M., Vasquez, J. C., Matas, J., Vicuna, L. G. d., & Castilla, M. (2011). Hierarchical Control of Droop-Controlled AC and DC Microgrids—A General Approach Toward Standardization. *IEEE Transactions on Industrial Electronics*, 58(1), 158-172. doi:10.1109/TIE.2010.2066534
- Guo, X., Lu, Z., Wang, B., Sun, X., Wang, L., & Guerrero, J. M. (2014). Dynamic Phasors-Based Modeling and Stability Analysis of Droop-Controlled Inverters for Microgrid Applications. *IEEE Transactions on Smart Grid*, 5(6), 2980-2987. doi:10.1109/TSG.2014.2331280
- Han, H., Liu, Y., Sun, Y., Su, M., & Guerrero, J. M. (2015). An Improved Droop Control Strategy for Reactive Power Sharing in Islanded Microgrid. *IEEE Transactions on Power Electronics*, 30(6), 3133-3141. doi:10.1109/TPEL.2014.2332181
- Han, Y., Li, H., Shen, P., Coelho, E. A. A., & Guerrero, J. M. (2017). Review of Active and Reactive Power Sharing Strategies in Hierarchical Controlled Microgrids. *IEEE Transactions on Power Electronics*, 32(3), 2427-2451. doi:10.1109/TPEL.2016.2569597
- Han, Y., Li, H., Xu, L., Zhao, X., & Guerrero, J. M. (2018). Analysis of Washout Filter-Based Power Sharing Strategy—An Equivalent Secondary Controller for Islanded Microgrid Without LBC Lines. *IEEE Transactions on Smart Grid*, 9(5), 4061-4076. doi:10.1109/TSG.2017.2647958
- Han, Y., Shen, P., Zhao, X., & Guerrero, J. M. (2016). An Enhanced Power Sharing Scheme for Voltage Unbalance and Harmonics Compensation in an Islanded AC Microgrid. *IEEE Transactions on Energy Conversion*, 31(3), 1037-1050. doi:10.1109/TEC.2016.2552497

- Han, Y., Shen, P., Zhao, X., & Guerrero, J. M. (2017). Control Strategies for Islanded Microgrid Using Enhanced Hierarchical Control Structure With Multiple Current-Loop Damping Schemes. *IEEE Transactions on Smart Grid*, 8(3), 1139-1153. doi:10.1109/TSG.2015.2477698
- Han, Y., Xu, L., Khan, M. M., Chen, C., Yao, G., & Zhou, L. (2011). Robust Deadbeat Control Scheme for a Hybrid APF With Resetting Filter and ADALINE-Based Harmonic Estimation Algorithm. *IEEE Transactions on Industrial Electronics*, 58(9), 3893-3904. doi:10.1109/TIE.2010.2093475
- Hao, X., Yang, X., Liu, T., Huang, L., & Chen, W. (2013). A Sliding-Mode Controller With Multiresonant Sliding Surface for Single-Phase Grid-Connected VSI With an LCL Filter. *IEEE Transactions on Power Electronics*, 28(5), 2259-2268. doi:10.1109/TPEL.2012.2218133
- Hasan, Z., Salman, K., & El-Hawary, M. E. (2016, 15-18 May 2016). *Linear quadratic regulator design for power system stabilizer using biogeography based optimization method*. Paper presented at the 2016 IEEE Canadian Conference on Electrical and Computer Engineering (CCECE).
- He, J., & Li, Y. W. (2012). Generalized Closed-Loop Control Schemes with Embedded Virtual Impedances for Voltage Source Converters with LC or LCL Filters. *IEEE Transactions on Power Electronics*, 27(4), 1850-1861. doi:10.1109/TPEL.2011.2168427
- He, J., Li, Y. W., Bosnjak, D., & Harris, B. (2013). Investigation and Active Damping of Multiple Resonances in a Parallel-Inverter-Based Microgrid. *IEEE Transactions on Power Electronics*, 28(1), 234-246. doi:10.1109/TPEL.2012.2195032
- He, Y., Chung, H. S., Ho, C. N., & Wu, W. (2016). Use of Boundary Control With Second-Order Switching Surface to Reduce the System Order for Deadbeat Controller in Grid-Connected Inverter. *IEEE Transactions on Power Electronics*, 31(3), 2638-2653. doi:10.1109/TPEL.2015.2441117
- Hoang, T. V., & Lee, H. (2020). Virtual Impedance Control Scheme to Compensate for Voltage Harmonics with Accurate Harmonic Power Sharing in Islanded Microgrids. *IEEE Journal of Emerging and Selected Topics in Power Electronics*, 1-1. doi:10.1109/JESTPE.2020.2983447
- Houari, A., Renaudineau, H., Martin, J., Nahid-Mobarakeh, B., Pierfederici, S., & Meibody-Tabar, F. (2015). Large-signal stabilization of AC grid supplying voltage-source converters with LCL-filters. *IEEE Transactions on Industry Applications*, 51(1), 702-711. doi:10.1109/TIA.2014.2328789

- Houari, A., Renaudineau, H., Nahid-Mobarakeh, B., Martin, J. P., Pierfederici, S., & Meibody-Tabar, F. (2014). Large Signal Stability Analysis and Stabilization of Converters Connected to Grid Through LCL Filters. *IEEE Transactions on Industrial Electronics*, 61(12), 6507-6516. doi:10.1109/TIE.2014.2320225
- Huerta, F., Bueno, E., Cobreces, S., Rodriguez, F. J., & Giron, C. (2008, 15-19 June 2008). *Control of grid-connected voltage source converters with LCL filter using a Linear Quadratic servocontroller with state estimator*. Paper presented at the 2008 IEEE Power Electronics Specialists Conference.
- Huerta, F., Pizarro, D., Cobreces, S., Rodriguez, F. J., Giro, x, Rodriguez, A. (2012). LQG Servo Controller for the Current Control of LCL Grid-Connected Voltage-Source Converters. *Industrial Electronics, IEEE Transactions on*, 59(11), 4272-4284. doi:10.1109/TIE.2011.2179273
- IEEE Recommended Practice and Requirements for Harmonic Control in Electric Power Systems - Redline. (2014). *IEEE Std 519-2014 (Revision of IEEE Std 519-1992) - Redline*, 1-213.
- Imran, R. M., Wang, S., & Flaih, F. M. F. (2019). DQ-Voltage Droop Control and Robust Secondary Restoration With Eligibility to Operate During Communication Failure in Autonomous Microgrid. *IEEE Access*, 7, 6353-6361. doi:10.1109/ACCESS.2018.2889806
- Jain, C., & Singh, B. (2015). Single-phase single-stage multifunctional grid interfaced solar photo-voltaic system under abnormal grid conditions. *IET Generation, Transmission & Distribution*, 09(10), 886-894.
- Javadi, A., Abarzadeh, M., Grégoire, L., & Al-Haddad, K. (2019). Real-Time HIL Implementation of a Single-Phase Distribution Level THSeAF Based on D-NPC Converter Using Proportional-Resonant Controller for Power Quality Platform. *IEEE Access*, 7, 110372-110386. doi:10.1109/ACCESS.2019.2934033
- Javadi, A., Hamadi, A., Ndtoungou, A., & Al-Haddad, K. (2017). Power Quality Enhancement of Smart Households Using a Multilevel-THSeAF With a PR Controller. *IEEE Transactions on Smart Grid*, 8(1), 465-474. doi:10.1109/TSG.2016.2608352
- Jayalath, S., & Hanif, M. (March 2017). Generalized LCL-Filter Design Algorithm for Grid-Connected Voltage-Source Inverter *IEEE Transactions on Industrial Electronics*, vol. 64(no. 3), pp. 1905-1915.
- Jianguo, W., Jiu Dun, Y., & Lin, J. (2016). Pseudo-Derivative-Feedback Current Control for Three-Phase Grid-Connected Inverters With LCL Filters. *Power Electronics, IEEE Transactions on*, 31(5), 3898-3912. doi:10.1109/TPEL.2015.2462331

- Jinwei, H., Yun Wei, L., Bosnjak, D., & Harris, B. (2013). Investigation and Active Damping of Multiple Resonances in a Parallel-Inverter-Based Microgrid. *Power Electronics, IEEE Transactions on*, 28(1), 234-246. doi:10.1109/TPEL.2012.2195032
- Joung, K. W., Kim, T., & Park, J. (2019). Decoupled Frequency and Voltage Control for Stand-Alone Microgrid With High Renewable Penetration. *IEEE Transactions on Industry Applications*, 55(1), 122-133. doi:10.1109/TIA.2018.2866262
- Juntunen, R., Korhonen, J., Musikka, T., Smirnova, L., Pyrhönen, O., & Silventoinen, P. (2015, 15-19 March 2015). *Identification of resonances in parallel connected grid inverters with LC- and LCL-filters*. Paper presented at the 2015 IEEE Applied Power Electronics Conference and Exposition (APEC).
- Kahrobaeian, A., & Mohamed, Y. A. I. (2014). Analysis and Mitigation of Low-Frequency Instabilities in Autonomous Medium-Voltage Converter-Based Microgrids With Dynamic Loads. *IEEE Transactions on Industrial Electronics*, 61(4), 1643-1658. doi:10.1109/TIE.2013.2264790
- Kaszewski, A., Grzesiak, L. M., & Ufnalski, B. (2012, 25-28 Oct. 2012). *Multi-oscillatory LQR for a three-phase four-wire inverter with L3nC output filter*. Paper presented at the IECON 2012 - 38th Annual Conference on IEEE Industrial Electronics Society.
- Kedjar, B., & Al-Haddad, K. (2009). DSP-Based Implementation of an LQR With Integral Action for a Three-Phase Three-Wire Shunt Active Power Filter. *Industrial Electronics, IEEE Transactions on*, 56(8), 2821-2828. doi:10.1109/TIE.2008.2006027
- Kedjar, B., Kanaan, H. Y., & Al-Haddad, K. (2014). Vienna Rectifier With Power Quality Added Function. *IEEE Transactions on Industrial Electronics*, 61(8), 3847-3856. doi:10.1109/TIE.2013.2286577
- Khadkikar, V., & Chandra, A. (2012, 17-20 June 2012). *Control of single-phase UPQC in synchronous d-q reference frame*. Paper presented at the 2012 IEEE 15th International Conference on Harmonics and Quality of Power.
- Khadkikar, V., Singh, M., Chandra, A., & Singh, B. (2010, 20-23 Dec. 2010). *Implementation of single-phase synchronous d-q reference frame controller for shunt active filter under distorted voltage condition*. Paper presented at the 2010 Joint International Conference on Power Electronics, Drives and Energy Systems & 2010 Power India.
- Komurcugil, H., Altin, N., Ozdemir, S., & Sefa, I. (2016). Lyapunov-Function and Proportional-Resonant-Based Control Strategy for Single-Phase Grid-Connected VSI With LCL Filter. *IEEE Transactions on Industrial Electronics*, 63(5), 2838-2849. doi:10.1109/TIE.2015.2510984

- Komurcugil, H., Bayhan, S., & Abu-Rub, H. (2017, 4-6 April 2017). *Lyapunov-function based control approach with cascaded PR controllers for single-phase grid-tied LCL-filtered quasi-Z-source inverters*. Paper presented at the 2017 11th IEEE International Conference on Compatibility, Power Electronics and Power Engineering (CPE-POWERENG).
- Komurcugil, H., Ozdemir, S., Sefa, I., Altin, N., & Kukrer, O. (2016). Sliding-Mode Control for Single-Phase Grid-Connected LCL-Filtered VSI With Double-Band Hysteresis Scheme. *Industrial Electronics, IEEE Transactions on*, 63(2), 864-873. doi:10.1109/TIE.2015.2477486
- Kundur, P. (2013). *Power System Stability and Control*. 15th ed. New Delhi, India: Tata McGraw Hill.
- Lal, V. N., & Singh, S. N. (2016). Modified particle swarm optimisation-based maximum power point tracking controller for single-stage utility-scale photovoltaic system with reactive power injection capability. *IET Renewable Power Generation*, 10(7), 899-907. doi:10.1049/iet-rpg.2015.0346
- Lazzarin, T. B., Bauer, G. A. T., & Barbi, I. (2013). A Control Strategy for Parallel Operation of Single-Phase Voltage Source Inverters: Analysis, Design and Experimental Results. *IEEE Transactions on Industrial Electronics*, 60(6), 2194-2204. doi:10.1109/TIE.2012.2193856
- Li, Y., & Fan, L. (2017). Stability Analysis of Two Parallel Converters With Voltage–Current Droop Control. *IEEE Transactions on Power Delivery*, 32(6), 2389-2397. doi:10.1109/TPWRD.2017.2656062
- Li, Z., Zang, C., Zeng, P., Yu, H., & Li, S. (2018). Fully Distributed Hierarchical Control of Parallel Grid-Supporting Inverters in Islanded AC Microgrids. *IEEE Transactions on Industrial Informatics*, 14(2), 679-690. doi:10.1109/TII.2017.2749424
- Liebst, B., & Robinson, J. (1991). *A linear quadratic regulator weight selection algorithm for robust pole assignment*.
- Liserre, M., Blaabjerg, F., & Hansen, S. (2005). Design and control of an LCL-filter-based three-phase active rectifier. *IEEE Transactions on Industry Applications*, 41(5), 1281-1291. doi:10.1109/TIA.2005.853373
- Liserre, M., Dell'Aquila, A., & Blaabjerg, F. (2002, 23-27 June 2002). *Stability improvements of an LCL-filter based three-phase active rectifier*. Paper presented at the 2002 IEEE 33rd Annual IEEE Power Electronics Specialists Conference. Proceedings (Cat. No.02CH37289).

- Liserre, M., Dell'Aquila, A., & Blaabjerg, F. (2003, 9-13 Feb. 2003). *Genetic algorithm based design of the active damping for a LCL-filter three-phase active rectifier*. Paper presented at the Eighteenth Annual IEEE Applied Power Electronics Conference and Exposition, 2003. APEC '03.
- Liu, B., Liu, Z., Liu, J., An, R., Zheng, H., & Shi, Y. (2019). An Adaptive Virtual Impedance Control Scheme Based on Small-AC-Signal Injection for Unbalanced and Harmonic Power Sharing in Islanded Microgrids. *IEEE Transactions on Power Electronics*, 34(12), 12333-12355. doi:10.1109/TPEL.2019.2905588
- Liu, Q., Peng, L., Kang, Y., Tang, S., Wu, D., & Qi, Y. (2014). A Novel Design and Optimization Method of an LCL Filter for a Shunt Active Power Filter. *IEEE Transactions on Industrial Electronics*, 61(8), 4000-4010. doi:10.1109/TIE.2013.2282592
- Liu, T., Liu, Z., Liu, J., Tu, Y., & Liu, Z. (2017). *An improved capacitor-current-feedback active damping for LCL resonance in grid-connected inverters*. Paper presented at the IEEE 3rd International Future Energy Electronics Conference and ECCE Asia (IFEEC 2017 - ECCE Asia), Kaohsiung.
- Lu, M., Wang, X., Loh, P. C., & Blaabjerg, F. (2015, 20-24 Sept. 2015). *Interaction and aggregated modeling of multiple paralleled inverters with LCL filter*. Paper presented at the 2015 IEEE Energy Conversion Congress and Exposition (ECCE).
- Luo, A., Chen, Y., Shuai, Z., & Tu, C. (2013). An Improved Reactive Current Detection and Power Control Method for Single-Phase Photovoltaic Grid-Connected DG System. *IEEE Transactions on Energy Conversion*, 28(4), 823-831. doi:10.1109/TEC.2013.2277658
- Maccari, L. A., Santini, C. L. d. A., Oliveira, R. C. d. L. F. d., & Montagner, V. F. (2013, 27-31 Oct. 2013). *Robust discrete linear quadratic control applied to grid-connected converters with LCL filters*. Paper presented at the 2013 Brazilian Power Electronics Conference.
- Maccari, L. A., Santini, C. L. d. A., Oliveira, R. C. L. F., & Montagner, V. F. (2014, 7-10 Dec. 2014). *Design and experimental implementation of a robust DLQR for three-phase grid-connected converters*. Paper presented at the 2014 11th IEEE/IAS International Conference on Industry Applications.
- Maccari, L. A., Santini, C. L. d. A., Pinheiro, H., Oliveira, R. C. L. F. d., & Montagner, V. F. (2015). Robust optimal current control for grid-connected three-phase pulse-width modulated converters. *IET Power Electronics*, 8(8), 1490-1499. doi:10.1049/iet-pel.2014.0787

- Mahmood, H., Michaelson, D., & Jiang, J. (2015). Accurate Reactive Power Sharing in an Islanded Microgrid Using Adaptive Virtual Impedances. *IEEE Transactions on Power Electronics*, 30(3), 1605-1617. doi:10.1109/TPEL.2014.2314721
- Majumder, R., Chaudhuri, B., Ghosh, A., Majumder, R., Ledwich, G., & Zare, F. (2010). Improvement of Stability and Load Sharing in an Autonomous Microgrid Using Supplementary Droop Control Loop. *IEEE Transactions on Power Systems*, 25(2), 796-808. doi:10.1109/TPWRS.2009.2032049
- Marnay, C., Chatzivasileiadis, S., Abbey, C., Iravani, R., Joos, G., Lombardi, P., Appen, J. v. (2015, 8-11 Sept. 2015). *Microgrid Evolution Roadmap*. Paper presented at the 2015 International Symposium on Smart Electric Distribution Systems and Technologies (EDST).
- Masson, G., Orlandi, S., & Rekinge, M. (2014). Global market outlook for photovoltaics 2014-2018 , *European Photovoltaics*
- Mehrizi-Sani, A., & Iravani, R. (2010). Potential-Function Based Control of a Microgrid in Islanded and Grid-Connected Modes. *IEEE Transactions on Power Systems*, 25(4), 1883-1891. doi:10.1109/TPWRS.2010.2045773
- Meza, C., Biel, D., Jeltsema, D., & Scherpen, J. M. A. (2012). Lyapunov-Based Control Scheme for Single-Phase Grid-Connected PV Central Inverters. *IEEE Transactions on Control Systems Technology*, 20(2), 520-529. doi:10.1109/TCST.2011.2114348
- Mirhosseini, M., Pou, J., & Agelidis, V. G. (2015). Single- and Two-Stage Inverter-Based Grid-Connected Photovoltaic Power Plants With Ride-Through Capability Under Grid Faults. *IEEE Transactions on Sustainable Energy*, 6(3), 1150-1159. doi:10.1109/TSTE.2014.2347044
- Mohamed, Y. A. I., & El-Saadany, E. F. (2008). Adaptive Decentralized Droop Controller to Preserve Power Sharing Stability of Paralleled Inverters in Distributed Generation Microgrids. *IEEE Transactions on Power Electronics*, 23(6), 2806-2816. doi:10.1109/TPEL.2008.2005100
- Mohamed, Y. A. I., Zeineldin, H. H., Salama, M. M. A., & Seethapathy, R. (2012). Seamless Formation and Robust Control of Distributed Generation Microgrids via Direct Voltage Control and Optimized Dynamic Power Sharing. *IEEE Transactions on Power Electronics*, 27(3), 1283-1294. doi:10.1109/TPEL.2011.2164939
- Niannian, C., & Mitra, J. (2010, 26-28 Sept. 2010). *A decentralized control architecture for a microgrid with power electronic interfaces*. Paper presented at the North American Power Symposium 2010.

- Nishida, K., Ahmed, T., & Nakaoka, M. (2014). Cost-Effective Deadbeat Current Control for Wind-Energy Inverter Application With LCL Filter. *IEEE Transactions on Industry Applications*, 50(2), 1185-1197. doi:10.1109/TIA.2013.2279900
- Olivares, D. E., Mehrizi-Sani, A., Etemadi, A. H., Cañizares, C. A., Iravani, R., Kazerani, M., Hatziargyriou, N. D. (2014). Trends in Microgrid Control. *IEEE Transactions on Smart Grid*, 5(4), 1905-1919. doi:10.1109/TSG.2013.2295514
- Ounejjar, Y., Al-Haddad, K., & Grégoire, L. A. (2011). Packed U cells multilevel converter topology: theoretical study and experimental validation. *IEEE Trans. Ind. Electron.*, 58(4), 1294-1306.
- Padilha Vieira, R., Stefanello, M., Varella Tambara, R., & Grundling, H. A. (2014, Oct. 29 2014-Nov. 1 2014). *Sliding mode control in a multi-loop framework for current control of a grid-tied inverter via LCL-filter*. Paper presented at the Industrial Electronics Society, IECON 2014 - 40th Annual Conference of the IEEE.
- Pan, D., Ruan, X., Bao, C., Li, W., & Wang, X. (2014). Capacitor-Current-Feedback Active Damping With Reduced Computation Delay for Improving Robustness of LCL-Type Grid-Connected Inverter. *IEEE Transactions on Power Electronics*, 29(7), 3414-3427. doi:10.1109/TPEL.2013.2279206
- Parker, S. G. (July 2014). *Discrete Time Current Regulation of Grid Connected Converters with LCL Filters. A thesis submitted in fulfilment of the requirements for the degree of Doctor of Philosophy.*
- Parker, S. G., McGrath, B. P., & Holmes, D. G. (2014). Regions of Active Damping Control for LCL Filters. *Industry Applications, IEEE Transactions on*, 50(1), 424-432. doi:10.1109/TIA.2013.2266892
- Pasha, A. M., Zeineldin, H. H., Al-Sumaiti, A. S., Moursi, M. S. E., & Sadaany, E. F. E. (2017). Conservation Voltage Reduction for Autonomous Microgrids Based on V-I Droop Characteristics. *IEEE Transactions on Sustainable Energy*, 8(3), 1076-1085. doi:10.1109/TSTE.2017.2651046
- Pen, x, a-Alzola, R., Liserre, M., Blaabjerg, F., Ordonez, M., & Kerekes, T. (2014). A Self-commissioning Notch Filter for Active Damping in a Three-Phase LCL -Filter-Based Grid-Tie Converter. *Power Electronics, IEEE Transactions on*, 29(12), 6754-6761. doi:10.1109/TPEL.2014.2304468
- Peña-Alzola, R., Liserre, M., Blaabjerg, F., Ordonez, M., & Yang, Y. (2014). LCL-Filter Design for Robust Active Damping in Grid-Connected Converters. *IEEE Transactions on Industrial Informatics*, 10(4), 2192-2203. doi:10.1109/TII.2014.2361604

- Peña-Alzola, R., Liserre, M., Blaabjerg, F., Sebastián, R., Dannehl, J., & Fuchs, F. W. (2013). Analysis of the Passive Damping Losses in LCL-Filter-Based Grid Converters. *IEEE Transactions on Power Electronics*, 28(6), 2642-2646. doi:10.1109/TPEL.2012.2222931
- Peña-Alzola, R., Liserre, M., Blaabjerg, F., Sebastián, R., Dannehl, J., & Fuchs, F. W. (2014). Systematic Design of the Lead-Lag Network Method for Active Damping in LCL-Filter Based Three Phase Converters. *IEEE Transactions on Industrial Informatics*, 10(1), 43-52. doi:10.1109/TII.2013.2263506
- Pilo, F., Pisano, G., & Soma, G. G. (2007, 23-27 June 2007). *Neural Implementation of MicroGrid Central Controllers*. Paper presented at the 2007 5th IEEE International Conference on Industrial Informatics.
- Pradhan, S., Hussain, I., Singh, B., & Panigrahi, B. K. (2017). Modified VSS-LMS-based adaptive control for improving the performance of a single-stage PV-integrated grid system. *IET Science, Measurement & Technology*, 11(4), 388-399. doi:10.1049/iet-smt.2016.0351
- Rafiei, S., Moallem, A., Bakhshai, A., & Yazdani, D. (2014, 16-20 March 2014). *Application of a digital ANF-based power processor for micro-grids power quality enhancement*. Paper presented at the 2014 IEEE Applied Power Electronics Conference and Exposition - APEC 2014.
- Rahim, N. A., Chaniago, K., & Selvaraj, J. (2011). Single-Phase Seven-Level Grid-Connected Inverter for Photovoltaic System. *Transactions on Industrial Electronics*, 58(06), 2435-2443.
- Rahmani, S., Al-Haddad, K., & Kanaan, H. Y. (2008). Two PWM techniques for single-phase shunt active power filters employing a direct current control strategy. *IET Power Electronics*, 1(3), 376-385. doi:10.1049/iet-pel:20070253
- Reznik, A., Simões, M. G., Al-Durra, A., & Mueeen, S. M. (2014). LCL Filter Design and Performance Analysis for Grid-Interconnected Systems. *IEEE Transactions on Industry Applications*, 50(2), 1225-1232. doi:10.1109/TIA.2013.2274612
- Ricchiuto, D., Liserre, M., Kerekes, T., Teodorescu, R., & Blaabjerg, F. (2011, 17-22 Sept. 2011). *Robustness analysis of active damping methods for an inverter connected to the grid with an LCL-filter*. Paper presented at the 2011 IEEE Energy Conversion Congress and Exposition.
- Ricchiuto, D., Liserre, M., & Santis, D. D. (2012). *Low-switching-frequency active damping methods of medium-voltage multilevel inverters*. Paper presented at the IEEE International Symposium on Industrial Electronics, Hangzhou.

- Rocabert, J., Luna, A., Blaabjerg, F., & Rodríguez, P. (2012). Control of Power Converters in AC Microgrids. *IEEE Transactions on Power Electronics*, 27(11), 4734-4749. doi:10.1109/TPEL.2012.2199334
- Ruiz, G. E. M., Muñoz, N., & Cano, J. B. (2015, 2-4 June 2015). *Modeling, analysis and design procedure of LCL filter for grid connected converters*. Paper presented at the 2015 IEEE Workshop on Power Electronics and Power Quality Applications (PEPQA).
- Š, B., Komrska, T., Šmídl, V., Glasbergerová, V., & Peroutka, Z. (2016, 6-7 Sept. 2016). *Multi-harmonic LQ control of single-phase converter with LCL filter*. Paper presented at the 2016 International Conference on Applied Electronics (AE).
- Sabzehgar, R. (2015, 9-9 Nov. 2015). *A review of AC/DC microgrid-developments, technologies, and challenges*. Paper presented at the 2015 IEEE Green Energy and Systems Conference (IGESC).
- Santini, C. L. d. A., Maccari, L. A., & Montagner, V. F. (2014, 7-10 Dec. 2014). *Design and analysis of robustness of DLQR controllers applied to grid-connected inverters*. Paper presented at the 2014 11th IEEE/IAS International Conference on Industry Applications.
- Savaghebi, M., Jalilian, A., Vasquez, J. C., & Guerrero, J. M. (2012). Secondary Control Scheme for Voltage Unbalance Compensation in an Islanded Droop-Controlled Microgrid. *IEEE Transactions on Smart Grid*, 3(2), 797-807. doi:10.1109/TSG.2011.2181432
- Savaghebi, M., Jalilian, A., Vasquez, J. C., & Guerrero, J. M. (2013). Autonomous Voltage Unbalance Compensation in an Islanded Droop-Controlled Microgrid. *IEEE Transactions on Industrial Electronics*, 60(4), 1390-1402. doi:10.1109/TIE.2012.2185914
- Sebaaly, F., Vahedi, H., Kanaan, H. Y., Moubayed, N., & Al-Haddad, K. (2016). Sliding Mode Fixed Frequency Current Controller Design for Grid-Connected NPC Inverter. *IEEE Journal of Emerging and Selected Topics in Power Electronics*, 04(04), 1397-1405.
- Sharma, R. K., Mishra, S., & Pullaguram, D. (2020). A Robust H_∞ Multivariable Stabilizer Design for Droop Based Autonomous AC Microgrid. *IEEE Transactions on Power Systems*, 35(6), 4369-4382. doi:10.1109/TPWRS.2020.3000312
- Silva, S. A. O. d., Sampaio, L. P., Oliveira, F. M. d., & Durand, F. R. (2017). Feed-forward DC-bus control loop applied to a single-phase grid-connected PV system operating with PSO-based MPPT technique and active power-line conditioning. *IET Renewable Power Generation*, 11(1), 183-193. doi:10.1049/iet-rpg.2016.0120

- Singh, B., Chandra, A., & Al-Haddad, K. (Eds.). (2015). *Power Quality: Problems and Mitigation Techniques*. Chichester, U.K.: Wiley.
- Singh, Y., Hussain, I., Mishra, S., & Singh, B. (2017). Adaptive neuron detection-based control of single-phase SPV grid integrated system with active filtering. *IET Power Electronics*, 10(6), 657-666. doi:10.1049/iet-pel.2016.0613
- Singh, Y., Hussain, I., Singh, B., & Mishra, S. (2017). Single-phase solar grid-interfaced system with active filtering using adaptive linear combiner filter-based control scheme. *IET Generation, Transmission & Distribution*, 11(8), 1976-1984. doi:10.1049/iet-gtd.2016.1392
- Sreekumar, P., & Khadkikar, V. (2016). A New Virtual Harmonic Impedance Scheme for Harmonic Power Sharing in an Islanded Microgrid. *IEEE Transactions on Power Delivery*, 31(3), 936-945. doi:10.1109/TPWRD.2015.2402434
- Sun, Y., Li, S., Lin, B., Fu, X., Ramezani, M., & Jaithwa, I. (2017). Artificial Neural Network for Control and Grid Integration of Residential Solar Photovoltaic Systems. *IEEE Transactions on Sustainable Energy*, 8(4), 1484-1495. doi:10.1109/TSTE.2017.2691669
- Trabelsi, M., Bayhan, S., Ghazi, K. A., Abu-Rub, H., & Ben-Brahim, L. (2016). Finite-Control-Set Model Predictive Control for Grid-Connected Packed-U-Cells Multilevel Inverter. *IEEE Transactions on Industrial Electronics*, 63(11), 7286-7295. doi:10.1109/TIE.2016.2558142
- Trivedi, A., & Singh, M. (2017). Repetitive Controller for VSIs in Droop-Based AC-Microgrid. *IEEE Transactions on Power Electronics*, 32(8), 6595-6604. doi:10.1109/TPEL.2016.2619367
- Tsai-Fu, W., Hung-Shou, N., Chih-Lung, S., & Tsung-Ming, C. (2005). A single-phase inverter system for PV power injection and active power filtering with nonlinear inductor consideration. *IEEE Transactions on Industry Applications*, 41(4), 1075-1083. doi:10.1109/TIA.2005.851035
- Tuyen, N. D., & Fujita, G. (2015). PV-Active Power Filter Combination Supplies Power to Nonlinear Load and Compensates Utility Current. *IEEE Power and Energy Technology Systems Journal*, 02(01), 32-42.
- Twining, E., & Holmes, D. G. (2002, 23-27 June 2002). *Grid current regulation of a three-phase voltage source inverter with an LCL input filter*. Paper presented at the 2002 IEEE 33rd Annual IEEE Power Electronics Specialists Conference. Proceedings (Cat. No.02CH37289).

- Ufnalski, B., Kaszewski, A., & Grzesiak, L. M. (2015). Particle Swarm Optimization of the Multioscillatory LQR for a Three-Phase Four-Wire Voltage-Source Inverter With an LCL Output Filter. *IEEE Transactions on Industrial Electronics*, 62(1), 484-493. doi:10.1109/TIE.2014.2334669
- Vahedi, H., Kanaan, H. Y., & Al-Haddad, K. (2015, 9-12 Nov. 2015). *PUC converter review: Topology, control and applications*. Paper presented at the IECON 2015 - 41st Annual Conference of the IEEE Industrial Electronics Society.
- Vahedi, H., Labbé, P. A., & Al-Haddad, K. (2016). Sensor-Less Five-Level Packed U-Cell (PUC5) Inverter Operating in Stand-Alone and Grid-Connected Modes. *IEEE Transactions on Industrial Informatics*, 12(01), pp. 361-370.
- Vahedi, H., Shojaei, A. A., Dessaint, L. A., & Al-Haddad, K. (2018). Reduced DC-Link Voltage Active Power Filter Using Modified PUC5 Converter. *IEEE Transactions on Power Electronics*, 33(2), 943-947. doi:10.1109/TPEL.2017.2727325
- Vandoorn, T. L., Kooning, J. D. M. D., Meersman, B., Guerrero, J. M., & Vandevelde, L. (2012). Automatic Power-Sharing Modification of P/ V Droop Controllers in Low-Voltage Resistive Microgrids. *IEEE Transactions on Power Delivery*, 27(4), 2318-2325. doi:10.1109/TPWRD.2012.2212919
- Vieira, R. P., Stefanello, M., Tambara, R. V., & Gründling, H. A. (2014, 29 Oct.-1 Nov. 2014). *Sliding mode control in a multi-loop framework for current control of a grid-tied inverter via LCL-filter*. Paper presented at the IECON 2014 - 40th Annual Conference of the IEEE Industrial Electronics Society.
- Villanueva, E., Correa, P., Rodriguez, J., & Pacas, M. (2009). Control of a Single-Phase Cascaded H-Bridge Multilevel Inverter for Grid-Connected Photovoltaic Systems. *IEEE Transactions on Industrial Electronics*, 56(11), 4399-4406.
- Wang, J., Yan, J. D., & Jiang, L. (2016). Pseudo-Derivative-Feedback Current Control for Three-Phase Grid-Connected Inverters With LCL Filters. *IEEE Transactions on Power Electronics*, 31(5), 3898-3912. doi:10.1109/TPEL.2015.2462331
- Wang, X., Blaabjerg, F., Liserre, M., Chen, Z., He, J., & Li, Y. (2014). An Active Damper for Stabilizing Power-Electronics-Based AC Systems. *IEEE Transactions on Power Electronics*, 29(7), 3318-3329. doi:10.1109/TPEL.2013.2278716
- Wang, X., Ruan, X., Liu, S., & Tse, C. K. (2010). Full Feedforward of Grid Voltage for Grid-Connected Inverter With LCL Filter to Suppress Current Distortion Due to Grid Voltage Harmonics. *IEEE Transactions on Power Electronics*, 25(12), 3119-3127. doi:10.1109/TPEL.2010.2077312

- Wang, Z., Yang, R., & Wang, L. (2011, 17-19 Jan. 2011). *Intelligent multi-agent control for integrated building and micro-grid systems*. Paper presented at the ISGT 2011.
- Wenli, Y., Yongheng, Y., Xiaobin, Z., & Blaabjerg, F. (2015, 15-19 March 2015). *Digital notch filter based active damping for LCL filters*. Paper presented at the Applied Power Electronics Conference and Exposition (APEC), 2015 IEEE.
- Wu, T.-F., Nien, H.-S., Shen, C.-L., & Chen, T.-M. A single-phase inverter system for PV power injection and active power filtering with nonlinear inductor consideration. *IEEE Transactions on Industry Applications*, 41(04), 1075-1083.
- Wu, W., He, Y., & Blaabjerg, F. (2012). An LLCL Power Filter for Single-Phase Grid-Tied Inverter. *IEEE Transactions on Power Electronics*, 27(2), 782-789. doi:10.1109/TPEL.2011.2161337
- Wu, W., Liu, Y., He, Y., Chung, H. S. H., Liserre, M., & Blaabjerg, F. (2017). Damping Methods for Resonances Caused by LCL-Filter-Based Current-Controlled Grid-Tied Power Inverters: An Overview. *IEEE Transactions on Industrial Electronics*, 64(9), 7402-7413. doi:10.1109/TIE.2017.2714143
- Xiaoqiang, L., Xiaojie, W., Yiwen, G., Xibo, Y., ChenYang, X., & Xue, Z. (2015). Wide Damping Region for LCL-Type Grid-Connected Inverter With an Improved Capacitor-Current-Feedback Method. *Power Electronics, IEEE Transactions on*, 30(9), 5247-5259. doi:10.1109/TPEL.2014.2364897
- Xu, H., Yu, C., Liu, C., Wang, Q., Liu, F., & Li, F. (2019). An Improved Virtual Capacitor Algorithm for Reactive Power Sharing in Multi-Paralleled Distributed Generators. *IEEE Transactions on Power Electronics*, 1-1. doi:10.1109/TPEL.2019.2898990
- Xue, D., Chen, Y., Atherton, D. P., Society for, I., & Applied, M. (2007). Linear feedback control : analysis and design with MATLAB.
- Xuehua, W., Xinbo, R., Shangwei, L., & Tse, C. K. (2010). Full Feedforward of Grid Voltage for Grid-Connected Inverter With LCL Filter to Suppress Current Distortion Due to Grid Voltage Harmonics. *Power Electronics, IEEE Transactions on*, 25(12), 3119-3127. doi:10.1109/TPEL.2010.2077312
- Yang, S., Lei, Q., Peng, F. Z., & Qian, Z. (2011). A Robust Control Scheme for Grid-Connected Voltage-Source Inverters. *IEEE Transactions on Industrial Electronics*, 58(1), 202-212. doi:10.1109/TIE.2010.2045998
- Yang, S. Y., Zhang, X., Zhang, C. W., & Xie, Z. (2009, 17-20 May 2009). *Study on active damping methods for voltage source converter with LCL input filter*. Paper presented at the 2009 IEEE 6th International Power Electronics and Motion Control Conference.

- Yang, Z., & Ho, C. N.-M. (2016, 22-26 May 2016). *A review on Microgrid architectures and control methods*. Paper presented at the 2016 IEEE 8th International Power Electronics and Motion Control Conference (IPEMC-ECCE Asia).
- Yao, W., Chen, M., Matas, J., Guerrero, J. M., & Qian, Z. (2011). Design and Analysis of the Droop Control Method for Parallel Inverters Considering the Impact of the Complex Impedance on the Power Sharing. *IEEE Transactions on Industrial Electronics*, 58(2), 576-588. doi:10.1109/TIE.2010.2046001
- Yao, W., Yang, Y., Zhang, X., & Blaabjerg, F. (2015, 15-19 March 2015). *Digital notch filter based active damping for LCL filters*. Paper presented at the 2015 IEEE Applied Power Electronics Conference and Exposition (APEC).
- Yazdani, M., & Mehrizi-Sani, A. (2016). Washout Filter-Based Power Sharing. *IEEE Transactions on Smart Grid*, 7(2), 967-968. doi:10.1109/TSG.2015.2497964
- Zeng, Z., Zhao, R., & Yang, H. (2014). Coordinated control of multi-functional grid-tied inverters using conductance and susceptance limitation. *IET Power Electronics*, 7(7), 1821-1831. doi:10.1049/iet-pel.2013.0692
- Zhang, H., Kim, S., Sun, Q., & Zhou, J. (2017). Distributed Adaptive Virtual Impedance Control for Accurate Reactive Power Sharing Based on Consensus Control in Microgrids. *IEEE Transactions on Smart Grid*, 8(4), 1749-1761. doi:10.1109/TSG.2015.2506760
- Zhao, W., & Chen, G. (2009, 6-7 April 2009). *Comparison of active and passive damping methods for application in high power active power filter with LCL-filter*. Paper presented at the 2009 International Conference on Sustainable Power Generation and Supply.
- Zhu, Y., Zhuo, F., Wang, F., Liu, B., Gou, R., & Zhao, Y. (2016). A Virtual Impedance Optimization Method for Reactive Power Sharing in Networked Microgrid. *IEEE Transactions on Power Electronics*, 31(4), 2890-2904. doi:10.1109/TPEL.2015.2450360
- Zongbin, Jiang, L., Zhang, Z., Yu, D., Wang, Z., Deng, X., (2017). A Novel DC-Power Control Method for Cascaded H-Bridge Multilevel Inverter. *Transactions on Industrial Electronics*, 64(9), 6874-6884.